2019

The Skin Remembers: Epigenetic Memories of Inflammation Past

Samantha B. Larsen

THE SKIN REMEMBERS: EPIGENETIC MEMORIES OF INFLAMMATION PAST

A Thesis Presented to the Faculty of

The Rockefeller University

in Partial Fulfillment of the Requirements for

the degree of Doctor of Philosophy

by

Samantha B. Larsen

June 2019

THE SKIN REMEMBERS: EPIGENETIC MEMORIES OF INFLAMMATION PAST

Samantha B. Larsen, Ph.D.

The Rockefeller University 2019

As one of the body's largest environmental interfaces, the skin is routinely exposed to a myriad of inflammatory stimuli. It functions as a barrier acting as the first line of defense against pathogens, while simultaneously protecting the organism from dehydration. Maintaining an intact barrier is therefore paramount to organismal survival, and the foremost torchbearers of this task are skin epithelial stem cells (EpSCs). EpSCs reside in the basal layer of the skin, survive long-term, and are capable of both self-renewing and differentiating into multiple skin lineages. To efficaciously maintain the barrier, EpSCs must be able to sense and respond to environmental cues. Here, I unearth an adaptive mechanism whereby EpSCs retain an epigenetic memory of prior inflammatory exposure that endows them with enhanced sensitivity and responsiveness to subsequent tissue damage. During secondary injury, inflammatory memory is mediated by cytosolic dsDNA sensor and activator of the inflammasome AIM2, and its downstream effectors caspase-1 and interleukin-1β. Characterization of the chromatin landscape in inflammation-experienced EpSCs reveals specific retention of monomethylation of histone 3 on lysine 4 in memory chromatin domains primed for reactivation. Altogether, this body of work identifies a novel mechanism by which EpSCs cope with and adapt to environmental stress in preparation for the next inflammatory trigger.

ACKNOWLEDGMENTS

This work would not have been possible without the support and guidance from my adviser, Elaine Fuchs. Initially, I entered Rockefeller believing I would join a neuroscience lab; however, it was Elaine who convinced me to try something different and to try that something in her lab. When I approached Elaine about studying inflammation in the skin, she encouraged the collaboration with then post-doc extraordinaire, Shruti Naik. Elaine is a champion of female scientists, a passionate mentor, and an absolute inspiration. It has been under her guidance that I have matured into an independent scientist, and progress in my career "being comfortable with being uncomfortable."

Shruti has been an incredible mentor, collaborator, life coach, and friend over the past 5 years. Her infectious energy for science is contagious, and working with her on a day-to-day basis was wonderful. I am looking forward to being reunited as colleagues at NYU.

The past year, I have had the pleasure of mentoring and working alongside fellow graduate student Chris Cowley. Chris is a bright and talented scientist, whose dedication to our work shows daily. I am excited to see all the great things Chris will achieve as he progresses in his graduate work at Rockefeller.

The biggest of thank yous to two individuals, Nick Gomez and Thomas Carroll, for their help in the bioinformatic analyses presented throughout this dissertation. Nick tackled the initial sets of ATAC-Seq data, and did their full work up. In doing so he simultaneously taught me the basics of bioinformatics so that when it came to analyzing the AIM2KO ATAC data, I was self-sufficient. Thank you for teaching me not to fear rejection and encouraging my basic bioinformatics education. Thank you

to Tom, who tackled the MINT-ChIP data sets (the equivalent of 20-40 ChIP-Seqs at one time!) and wrote a pipeline that would make subsequent analyses faster and streamlined. Tom has been instrumental in teaching me to handle these large data sets and using the correct bioinformatic tools to analyze them. Thank you both!

The work presented in this dissertation required constant FACS sorting and analyses to isolate skin epithelial stem cells. Thank you to the entire FCRC team, who have been helpful during each and every sort, accommodating when our sorts need more time, and resourceful in shuffling the schedule when we have needed emergency sorts. Thank you to Rockefeller's GRC for their assistance and guidance in preparing for the genomics experiments.

Thank you to the Dean's Office, who initially made my decision to attend Rockefeller one of the easiest choices I have ever made. Their organization, attentiveness, and availability have made it an absolute pleasure to be a graduate student at Rockefeller.

One of the best things about the Fuchs lab is the colleagues. While during group and subgroup meetings every one has contributed in one way or another to this work, for which I am grateful, I would like to thank Phoenix, Leo, Rachel, Sanjee, Felipe, Matt, Rene, Hanseul, and Yejing for their helpful discussion and/or teaching a specific technique. A big thank you to the Fuchs lab mouse team, who have been helpful in breeding, weening, ordering, and organizing mice. Specific thanks to Lisa for teaching mouse techniques and to John for lentivirus injections. Also a big shout out to the Fuchs lab running team!

Lastly, thank you to my amazing family and friends. Thank you to my mom, Beth, who has encouraged and cultivated my love of science since I was a child. She bought my first set of test tubes when I was 10 and helped realize my dream of becoming a scientist. To Hanna, for being my best friend, answering the phone no matter the time, and for being my personal stylist. To my dad, Tommy, for the dad

jokes and Friday funnies. To Matt, thank you for the endless laughs, knowing the right thing to say, indulging my need to walk miles before dessert, being a low key interior decorator, jumping into sub-freezing water, encouraging our SCUBA certification and for all around being one of the best people I know. To the friends I have made along the way at Rockefeller, I am so fortunate that we were in the same place at the same time: Anneloor, Koen, Till, Leon, Bryan, Felipe, Mariya, Brooke, Kate, and Jon. Lastly, to the group of friends here in the city, you make every weekend wonderful. Thank you YELLOW and SALSAA for the dodgeball skills, and to Anna, Amy, Lauren, and Maddie for the FTC. I love you all!

Significant Contributions

The work presented in this dissertation reflects a large collaborative effort. While I have had direct involvement in collection and analysis of all data presented, I will refer to the collective effort of all scientists involved and predominantly use the pronoun ”we” throughout the text. Major contributors to this work include Shruti Naik (SN), Christopher Cowley (CC), Nicholas Gomez (NG), and Thomas Carroll (TC).

SN and NG were significant contributors to the work presented in Chapter 2. SN and I independently performed and validated all wound healing experiments. SN performed flow cytometric analysis for lineage tracing experiments and the skin immune cell panels, while I performed all microscopy. SN and I each did a biological replicate for D6 and D30 RNA-Sequencing. SN did 12 hour RNA-Sequencing. I did D6, D30, and D180 WT ATAC-Seq experiments. CC and I performed D6 and D30 AIM2KO ATAC experiments. SN and I did the tumor study. NG performed the ATAC-Seq analyses for WT samples and I performed AIM2KO ATAC analyses. I cloned and designed all the vectors presented throughout this chapter with the exception of TRE-AIM2 cloned by Kirill Alaverdyan.

TC and CC were significant contributors to the work presented in Chapter 3. TC designed and coded a MINT-ChIP pipeline that performs demultiplexing, sequence

alignment, peak calls, and motif analysis on FASTQ files. CC and I performed mouse treatments, skin preps, and EpSC isolation for MINT-ChIP. CC and I performed MINT-ChIP experiments and all analyses downstream from the pipeline.

Other contributions to the work presented include: Leo Yuan for developing the methodology and performing the culturing of our adult stem cell populations. Kirill Alaverdyan for genotyping. John Levorse for all *in utero* lentiviral injections. Lisa, Megan, and Lynette for breeding, weening, and maintenance of mouse colonies.

TABLE OF CONTENTS

LIST OF TABLES

LIST OF FIGURES

LIST OF ABBREVIATIONS

ATAC	Assay for Transposase-Accessible Chromatin
ChIP	Chromatin Immunoprecipitation
DAMP	Danger Associated Molecular Pattern
DT	Diptheria Toxin
EGFP	Enhanced Green Fluorescent Protein
EpSC	Epithelial Stem Cell
FACS	Fluorescence Assisted Cell Sorting
HFSC	Hair Follicle Stem Cell
IMQ	Imiquimod
KO	Knock Out
LV	Lentiviral Vector
PAMP	Pathogen Associated Molecular Pattern
PI	Post-inflamed
qPCR	Quantitative Polymerase Chain Reaction
rtTA	Reverse Tetracycline-Controlled Transactivator
RFP	Red Fluorescent Protein
SE	Super-enhancer
TAM	Tamoxifen
TCR	T Cell Receptor
TF	Transcription Factor
TLR	Toll Like Receptor
TRE	Tetracycline Response Element
TSS	Transcription Start Site
UTR	Untranslated Region
WT	Wild Type
YFP	Yellow Fluorescent Protein

CHAPTER 1

INTRODUCTION

1.1 Inflammatory Skin Disease

The skin can be subdivided into two compartments: the epidermis and the dermis. The epidermis is the outermost layer that creates a sealed barrier to the external environment and is separated from the underlying dermis by a thin fibrous basement membrane. The epidermis is populated by skin cells called keratinocytes, which stratify into multiple layers including the stratum basale (innermost), stratum spinosum, stratus granulosum, and stratum corneum (outermost) to ensure formation of a protective barrier. These keratinocytes reside in a complex niche replete with a diverse network of cellular members that are in constant communication to ensure healthy tissue regulation and maintenance of the barrier. One of the most important cell types in the skin niche are immune cells, which are present in the skin to sample different antigens, alert the body to pathogen invasion, and serve as rapid responders in orchestrating tissue repair after injury. The crosstalk between keratinocytes and immune cells is a fine-tuned balance, where any dysregulation can lead to the formation of inflammatory skin disorders.

One of the most common skin inflammatory diseases is psoriasis, which affects approximately 2$\%$ of the population [1]. It is a remitting and relapsing chronic disease, where skin lesions reoccur in the same body sites over and over again. These skin lesions are caused by hyperproliferative keratinocytes that fail to produce an effec-

tive cornified layer leading to a hyperthickened epidermis (acanthosis) and retention of nuclei in the stratum corneum (parakeratosis) [2]. These lesions are hypervascularized leading to their red color and are hyperennervated making the skin region more sensitive to pain. Psoriasis is associated with a large immune cell infiltrate in the dermis consisting of dendritic cells, macrophages, neutrophils, and T cells with a concurrent elevation of T cells in the epidermis. While there is a large immune component to psoriasis, it remains unclear whether this disease is epithelial or immunological in nature. What we do know is the importance of the crosstalk between immune cells and keratinocytes.

Infiltrating immune cells create an inflammatory microenvironment rich in cytokines that fuel keratinocyte proliferation including type I interferons, TNF-α, IL-17, and IL-22 [2] [3]. Stimulated keratinocytes in turn secrete chemokines such as CXCL8, CXL10, and CCL20 that recruit immune cells to the lesion [4]. Keratinocytes themselves propagate the inflammatory milieu by secreting cytokines such as IL-1β, IL-6, and TNF-a that induce the proliferation of neighboring keratinocytes [5]. A recently appreciated component of psoriatic pathogenesis is the detection of abundant levels of cytosolic self-DNA within skin lesions. Aberrant cytosolic DNA is a danger signal, which keratinocytes respond to via activation of the AIM2 inflammasome which leads to processing and release of IL-1β [6]. Cytosolic DNA can also complex with keratinocyte-derived antimicrobial cathelicidin peptide LL-37, which activates dendritic cells via TLR9 providing a potential mechanism by which cytosolic self-DNA functions as a pro-inflammatory danger associated molecular pattern leading to a break in immunologic tolerance thereby contributing to the chronic nature of psoriasis [7].

At present there is no cure for psoriasis, and a paucity of efficacious therapies to offer patients. Therapies can be broken into multiple classes including: biologics (must be injected or via IV), oral treatments, phototherapy (i.e. regular exposure to

UV light), or topicals (i.e. corticosteroids). Each of these classes has major drawbacks, take for example prolonged exposure to UV light increasing the risk of skin cancer. The most commonly used treatment for psoriasis, which has not responded to other treatments, is biologics. Biologics aim to do one of two things: directly target and block T cells or block their proinflammatory cytokines (TNFa, IL-17a, IL-12, and IL-23) [8] [9]. Because these therapies are injected or taken via IV, they have deleterious systemic side effects such as an increased risk of infection, inflammatory bowel disease, or new/worsening heart failure to name a few. What the current biologics and therapies all have in common is that they aim to target the immune system, but as discussed before the origins of psoriatic pathogenesis remain unknown. With the need for more efficient therapies, there is a need to consider psoriatic pathogensis from an epithelial angle.

One of the most curious and perplexing aspects of psoriasis is that the lesions relapse in the same body site. Recent work highlights that skin in different body locations can be replete with distinct populations of commensal microbiota, which affect the immune cell milieu [10]. In fact, the skin on the back of a person's elbow is more similar to another person's elbow than to their own palms or other body site [11]. One can imagine this having an effect on the propensity for the disease to develop in common body sites between patients. Nevertheless, the skin itself is still fundamentally the same from one body site to another, and offers a tremendous opportunity to gain insight into how psoriatic pathogenesis affects skin biology. To begin there are some outstanding questions that need be addressed such as: what are the long-term consequences of inflammation on keratinocytes and how do these keratinocytes cope with and adapt to inflammatory stress? Answering these questions will offer insights into psoriatic pathogenesis that one day can be used for the development of a novel therapeutic intervention.

1.2 The skin is maintained in health and disease by epithelial stem cells

Adult tissue stem cells in the skin reside in the hair follicle, sebaceous gland, and the epidermis [12] [13] [14]. Basal interfollicular epidermal stem cells (EpSCs) reside in one single layer that adheres to the basement membrane, which is rich in extracellular matrix and growth factors. The main role of EpSCs is to continuously replenish the skin during homeostasis and re-epithelialize the skin barrier after tissue injury. They accomplish this role through their ability to both self-renew, giving rise to 'sister' stem cells, and to execute a terminal differentiation program that gives rise to the outer layers of the skin including the spinous, granular, and corneum layers [15] [16]. When a basal cell commits to terminally differentiate, it goes through major transcriptional and morphological changes that results in an enucleated cell at the stratum corneum later, which eventually gets sloughed off. The progression from basal cell to sloughing takes approximately 4 weeks in humans, and in mice, the minimum transit time from basal layer to cornified layer is about 1-2 weeks [17] [18]. EpSCs are retained long-term, and individual clones can remain in the basal layer for over 50 weeks in mice [19] [20] [17].

Following tissue injury such as a full thickness wound where both the epidermal and dermal layers of skin are removed, EpSCs are activated and begin to proliferate. Stem cells near the wound edge coordinate their behavior by balancing proliferation, differentiation, and migration to re-epithelialize the breached barrier. EpSCs become highly proliferative, and begin to directionally divide towards the wound edge while simultaneously conducting collective migration, which leads to an elongated epithelial tongue that extends into the wound bed until the barrier is sealed [21] [22]. The balance between EpSCs' wound healing response and homeostasis is carefully regulated, and when this balance is disturbed there is an increased propensity for tissue dysregulation that could result in the development of dysfunctional tissue states such

as hyperproliferative inflammatory skin disorders, non-healing wounds, or squamous cell carcinoma [23] [22] [24].

1.3 Stem cells modulate their behavior upon detection of environmental cues

1.3.1 Stem cells during infection and inflammation

Adult stem cells are importantly tasked with maintaining their tissues both in health and disease. This function is made possible by their ability to sense and respond to various environmental cues. Stem cells (SCs) express a number of membrane-bound receptors that enable them to identify changes or danger in their extracellular environment such as cytokine and pattern recognition receptors. Similar SCs express cytoplasmic sentinels to alert them to foreign material within the cell. Each of these sensors is upstream of well-defined pathways that influence stem cell behavior. These pathways result in decisions between quiescence and activation, self-renewal and differentiation, metabolic state, and lineage bias. These sensors are expressed and active during both homeostasis and disease, and are critical to enabling stem cells to adequately maintain their tissue.

In the skin, EpSCs express a variety of cytokines and chemokines that enable them to identify cues and initiate reactionary transcriptional programs. One example, EpSC bound epidermal growth factor receptor (EGFR), plays a crucial role in regulating innate immune cell-driven inflammation, maintaining barrier function, and contributing to antimicrobial defense [25] [26]. If EGFR signaling is inhibited or impaired, the result is an uncontrolled inflammatory cascade with a huge immune cell surge, the production of a multitude of proinflammatory cytokines, and increased susceptibility to infection. Hair follicle stem cells (HFSCs), whose primary task is to fuel hair regrowth, reside in the bulge niche, which is an orifice to the external environment and provides a potential entry point for external pathogens. HFSCs can sense junctional perturbations in their niche that disturb barrier function, and quickly coor-

dinate a transcriptional response that results in direct signaling and recruitment of immune cells via secretion of CCL2. HFSCs begin to proliferate, but rather than exit their niche which is their homeostatic response to proliferation, they remain in the bulge to contain the breach and reinforce the barrier [27].

Aging impacts the ability of skin EpSCs to be as sensitive to environmental signals as their younger selves. Aged mice have significantly delayed wound healing and barrier restoration, as the EpSCs are less capable of interpreting signals and upregulating the necessary transcriptional response. Specifically, the inefficient upregulation of *Skints* and phosphorylation of STAT3 results in the inability to activate and maintain dendritic epidermal T cells (DETCs), which promote re-epithelialization after injury [22].

Looking broadly to other adult stem cell compartments provides additional insight into the capability and mechanisms by which SCs sense and respond to environmental cues. Hematopoietic stem cells (HSCs) reside in the bone marrow and give rise to both myeloid and lymphoid lineages of immune cells. During a bacterial or viral infection, HSCs are activated in what is known as emergency hematopoiesis to replenish innate immune cells. This process involves a biased lineage decision towards myelopoiesis, since T cells are capable of proliferating in response to infection. HSCs must therefore detect an infection, interpret the inflammatory cues, and generate myeloid cells. One mechanism by which emergency hematopoiesis is regulated is through IFNγ secretion by cytotoxic $CD8^+$ T cells, which induces mesenchymal stromal cells (resident bone marrow niche cells) to release IL-6. Multipotent hematopoietic stem and progenitor cells (HSPCs) in turn sense IL-6, resulting in the reduced expression of transcription factors *Runx1* and *Cebpa*, which are important to progenitor self-renewal. IL6-induced downregulation of *Runx1* and *Cebpa* in myeloid progenitors leads to increased differentiation, and the production of more myeloid cells enabling efficacious control of the infection [28].

Additionally, HSPCs can directly detect infection via membrane-bound toll like receptors (TLR) that recognize specific pathogen associated molecular patterns (PAMPs). HSPCs express TLR4, which recognizes LPS, a paradigmatic gram-negative bacterial product. LPS-induced TLR4 signaling results in emergency hematopoiesis via stem cell activation, cytokine production, and myeloid differentiation [29]. HSCs also express cytoplasmic sensors such as NLRP1, which recognizes intracellular PAMPs, and leads to inflammasome formation. Activation of the inflammasome leads to HSC pyroptosis and the release of IL-1β, which alerts neighboring cells of an infection so they can act to neutralize the threat. Activation of these pathways must be tightly regulated, as prolonged stimulation can lead to impaired HSC self-renewal and reduced competitive repopulation activity [30].

The response of HSPCs to infection is mosaic due to their heterogeneous expression of *Il6ra* and *Tlr4*. Within the broad population of HSPCs, there are multiple subtypes including long-term-HSCs, short-term-HSCs, multipotent progenitors, and lymphoid-primed multipotent progenitors. Single cell proteomics highlights a dynamic communication between these HSPC sub-populations in response to the sensing of danger signals. Varied receptor expression between sub-populations leads to distinct activation patterns and cytokine profiles based on the class of infection or signal received. This dynamic communication and heterogeneous cytokine release leads to an efficient and robust immune response with rapid myeloid cell recovery [31].

Intestinal epithelial stem cells (ISCs) also directly respond to changes in their microenvironment. During inflammation, direct sensing of tissue resident innate lymphoid cell (ILC)-derived IL-22 promotes ISC proliferation through the activation of the STAT3 pathway. STAT3 activation is important to ISC maintenance and ISC production of innate antimicrobial molecules REG3b and REG3g [32]. Crosstalk between immune cells and ISCs is therefore imperative to survival and maintenance of intestinal tissues during inflammation.

1.3.2 Stem cells during homeostasis

Beyond foreign infections, adult stem cells are equipped to respond to cues from their homeostatic microenvironment. In HSCs, multiple cytokine receptor families converge and rely on JAK1 to relay critical information from the extracellular space to HSCs to modulate their behavior. JAK1 has been implicated in different immunological and neoplastic diseases and is important in normal cytokine production and autocrine feedback. Without JAK1, in homeostasis, HSCs lack the ability to self-renew and bias their differentiation to towards the myeloid lineage. Transcriptional analysis of *Jak1* deficient HSCs reveals that STAT1, STAT2, and IFN-regulated transcription factors, which are activated dowstream of JAK1 signaling, inadequately transcribe their target genes. Failure to link JAK1 signaling to transcriptional ouput results in HSC inability to sense hematopoeitc stress and regulate hematopoiesis [33].

Intestinal epithelial stem cells (ISCs) residing in the crypt exist in a symbiotic relationship with commensal gut microbiota. These gut microbiota help to protect the host from pathogenic microorganisms, and communicate with ISCs through the release of microbe-associated molecular patterns (MAMP). ISCs sense the presence of MAMPs through TLR4 and NOD2, which is an intracellular innate immune sensor. When NOD2 is activated by its ligand muramyldipeptide, a peptidoglycan motif, downstream signaling promotes stem cell survival [34]. This ISC adaptation is handy both during routine tissue regeneration, but also during pathogenic infections that require stem cell survival and tissue repair.

ISCs also communicate with different subsets of T cells through their expression of MHCII, which influences their decision between differentiation and self-renewal. Helper T cells promote ISC differentiation through secretion of IFNγ, IL-17A, or IL-13, and Tregs promote ISC self-renewal via IL-10 [35]. Lastly, ISC sensing of ILC and $\gamma\delta$T cell derived IL-22 was found to contribute to ISC homeostasis through regulation of the DNA damage response. ILCs and $\gamma\delta$T cell sense genotoxic compounds in

the diet and secrete IL-22, which induces ISCs to initiate a protective response that preserves their and their progeny's genomic integrity [36].

All together these studies highlight the importance of adult tissue stem cells in being able to sense and respond to various environmental cues. Whether by membrane-bound receptors, cytosolic sentinels, or direct cell-cell contact, stem cells have evolved to efficiently react to changes in their microenvironment that enable them to effectively maintain tissue integrity both in health and disease.

1.4 Stem cell intrinsic immunity

Intrinsic immunity is a cellular defense mechanism, whereby cells routinely produce defense proteins and cytosolic sentinels to stand guard and detect pathogen invasion. Intrinsic immunity enables tissue stem cells to evade infections from viruses and pathogens, to regulate the delicate balance between their activation and quiescence, as well as to avoid detection from the adaptive immune system.

Adult stem cells representing each of the three multipotent germ layers including neural, pancreatic, and mesenchymal stem cells express at baseline Interferon Stimulated Genes (ISGs) despite being refractory to interferon. The intrinsic expression of these genes protects stem cells from viral infection; however, upon terminal differentiation these genes are downregulated making downstream progeny more susceptible to reduced interferon signaling and infection. Dynamic regulation of chromatin modifications including H3K4me3 and H3K27ac at ISG-associated loci correlates to ISG expression as stem cells differentiate. Loss of ISG expression from the IFTM gene family in stem cells make them susceptible to a myriad of viral infections, including respiratory viruses, flaviviruses and zoonotic virus, leading to their inability to regenerate their respective tissues. While distinct tissue stem cells express cell-type-specific groups of ISGs, the role of ISGs in endowing intrinsic immunity to stem cells is conserved [37].

An additional mechanism cells utilize to sense viral infection is through cytosolic sensors that detect ds/ssDNA. Mesenchymal stem cells (MSCs) detect infection of murine gammaherpesvirus through cytosolic dsDNA sensor cGAS. The cGAS-STING pathway is imperative for the induction of ISGs and protection against viral infection and replication in MSCs [38]. dsDNA sensors also have inflammasome-independent mechanisms to regulate cellular adaptation to environmental signals. Canonically when AIM2 senses dsDNA, it activates the cell to respond by binding ASC resulting in cleavage of pro-CASP1 and downstream release of proinflammatory cytokines IL-1β and IL-18 orchestrating the host's defense to pathogen infection. However, recent work in intestinal stem cells, highlights that AIM2 also plays a dual role by functioning as a negative regulator of cell proliferation. In AIM2 deficient mice there is increased proliferation of ISCs due to enhanced susceptibility of these cells to aberrant Wnt-signaling, elevated phosphorylation of AKT, and expression of c-Myc [39]. These studies highlight the overarching role that cytosolic sensors play in protecting tissue stem cells from infection and maintaining homeostasis.

Tissue stem cells can be immune privileged and are capable of avoiding detection from the innate and adaptive immune system. Stem cells that remain in a quiescent state and are slow cycling, such as HFSCs and satellite cells, evade T-cell detection by downregulating antigen presentation machinery, such as MHCI. This protects their integrity and allows them to evade T-cell mediated cell death. Notably, faster cycling stem cells that are responsible for continuous tissue maintenance such as intestinal, ovary, and mammary stem cells express antigen presenting machinery and are thus able to be detected and targeted for T-cell mediated clearance [40].

We can glean insight into intrinsic immune proteins from the transcriptional and chromatin landscapes of stem cells at baseline and following tissue injury. This information can elucidate the preparedness of a stem cell to rapidly respond to injury, the type of response the cell can mount, and identify if there are long term or persisting

changes that would affect cell behavior.

1.5 Dynamic regulation of chromatin landscape enables cellular training

Gene expression patterns within a cell are controlled by the epigenome, which is a complex network of chromatin and histone modifications that cooperate to stimulate or repress gene activity. These modifications exist in a cell-type specific manner, conferring cell-type identity. Importantly, however, these marks are dynamic allowing for changes in transcriptional output to exact a shift from homeostasis to an injured state. Understanding these marks, their influence on gene expression, and their regulatory mechanisms will provide mechanistic insight into a stem cell's response to inflammation.

Chromatin exists in either active or repressed states, the latter of which leads to gene silencing. Chromatin repression can occur through several mechanisms including DNA methylation and histone modifications [41]. DNA methylation most commonly occurs through 5-methylcytosine (5mC), which is transferred to DNA via DNA methyltransferases (DNMTs). This mark is commonly found in CpG islands, and when enriched at promoters, the associated gene is repressed via the prevention of positive transcription factor binding or the promotion of negative regulators [42]. This mark is readily passed on to daughter cells after cell division via the function of DNMTs. Importantly, however, this mark is reversible and through the TET enzyme catalyzed oxidation of 5mc to 5-hydroxymethylcytosine (5-hmc), DNA can be demethylated. Histone methylation on certain residues such as H3 Lysine 9 (K9) and H3 Lysine 27 (K27) also leads to gene repression [43]. Histone lysines are methylated via lysine methyltransferases (KMTs), and specific lysine residues often have their own KMT [44]. For instance, G9a methylates H3K9me2, Polycomb methylates H3K27me3. In the case of histone modifications, methylation is not always silencing, such as in the case of methylation of H3 lysine 4 (K4), which results in gene acti-

vation. Like DNA methylation, histone methylation is also reversible and can be dynamically changed. Methyl groups can be removed by histone demethylases such as Jumonji-domain containing proteins (JMJC) or lysine-specific histone demethylases (LSD) [44].

Euchromatin is considered active or open, and enables binding of transcriptional machinery to drive gene expression. The predominant histone modification that marks active chromatin is lysine acetylation. Lysines are acetylated via histone acetyltransferases (HATs)

The chromatin landscape of non-coding regions of DNA, specifically cis-regulatory elements such as promoters and enhancers, elucidates how transcription of the associated gene is regulated [43]. Active promoters are marked by H3K4me3. H3K4me3 recruits chromatin remodeling factors such as CHD1 and BPTF, which open chromatin making it permissive to transcription [45] [46]. Simultaneously, H3K4me3 prevents the binding of repressive complexes such as NuRD and INHAT [47] [48]. H3K4me3 is also a good example of the integration of the histone code and DNA methylation status, where H3K4me3 blocks the binding of the DNMT3, which is capable of binding unmodified H3K4, preventing methylation/ repression of the promoter. Repressive histone marks such as H3K27me3 can also be found at promoters, which functions to shut transcription down.

Enhancers are cis regulatory elements that can be upstream, downstream, intronic, proximal or distal and act to increase transcription of their associated genes [49] [50]. Enhancers can exist in multiple states including inactive, poised, primed, and active. Inactive enhancers are often methylated and have histone marks such as H3K9me2 indicating a heterochromatic closed state. Active enhancers are marked by H3K27ac [51]. Often when an enhancer is decommissioned meaning the associated gene is no longer actively transcribed, it will lose its H3K27ac mark but retain H3K4me1 indicating it is primed. Primed enhancers are also typically marked by

5mC hypomethylation or the hydroxylated version, 5hmC. Poised enhancers contain the primed H3K4me1 mark, but also acquire H3K27me3 suggesting a more inactive state. Often H3K4me1 at distal enhancers will precede H3K27ac, and the mechanism by which methyltransferase such as MLL1/2 is initially recruited to these regions remains an open question [52]. One leading hypothesis is that cell-type specific or signaling dependent transcription factors interact with KMTs and guide them to these regions [53].

CHAPTER 2

INFLAMMATORY MEMORY SENSITIZES SKIN EPITHELIAL STEM CELLS TO TISSUE DAMAGE

2.1 Introduction

The skin is an epithelial barrier that functions as the body's first line of defense against environmental assaults, and as such is especially vulnerable to a range of pathogens and noxious agents. Maintaining the skin as an intact barrier is the key function of long-lived epithelial stem cells (EpSCs), which reside in in the innermost (basal) layer of the skin epithelium. These EpSCs can both self-renew and execute a terminal differentiation program that generates a continuous upward flux of barrier cells. Signals emanating from the basement membrane and underlying dermal niche constituents, facilitate EpSC function by inducing molecular programs that maintain EpSC identity and lineage commitment. EpSCs additionally sense and respond to cues from their microenvironment that signal danger, resulting in initiation of programs aimed at recruiting immune cells and reinforcing barrier integrity.

To this end, recent studies have identified a fine-tuned crosstalk between EpSCs and immune cells as critical to efficacious tissue repair [22]. Resident immune cells aid to alert EpSCs to danger, inducing them to initiate repair programs involving proliferation, migration, and recruitment of additional immune cells to the site of injury [27] [22]. EpSC proliferation and migration in tissue repair are carefully regulated, and when this process goes unchecked there is an increased propensity for

tissue dysregulation resulting in the development of dysfunctional tissue states such as hyperproliferative inflammatory skin disorders or tumorigenesis. Considering the vulnerability of EpSCs to inflammatory pressures, neither their involvement in the primary response to inflammation nor the enduring consequences are well understood. To address these open questions, I chose a well-characterized model of acute Imiquimod-induced skin inflammation to assess the long-lasting consequences of inflammation on EpSCs.

2.2 Results

2.2.1 Imiquimod is a self-resolving model of acute skin inflammation

Imiquimod (IMQ) is a Toll Like Receptor (TLR) 7/8 and NALP3 ligand that is applied as a topical cream to the back skin of mice for six consecutive days, where it induces a robust inflammatory response [54] [55] [25]. Skin resident sentinel dendritic cells sense IMQ and migrate to lymph nodes where they secrete IL-23 to induce the expansion of RORC+ $\gamma\delta$ T cells and Th17 cells. These activated lymphocytes travel back to the skin secreting IL-17 and IL-22 among other pro-inflammatory cytokines that are directly sensed by EpSCs inducing their hyperproliferation (Figure 2.1 A). In agreement with prior reports, after six days of treatment there is a psoriatic-like pathology characterized by epidermal hyperthickening, parakeratosis, hypervascularization, hyperinnervation, immune cell infiltrate, aberrant STAT3 signaling, and apoptosis [55] (Figure 2.1 B).

Importantly, IMQ-induced inflammation self-resolves after cessation of treatment, whereby day 30 all notable perturbations subsided and the skin's homeostatic architecture was restored (Figure 2.1 B, C). Given these self-resolving features, we wondered whether inflammation-sensitized stem cells and/or their progeny contribute to epidermal homeostasis after resolution of inflammation.

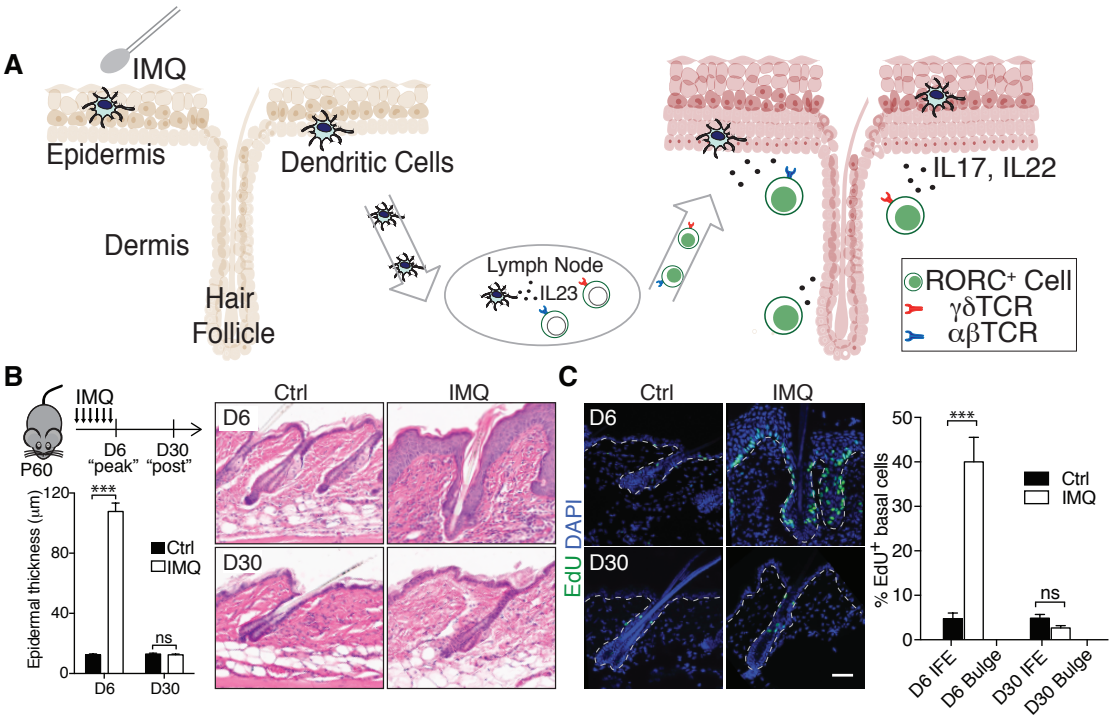

Figure 2.1: Imiquimod is a self-resolving model of skin inflammation **A** Mechanism for imiquimod (IMQ)-induced skin inflammation. **B** Schematic depicting timeline of Control (Ctrl) or IMQ treatment with corresponding histopathology and epidermal thickness quantifications. n= 3. **C** Immunofluorescence images and corresponding quantifications of EDU⁺ epidermal (IFE) and HF (bulge) basal cells at D6 of IMQ or Ctrl treatment and at D30 following treatment. n=3. DAPI, 4'6-diamidino-2-phenylindole.

2.2.2 Lineage tracing skin stem cells in inflammation

To track SC dynamics during and after inflammation, we utilized inducible-marker based fate mapping to delineate in vivo cellular behavior (Figure 2.2) [16]. Specifically, we crossed *Rosa-LSL-YFP* reporter mice that contain the Cre recombinase-oestrogen receptor fusion protein (CreER) driven by keratin (Krt) promoters active in either EpSCs (*Krt14*) or their transient progeny (*Krt10*). Krt14 is present in all skin EpSCs, and at low doses of tamoxifen, *Krt14-CreER* preferentially labels EpSCs of the interfollicular epidermis (and infundibulum). By contrast, *Krt10-CreER* is expressed in differentiating layers. Since hair follicle SCs (HFSCs) can transiently contribute to wound-repair, we also tested *Krt19-CreER*, specific to the HF bulge SC

niche [56] [57].

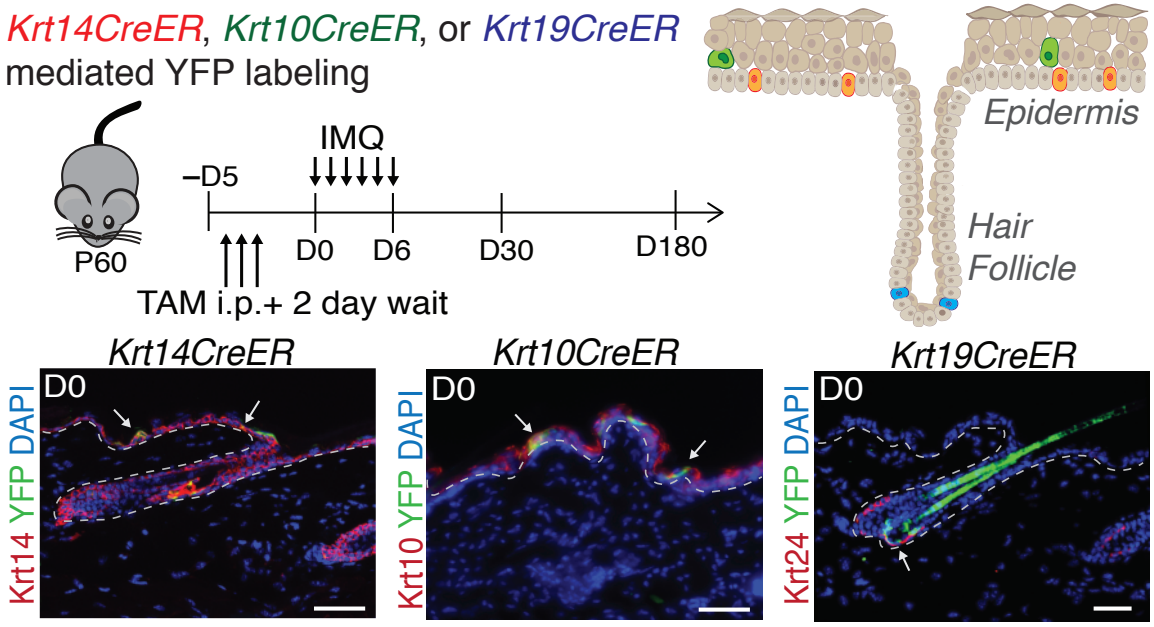

Figure 2.2: Lineage tracing strategy for skin stem cells. Tamoxifen (TAM)-induced *RosaYFP* reporter lineage tracing with *Krt14CreER*, expressed by Krt14$^+$ EpSCs; *Krt10CreER*, expressed by Krt10$^+$ terminally differentiating epidermis; and *Krt19CreER*, expressed by Krt24$^+$ HFSCs. n=4. Arrows mark YFP+ keratinocytes.

Two days after administering tamoxifen, YFP$^+$ cells co-localized with Krt14 in the basal layer (*Krt14-CreER*), Krt10 in the suprabasal layer (*Krt10-CreER*), or Krt24 in the HF bulge (*Krt24-CreER*) [58] [17] (Figure 2.2 and Figure 2.3 A-C). When IMQ was subsequently administered to the skin of *Krt14-CreER;Rosa-LSL-YFP* mice and then lineage-traced, YFP$^+$ cells persisted in the IMQ-treated skin at equivalent numbers to naive (vehicle control) skin for up to 180 days post-inflammation (Figure 2.3 D). Because Cre recombinase was not activated without tamoxifen, the YFP$^+$ EpSCs were long-lived and had survived the inflammatory assault. By contrast, *Krt10-CreER*-activated YFP$^+$ cells (although initially present) were shed within six days, indicating that once progenitors commit to terminal differentiation, they do not revert even in response to IMQ (Figure 2.3 B, E). Lastly, characteristic of their stemness *Krt19-CreER*-activated YFP$^+$ HFSCs persisted and were detected in the bulge niche

30 days after inflammation (Figure 2.3 C, E). However, they did not contribute to the epidermal pathology that typified the IMQ inflammatory response. These results led us hereafter to focus on Krt14^{+} EpSCs.

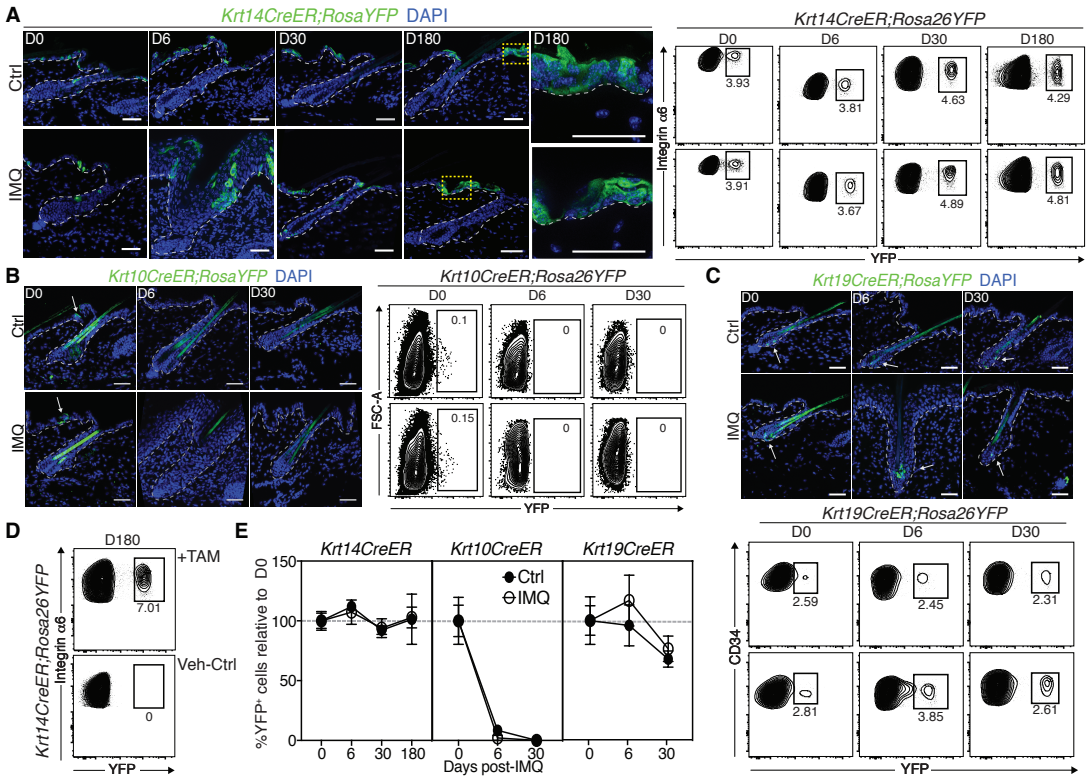

Figure 2.3: Lineage tracing of skin stem cells and progeny during and after inflammation. **A** Lineage tracing of *Krt14-CreER;RosaYFP* at indicated times. Left, immunofluorescence of TAM-activated (or corn-oil control) EpSCs (n=3). Right, flow cytometric analysis of integrin α6^{+} Sca1^{+} CD34^{-} YFP^{+} keratinocytes. **B** Analysis of skin from *Krt10-CreER;RosaYFP* mice that were lineage traced at indicated times. Left, representative immunofluorescence images. Right, flow cytometric analysis YFP^{+} keratinocytes (n=3).**C** Analysis of YFP^{+} keratinocytes of *Krt19-CreER;RosaYFP* skin post TAM treatment. Top, representative immunofluorescence images. Bottom, flow cytometric analysis of integrin α6^{+} Sca1^{-} CD34^{+} YFP^{+} keratinocytes (n=3). **D** Flow cytometric analysis of *Krt14-CreER;RosaYFP* cells from the epidermis of animals that were lineage traced starting from IMQ treatment and analyzed at day 180 (n=2). **E** Plots depict percentage of YFP^{+} cells relative to pre-IMQ (day 0) baselines (corresponding flow cytometric plots shown in **A**, **B**, and **C**. Scale bars, 50μm. Dotted lines demarcate the dermo-epidermal border. Arrows denote YFP^{+} keratinocytes. Data are $\pm$s.e.m. *n* denoted the number of biologically independent anaimals per group. Significance for all plots was determined using two-tailed *t*-test at 95% confidence interval. All experiments have been replicated at least twice.

2.2.3 Enhanced wound healing after inflammation

The persistence of inflammation-experienced EpSCs long after epidermal homeostasis had been restored led us to wonder whether this assault may have had a lasting effect on them and/or their microenvironment. To address this question, we challenged inflammation-recovered skin with a secondary assault, in this case wounding (Figure 2.4 A). Notably, post-inflamed mice closed their wounds approximately 2.5 times faster than naive control mice (Figure 2.4 B, C). The enhanced wound-healing response exhibited by inflammation-experienced skin was observed even when the initial assault had occurred 180 days earlier (Figure 2.4 D).

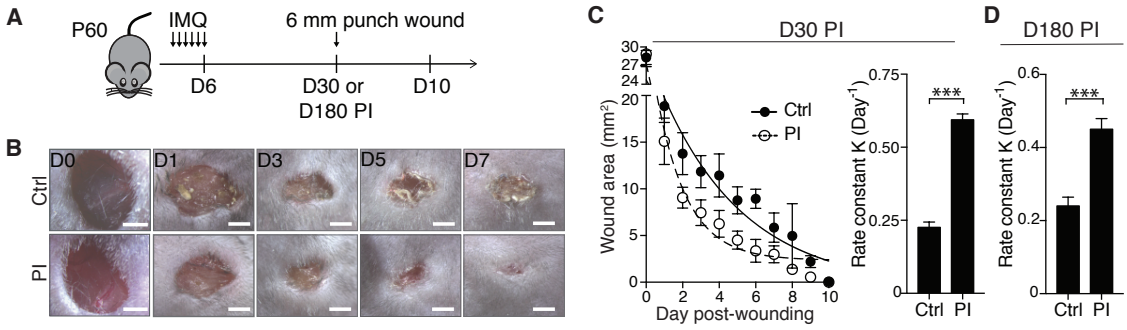

Figure 2.4: Epidermal wound repair post-inflammation. **A** Schematic of wound healing experiment timeline. **B** Images of wound healing in skin 30 days post-inflammation (PI) versus control (Ctrl). Scale bars = 2mm. **C** Accelerated wound healing in day 30 PI skin: Left plots area of wound over time and right plots the rate constant K of wound closure using one-phase decay model (n=17; ***P-value¡0.0001).**D** Accelerated wound healing observed 180 days after inflammation; graph plots rate constant K of wound closure using a one-phase decay model (n=5; ***P-value=0.0003). Data are mean $\pm$s.e.m. n denotes the number of biologically independent animals. Experiments replicated twice and significance determined by two-tailed t-test (95$\%$ confidence). NS, not significant ($P>0.05$).

To determine whether this heightened sensitivity could be elicited broadly by different primary skin irritants that provoke robust epidermal hyperproliferation, we replaced IMQ with various other treatments such as topical application of vitamin D analogue calcipotriol (MC903, to model atopic dermatitis); topical application of 12-O-tetradecanoylphorbol 13-acetate (TPA; to induce hyperplasia; epidermal abrasion

wounding; or infection with the fungal pathogen *Candida albicans* [59] [60] [61] [62]. Following restoration of epidermal homeostasis and skin barrier function, mice were wounded. In all cases, wounds healed faster in inflammation-experienced skin. These results highlighted the generality of the response, indicating that once skin is sensitized to inflammation, it reacts faster when faced with a secondary assault (Figure 2.5).

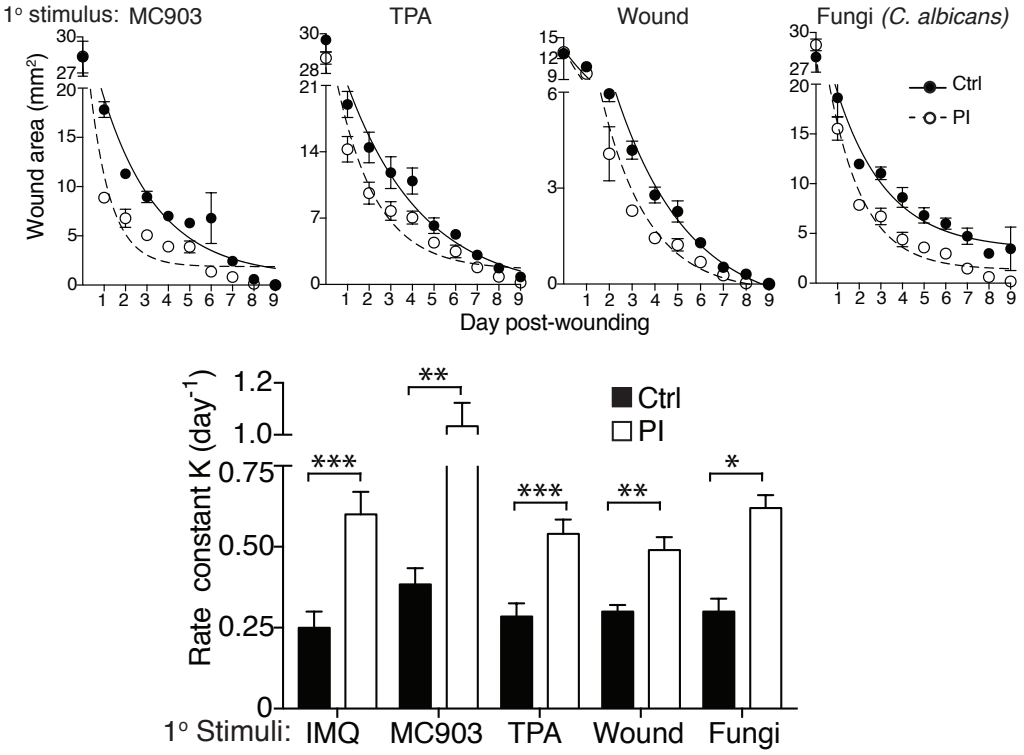

Figure 2.5: Distinct initial inflammatory stimuli result in accelerated wound healing post-inflammation. Top plots depict area of wound each day during closure, and bottom plots rate constant K of wound closure response for each initial inflammatory stimulus (n$\geq$4). IMQ, *** P¡0.0001; MC903 (also known as calcipotriol, ***P=0.0001; TPA, **P=0.0014; epidermal abrasion, **P=0.0027; infection with 10^6 fungal cells (*C. albicans*) **P=0.0029. Rate calculated from wound area in top plots. Data are mean $\pm$s.e.m. n denotes the number of animals. Experiments replicated twice and significance determined by two-tailed t-test (95$\%$ confidence).

After a full-thickness wound, re-epithelialization is mediated by sensitized epi-

dermal EpSCs, which transiently express Krt17. These EpSCs first multiply along the wound edge and then migrate into the wound bed to repair the skin barrier breach [22]. Inflammation-experienced skin displayed augmented epidermal thickness and accelerated re-epithelialization, but showed similar rates of proliferation (Figure 2.6 A-C). Re-epithelialization by the migrating Krt14$^+$ and integrin α5$^+$ epidermal tongue was considerably longer in post-inflamed wounds by day 3, and by day 5 the post-inflamed wounds were entirely re-epithelialized, a full 2 days faster than their control counterparts (Figure 2.6 B).

To exclude myofibroblast-mediated dermal contraction as a notable contributor to the post-inflamed augmented rate of wound closure, we affixed a silicone splint around the wound leaving re-epithelialization via migrating EpSCs as the sole means of healing [63]. Without tissue contraction, inflammation-experienced mice still exhibited enhanced re-epithelialization and accelerated wound repair (Figure 2.6 D). Moreover, using an assay that specifically measures keratinocyte migration, we found that keratinocyte outgrowth from *ex vivo* explants was more robust after inflammation than in controls (Figure 2.6 E) [22]. These findings suggest that inflammation induces long-term changes in EpSCs that enhance their capacity to react swiftly to a secondary assault.

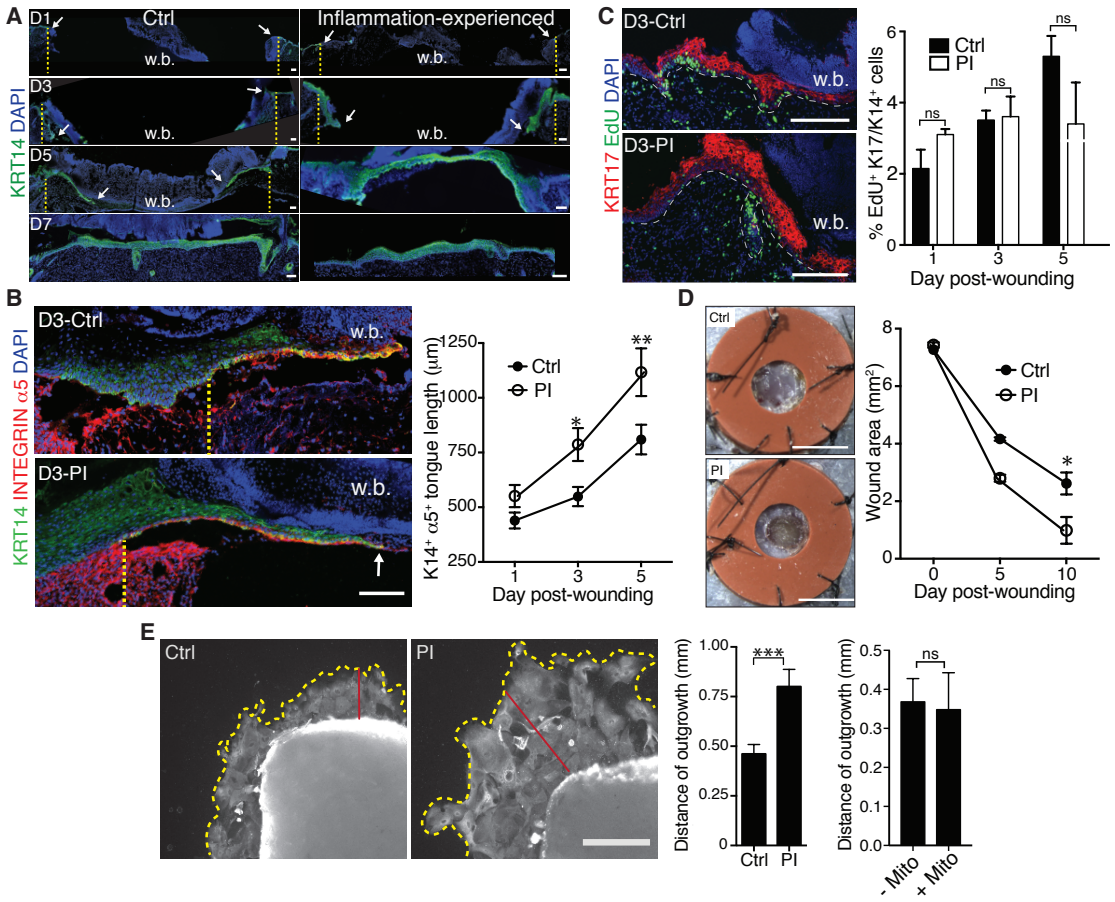

Figure 2.6: Inflammation-sensitized EpSCs are faster at re-epithelializing the wound. **A** Accelerated re-epithelialization in inflammation-experienced skin (n=3). Lines denote initial wound edges and arrows mark the edge of the wound bed (w.b.). Scale bars = 200μm. **B** Immunofluorescence images of wound edges labeled with integrin α5 to mark the migrating wound tongue that repithelializes the w.b., and Keratin 14 (KRT14), which markes the epidermal progenitors, expanded at the wound site. Vertical dotted lines denote the initial wound edges and arrows mark the edge of the extended epithelial tongue (n=3). Scale bars = 100μm. Plot depicts quantification of the length of the integrin $\alpha5^+$ Krt14$^+$ migrating epithelial tongue (n4; *P=0.034 (day 3), **P=0.0037 (day 5)). **C** Immunofluorescence images of wound edges labeled with anti-EdU to mark proliferating cells and anti-Keratin 17 (KRT17) to mark wound-sensitized keratinocytes ($n\geq3$). Scale bars = 100μm. Plot depicts quantification of proliferating wound-edge keratinocytes after a 4 hour EdU pulse. **D** Representative images and quantification of D10 silicone splinted 3 mm full thickness wounds from day 30 control and post-inflamed animals (n=4). Scale bars,3mm. **E** Analysis of Krt14$^+$ keratinocyte outgrowth from day 10 *ex vivo* skin explants. Yellow and red lines mark outgrowth boundary and distance, respectively ($n\geq14$; ***P=0.0006). Scale bars, 500μm. Data are mean $\pm$s.e.m. n denotes the number of biologically independent animals. Experiments replicated twice and significance determined by two-tailed t-test (95$\%$ confidence). NS, not significant ($P>0.05$).

2.2.4 IMQ intrinsically sensitizes EpSCs

EpSCs receive cues from their local milieu as well as from infiltrating immune cells and circulating factors that direct wound repair. We thus sought to evaluate the relative importance of these secondary effectors on the sensitization of inflammation-experienced skin to wounding. When IMQ was administered to half the dorsal skin, skin pathology was restricted to direct application sites (Figure 2.7 A). With this observation, we hypothesized that if the post-inflamed accelerated wound healing was due to systemic (circulating) factors that wounding distal to the site of inflammation should also result in augmented tissue repair. We thus treated half of the dorsal skin and wounded the contralateral side, and found that the distal site closed at a rate comparable to control skin ruling out substantial contribution from systemic factors (Figure 2.7 B).

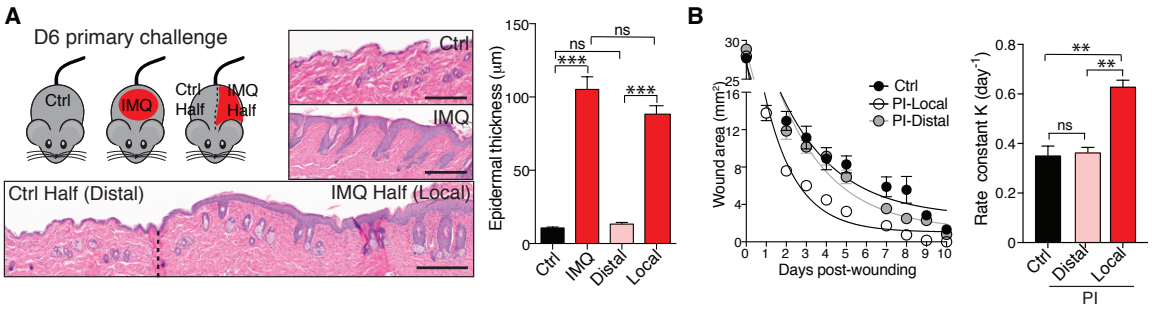

Figure 2.7: Accelerated wound healing occurs only at direct sites of prior inflammation. **A** Epidermal hyperthickening is confined to the initial site of inflammation (n=3, $\geq$3 images per animal). Scale bars, 200μm. $^{**}P$=0.0019,$^{***}P$=0.0009. **B** Wound closure at day 30 is enhanced only at sites of previous IMQ treatment (n=12). $^{***}P<0.0001$. Rate calculated from wound area in left plot. Data are mean $\pm$s.e.m. n denotes the number of biologically independent animals. Experiments replicated at least twice and significance was determined using a two-tailed t-test (95% confidence).

We next addressed whether the heightened responsiveness of inflammation-experienced EpSCs was secondarily dependent on the memory of resident innate and adaptive immune cell populations [64]. CD45^{+} cells including innate immune cells such as

Langerhans cells, dermal dendritic cells, macrophages, and eosinophils, and adaptive immune cells such as dendritic epidermal $\gamma\delta$ T cells (DETCs, $\gamma\delta$ T cell receptor (TCR)^{high}), returned to baseline levels 30 days after inflammation (Figure 2.8 A, B). While macrophages returned to basal levels in the skin post-inflammation, we wanted to rule out contribution of innate immune cell memory. To this end we used clodronate, which induces apoptosis after being taken up by phagocytic cells (CITATION) and effectively reduced skin-resident macrophage numbers by 90$\%$. We clodronate-depleted skin-resident macrophages before wounding and found no obvious effect in the wound repair advantage displayed by EpSCs after inflammation (Figure 2.8 C).

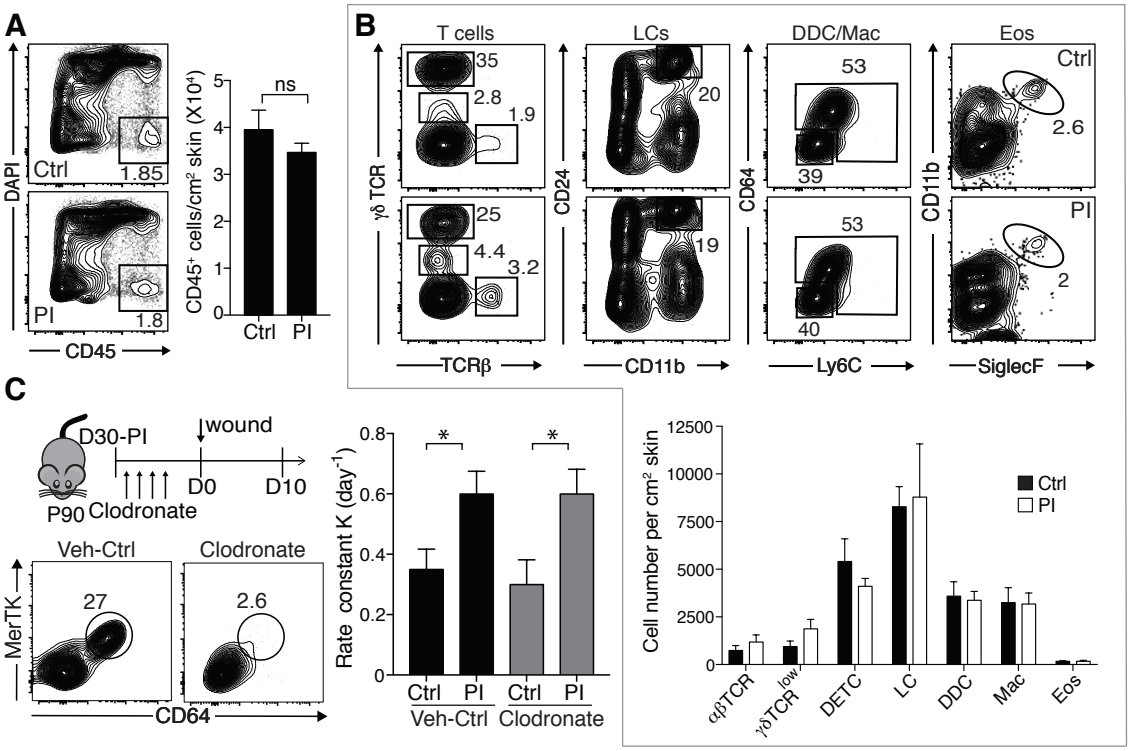

Figure 2.8: Immune cell populations return to baseline after inflammation.**A** Flow cytometric analysis and quantification of total immune cells (CD45⁺). **B** Flow cytometric analysis and quantification of $\alpha\beta$ T cell receptor (TCR) T cells, dermal $\gamma\delta$ T cells ($\gamma\delta$TCR^{low}), dendritic epidermal T cells (DETC; $\gamma\delta$TCR^{high}), Langerhans cells (LC), dermal dendritic cells (DDC), macrophages (Mac), and eosinophils (Eos) from control and day 30 post-inflamed skins (n$\geq$3). **C** Clodronate liposome-mediated resident macrophage depletion before wounding does not alter the wound repair advantage after inflammation (flow cytometry *n*=2; wound rate *n*$\geq$4). **P*=0.0419 (vehicle control; veh-ctrl), **P*=0.0266 (clodronate). Data are mean $\pm$s.e.m. *n* denotes the number of biologically independent animals. Experiments replicated at least twice and significance was determined using a two-tailed *t*-test (95$\%$ confidence).

Next, taking into consideration, that the initial IMQ response is triggered by a specific subset of immune cells, namely $\gamma\delta$ T lymphocytes that express the transcription factor (TF) retinoic acid receptor-related orphan receptor C (RORC), we assessed if there was a change in the frequency of this subset of immune cells in the skin (Figure 2.9 A) [25]. In contrast to innate immune cells and DETCs, which showed comparable representation in control and post-inflamed skin, RORC⁺ adaptive immune cells were increased in IMQ-treated skin both at the peak of inflammation (5.0 times) and after

resolution (1.8 times). In agreement with prior reports, these persistent RORC$^+$ cells were located in close proximity to the epidermis and hair follicles (Figure 2.9 B). To probe if these lingering RORC$^+$ cells were responsible for accelerated wound healing post-inflammation, we generated a *RorcCre;Rosa-iDTR* mouse model whereby RORC$^+$ cells were inducibly depleted after the initial inflammatory response, but prior to wounding. Delivery of diphtheria toxin (DT) resulted in $>90\%$ depletion of RORC$^+$ cells without a compensatory increase in other skin effector T cell populations. Consistent with involvement of tissue-resident T cells in wound and pathogen responses, depletion of RORC$^+$ cells in post-inflamed and control mice resulted in delayed wound closure relative to their wild-type counterparts [62] [65]. Importantly, however, even after RORC$^+$ depletion, inflammation-experience skin still exhibited a two-fold increase in wound closure rate compared to naive control skin (Figure 2.9 C).

To more rigorously establish that the heightened wound healing in inflammation-experienced skin went beyond adaptive immune cell changes, we investigated the phenomenon in *Rag2*-null mice, which still mount an inflammatory response to IMQ despite the absence of T and B cells (Figure 2.9 D). In *Rag2*-null mice, post-inflamed skin closed wounds significantly faster than naive skin. These results provide compelling evidence that the augmented tissue repair response exhibited by inflammation-experienced skin occurred independently of an enhanced T cell response (Figure 2.9 E).

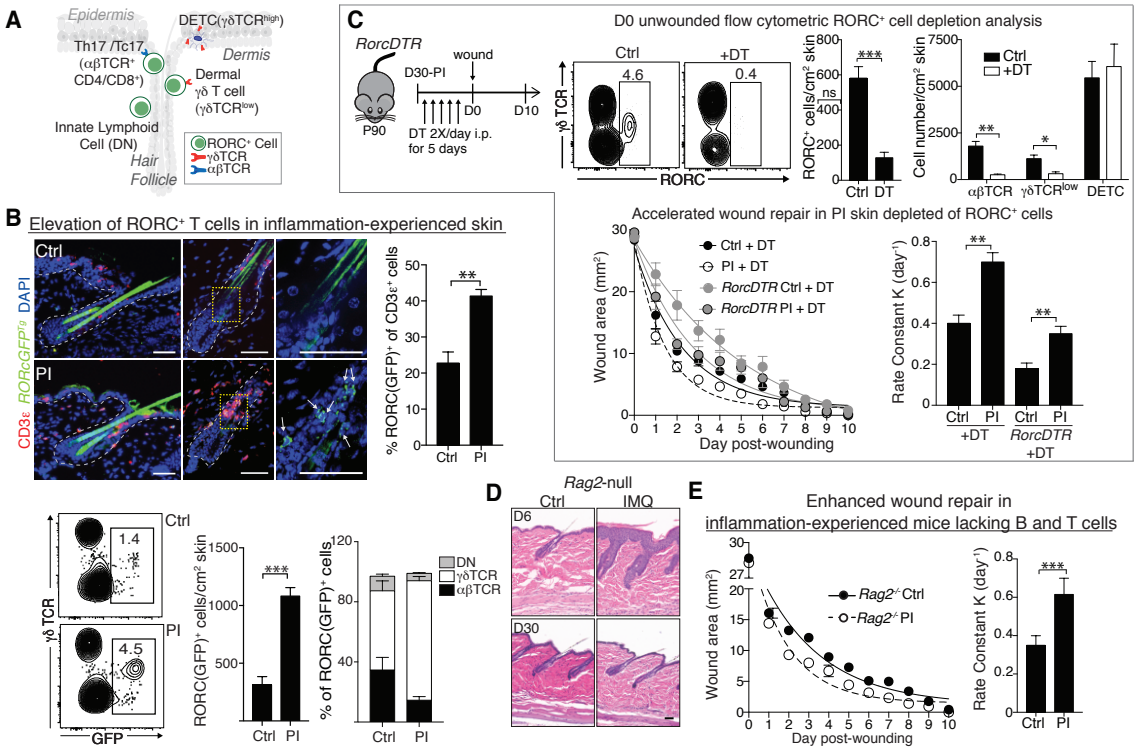

Figure 2.9: Resident RORC⁺ and T cells are dispensable for enhanced wound closure after inflammation. **A** DETC, dendritic epidermal $\gamma\delta$ T cells; RORC⁺ cell populations: dermal $\gamma\delta$ TCR^{low} T cells; DN, double negative ($\alpha\beta$ and $\gamma\delta$ TCR^{neg}); TC17, IL-17-producing cytotoxic T cells; TH17, IL-17-producing T helper cells. **B** RORC⁺ T cells (white arrows) are increased at day 30 post-inflammation ($n \geq 3$, 3 images per animal). Scale bars 50μm, $^{**}P$=0.0056. Experiments performed with *Rorc-eGFP* mice. Lines denote dermo-epidermal border, asterisk denotes autofluorescence, and yellow boxes denote magnified areas in the adjacent panels. **C** Wounds heal faster in post-inflamed skin despite the ablation of skin RORC+ (flow cytometry, n=4, $^{***}P$=0.0008). Schematic of RORC⁺ T cell depletion and wound repair using *Rosa-LSL-iDTR* (control) and *Rorc-cre;Rosa-LSL-iDTR* (*Rorc-DTR*) mice, which activate the diptheria toxin receptor (DTR) from the *Rosa26* locus only in RORC⁺ cells, enabling their selective ablation (n=5; $^{**}P$=0.005 (control), $^{**}P$=0.0053 (*RORc-DTR*)).**D,E** *Rag2*-null mice mount an IMQ response (n=3, 3 images per animal) and display accelerated wound healing 30 days after inflammation. Scale bars 50μm, n=5, $^{*}P$=0.0136. Data are mean $\pm$s.e.m. n denotes the number of biologically independent animals. Experiments replicated at least twice and significance was determined using a two-tailed t-test (95% confidence).

2.2.5 EpSC memory at the chromatin level

A memory of prior exposure to inflammatory stimuli has long been thought to be a property unique to immune cells. We posited that the heightened responsiveness to tissue damage observed in inflammation-experienced EpSCs may involve inflammation-induced changes in chromatin dynamics analogous to those recently described for innate immune memory in macrophages and natural killer cells [66] [67]. To explore this possibility, we purified epidermal EpSCs from IMQ-treated skin at the peak of inflammation (day 6) and after their return homeostasis (days 30 and 180). We next employed Assay for Transposase Accessible Chromatin with high-throughput sequencing (ATAC-seq) [68]. Agnostic to specific types of epigenetic modfications, this strategy enables global identification of accessible chromatin states.

To purify epidermal EpSCs, we devised a stringent purification strategy based upon the unique combination of surface markers Sca-1 and integrins α6 and β1, expressed by both post-inflamed and naive EpSCs (Figure 2.10 A). We then employed fluorescent activated cell sorting (FACS) to purify EpSCs, while excluding CD45 (immune), CD117 (melanocytes), CD140a (fibroblasts), and CD31 (endothelial) skin cells (Figure 2.10 B). Quantitative PCR (qPCR) confirmed the purity of our EpSCs (Figure 2.10 C).

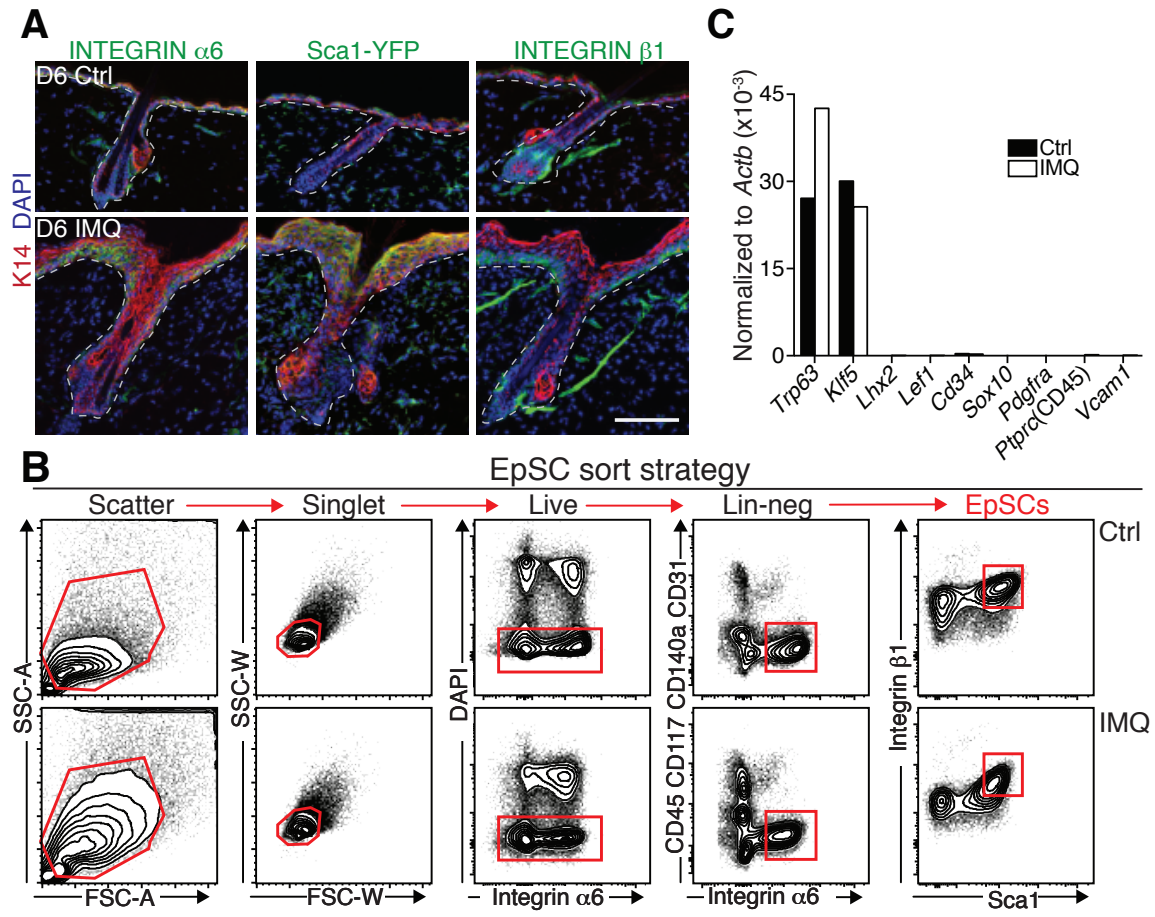

Figure 2.10: Isolation of a purified population of Epidermal EpSCs from inflamed and naive skin. **A** Immunofluorescence analysis of basal EpSC-specific markers in inflamed and control skin. Scale bar, 100 μm. **B** FACS strategy for isolation of EpSCs (integrin $\alpha6^{+}\beta1^{+}$Sca1^{+}), with exclusion of CD45^{+}, CD31^{+}, CD117^{+}, and CD140a^{+} non-epidermal cells, as well as dead (DAPI^{+}), doublets (side-scatter width (SSC-W^{high}) and forward-scatter width (FSC-W^{+})). **C** qPCR validation of EpSC purity. *Trp63* and *Klf5* are specific for EpSCs; the others are not expressed by EpSCs (n=3 mice pooled per group). *n* denotes the number of biologically independent animals.

ATAC-Seq was next performed in duplicate on EpSCs at D6 (peak), D30, and D180 post-inflammation. Independent biological replicates showed strong correlation (R2$\geq$0.97). As expected, ATAC signals were enriched at transcription start sites (TSS) and binding sites for distal regulatory element CCCTC-binding factor (CTCF) sites, and were similarly distributed over various genomic and intergenic regions in all samples (Figure 2.11 A, B). EpSC-specific genes such as *Klf5* and *Krt14* demon-

strated similar chromatin accessibility patterns (Figure 2.11 C).

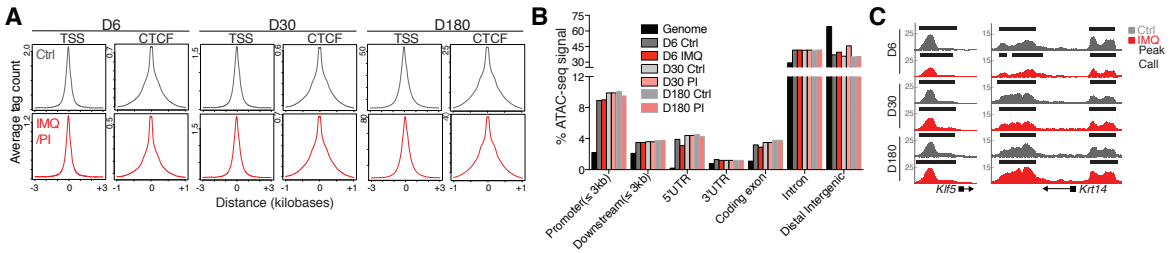

Figure 2.11: ATAC-Seq quality control in EpSCs. **A** Density plots depicting enrichment of ATAC-seq signals at TSSs $\pm$ 3kb and arount CTCF factor-binding sites. The x axis depicts respective distance $\pm$ 1kb from each of these domains. **B** Distribution of ATAC-seq peaks with defined genomic regions. UTR, untranslted regions of predicted mRNAs. **C** Genomic browser shots of peaks enriched in EpSC-specific genes *Klf5* and *Krt14* and unaffected by IMQ. Arrows denote direction of transcription.

By contrast, striking differences were seen between D6 IMQ-treated and control EpSCs. A total of 44,414 unique peaks (31% of total) were identified at the peak of inflammation [69] (Figure 2.12 A). These open chromatin regions associated with ontologies that typify inflammatory crosstalk in skin disease and inflammation: JAK-STAT, LPS-mediated, and EGFR signaling. Associated genes were enriched ($P10^{-12}$) in motifs for key epidermal transcription factors (such as AP-1 (Jun, Fos and ATF members), AP2γ, KLF5, ETS2, GRHL2/3 and p63), as well as factors such as NF-κB and STAT1/3, the activation of which as been associated with inflammation [70].

By day 30 after IMQ exposure, many peaks had resolved. Notably, however, more than 2,000 IMQ-induced peaks were maintained, suggestive of an inflammatory memory (Figure 2.12 B). Some peaks were even present at day 180, long after inflammation has resolved (Figure 2.12 A, B). PANTHER pathway analysis of their associated genes revealed enrichment for inflammation- and hyperproliferation-associated pathways including apoptosis signaling, interleukin signaling, oxidative stress response, RAS, and PI3 kinase pathways (Figure 2.12 C). Strikingly, these genomic regions also showed a strong enrichment for stress-associated TF binding motifs ATF3, AP-1, NRF2, P63, ETS2, CEBPB, ELK3, KLF5, and STAT3. STAT3 was

notable as it is known to be phosphorylated and activated after IMQ treatment [25]. Although, it was re-activated in the secondary response, STAT3 activity was not maintained during the interim (Figure 2.12 D). Thus, remarkably, many of the IMQ-induced changes to the EpSC chromosomal landscape were maintained long after resolution of the initial inflammatory assault and restoration of epidermal homeostasis.

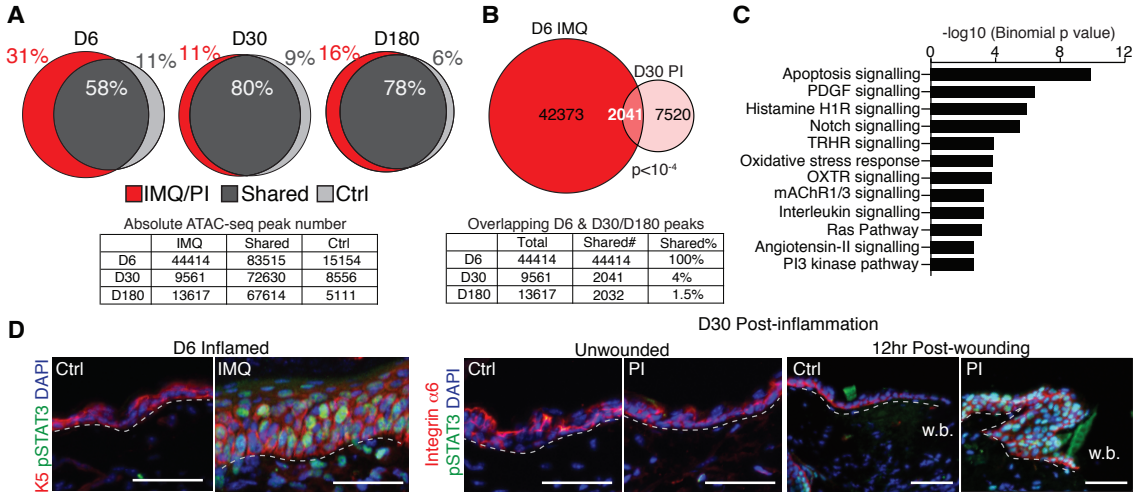

Figure 2.12: EpSCs possess memory of inflammation at the chromatin level. **A** Venn diagrams of ATAC-seq signals of day 6 inflamed and day 30/ 180 post-inflamed versus age-matched naive EpSCs (*n*=3 pooled mice per group, in duplicate). Table depicts absolute numbers of ATAC-seq peaks. Peak percentages are indicated on diagrams. **B** Venn diagram of ATAC-seq peaks (numbers indicated) unique to day 6 IMQ and day 30 post-IMQ EpSCs (random permutation, P¡10^{-4}). Table depicts numbers and frequencies of ATAC-seq peaks that are shared in day 6 inflamed and either day 30 or day 180 post-inflamed EpSCs. **C** PANTHER pathways analysis of 2,041 shared, inflammation-induced peaks between day 6 IMQ and day 30 post-IMQ EpSCs. **D** Epidermal STAT3 activation (pSTAT3(Tyr705)) in day 6 inflamed and day 30 post-inflamed skin 12 hours after wounding, but not in day 30 post-inflamed unwounded skin (*n*=3). *n* denotes the number of biologically independent animals. Experiments replicated at least twice.

2.2.6 Inflammation-sensing chromatin elements

Our data thus far suggests a model, whereby inflammation-activated transcription factors and other chromatin modifiers facilitate the initial opening of certain chromatin domains. Both epidermal transcription factors and chromatin modifiers present in

both inflammatory/stress and/or post-inflamed homeostatic conditions can then bind maintaining these regions accessible. The model further predicts these accessible domains retained after resolution of inflammation would serve as accessible platforms for accelerated re-activation upon a secondary assault (Figure 2.13 A).

Two important facets of this model were tested in this initial publication, and remaining aspects are works in progress. First, we interrogated the ability of the retained post-inflamed chromatin peaks to function as inflammation-sensing elements. To this end, we cloned individual peaks sustained post-inflammation (associated with *Cotl1, Armc6, Aoah,Aim2*) from genomic DNA isolated from inflammation-experienced EpSCs. The peaks were then cloned into a pLKO vector just before a minimal sv40 promoter followed by the *eGFP* transgene. The construct also included an internal reporter *Pgk-H2B-RFP*. This vector was then packaged into a lentivirus (LV), and transfected into 293T cells to produce high titer LV. Using the Fuchs lab well-established *in utero* LV delivery system, high titer LV was injected into the amniotic sac of developing embryos at E9.5, when the developing epidermis is one single cell layer (Figure 2.13 B). LV stably transduces only the first cell layer it encounters ensuring that only epidermal progenitors and their progeny would be infected (Figure 2.13 C). Viral positive cells would stably express *H2B-RFP*, but *eGFP* would only be detectable if the peaks cloned into the vector were capable of driving gene expression.

Mice were aged to P21, where *H2B-RFP* was detected uniquely throughout the epidermis indicating efficient viral transduction of the skin epithelium. *eGFP* was not activated until IMQ was administered, underscoring the potential of the post-inflamed unique chromatin domains to drive gene expression and to act as sensors of tissue damage (Figure 2.13 D).

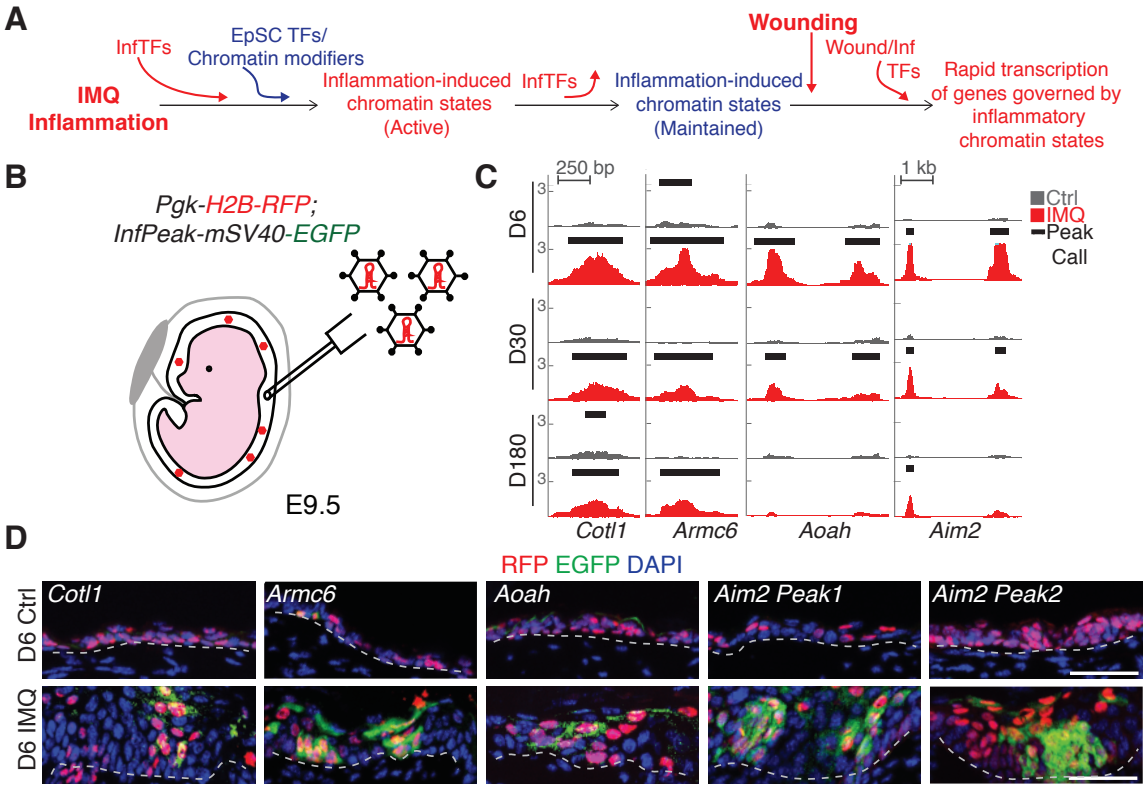

Figure 2.13: EpSC memory encodes inflammatory sensors. **A** Model of EpSC inflammatory memory. InfTFs, inflammation-induced transcription factors. **B** Schematic of *in utero* lentiviral transduction of skin epithelium. *Pgk-H2B-RFP* expression marks transduced EpSCs. **C** Snapshot of genomic loci in which the chromatin-accessible peaks are opened by inflammation at day 6 and persist up to 180 days after resolution. **D** Persisting accessible chromatin domains induced by inflammation can drive inflammation-specific eGFP reporter activity in EpSCs *in vivo* (n=2). Lines denote the dermo-epidermal border. Scale bars, 50μm. Experiments replicated at least twice.

Next, we hypothesized if persisting inflammation-induced open chromatin domains are physiologically relevant to the functional EpSC memory, then they should participate in the accelerated wound-repair response that we observed in inflammation-experienced mice. To test this possibility, we wounded the skin of day 30 post-inflamed mice, and 12 hours later we evaluated the transcriptional response of EpSCs within an approximately 0.5 mm$^+$ radius of the wound edge (Figure 2.14 A). In parallel, we performed RNA-Seq on epidermal EpSCs from control and IMQ-treated skin at the peak (D6) and post (D30) inflammation (Figure 2.14 B). Consistent with epidermal

pathology at the peak of inflammation, EpSCs isolated from D6 IMQ skin displayed notable changes in the transcriptome relative to their control counterparts. Changes correlated well with genes featuring newly acquired ATAC-seq peaks with 91% of differentially expressed genes being associated with newly acquired ATAC-peaks (Figure 2.14 C). While only a few of these genes were still transcribed at day 30 (false discovery rate (FDR)¡0.5), this picture rapidly changed upon wounding. Of the 140 genes differentially upregulated in post-inflamed wound-edge EpSCs 12 hours following injury, 73 (52%) were associated with ATAC-seq peaks that were acquired during and sustained after IMQ treatment (FDR0.05) (Figure 2.14 D). Given that wound re-epithelialization did not peak until day 5 after wounding, this early activation of genes associated with inflammation-experienced chromatin accessible regions was notable.

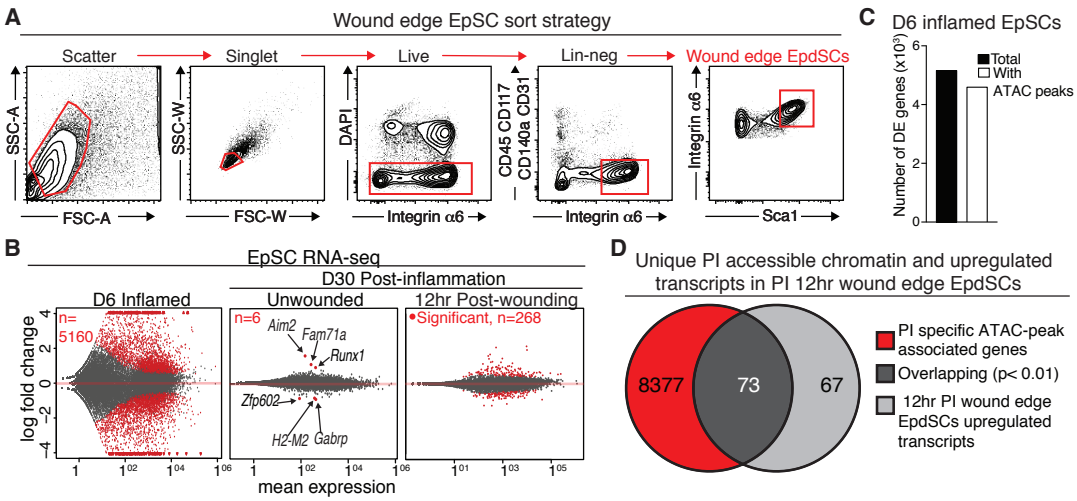

Figure 2.14: Inflammation-induced accessible chromatin rapidly induce transcription of associated genes upon secondary assault. **A** FACS strategy of wound-edge EpSC purity from skin that was treated with either IMQ or vehicle and then allowed to return to homeostasis before wounding at day 30 (*n*=3 pooled mice per group). **B** Differences between transcriptomes of day 6 inflamed or day 30 post-inflamed EpSCs with or without wounding, relative to respective control EpSCs. Shown are MA plot (log ratio versus mean averafe); the numbers of significant differentially expressed transcripts (FDR ¡0.05)are stated and depicted by red dots (*n*=4 pooled mice per group, in duplicate). **C** Matched ATAC-seq and RNA-seq analysis reveals that 91% of differentially expressed genes in day 6 inflamed versus control EpScs are associated with newly acquired ATAC-Seq peaks. **D** Of the 140 transcripts upregulated rapidly after wounding of post-inflamed versus control skin (grey), 73 (dark grey) were encoded by genes (red) associated with chromatin accessible domains that were unique to post-inflamed EpSCs (random permutation, P¡10^{-4}). Experiments replicated at least twice.

2.2.7 Downstream effectors of EpSC memory

To understand how these 'inflammatory memory' chromatin elements might confer a wound repair advantage, we first performed pathway analysis of the rapid-response transcripts (adjusted *P*0.05) of the genes that contain these chromatin domains. One of the top most enriched pathways was 'inflammasome signaling' (Figure 2.15 A). This pathway included *AIM2*, which has previously been implicated in skin disease and cancer, as well as other downstream components of the AIM2 inflammasome including *Casp1* and *Il18*. Notably in EpSCs, both *Aim2* and *Il18* loci exhibited

inflammation-induced chromatin accessibility, which was sustained long-term. *Aim2* was of particular intrigue because it was one of three genes differentially upregulated in EpSCs at days 30 and 180 after inflammation, as well as after wounding (Figure 2.15 B). Furthermore, *Aim2* upregulation was sustained in inflammation-experienced skin depleted of its RORC population reaffirming that the EpSC memory response did not rely on RORC^{+} cells (Figure 2.15 C).

To test the role of AIM2 in inflammatory memory, we performed loss- and gain-of-function studies. For loss of function studies, we used *Aim2*-null mice, which mounted a full inflammatory response to IMQ. However, post-inflamed *Aim2*-null mice failed to show a wound healing advantage (Figure 2.15 D). To determine if upregulated *Aim2* gene expression was sufficient to endow mice with accelerated tissue repair, we engineered and tested mice whose skin epithelium contained a lentiviral-transduced doxycycline-inducible *Aim2* cDNA (*TRE-Aim2*) (Figure 2.15 E). In the absence of IMQ preconditioning, increased expression of *Aim2* was sufficient to enhance wound repair (Figure 2.15 F). All together, these experiments revealed AIM2 as a key mediator in endowing inflammation-experienced EpSCs with their heightened sensitivity to a secondary assault.

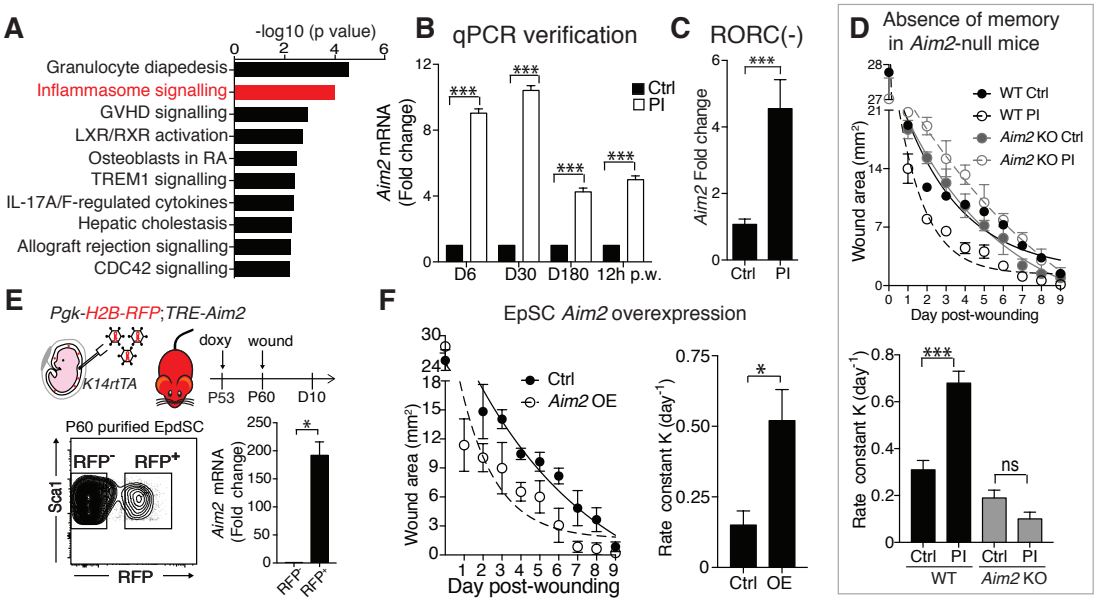

Figure 2.15: AIM2 is necessary and sufficient for post-inflamed wound healing advantage. **A** Ingenuity pathways analysis of upregulated transcripts in post-inflamed 12h wound-edge EpSCs relative to control cells (n=4 P¡10^{-4}). **B** Increased *Aim2* transcription associated with inflammation, memory, and rapid wound response in post-inflamed skin, post-wounding (PW) (n2, two-tailed t-test, day 6 and 12h post-wounding, ***P¡0.0001; day 180, ***P=0.0001). **C** Sustained *Aim2* transcription at D30 post-inflammation in mice depleted of RORC^{+} cells, n=3. **D** *Aim2*-null mice do not show enhanced wound healing after inflammation (n2, two-tailed textitt-test, ***P=0.0002). KO, knockout. **E** Schematic and qPCR validation of overexpression (OE) of epithelial *Aim2*. **F** OE of *Aim2* is sufficient to augment wound healing in naive mice (n=2). Data are mean ± s.e.m. Rate calculated from wound area. TRE, tetracycline response element. n denotes the number of biologically independent animals. Experiments replicated at least twice.

After confirming AIM2's importance to post-inflamed accelerated wound healing, we sought to determine if the effect was due to AIM2's canonical role in the inflammasome pathway or as recent reports indicate its suppression of stem cell proliferation. In the intestine, AIM2 suppresses stem-cell proliferation in indirectly inhibiting phosphorylated AKT(Ser473). However, in the epidermis, post-inflamed wounds had higher levels of pAKT (Ser473) and equal numbers of proliferating EpSCs to control wounds (Figure 2.16 A). Taken together, we decided to focus on AIM2's role in the inflammasome pathway that is triggered after infection or tissue damage.

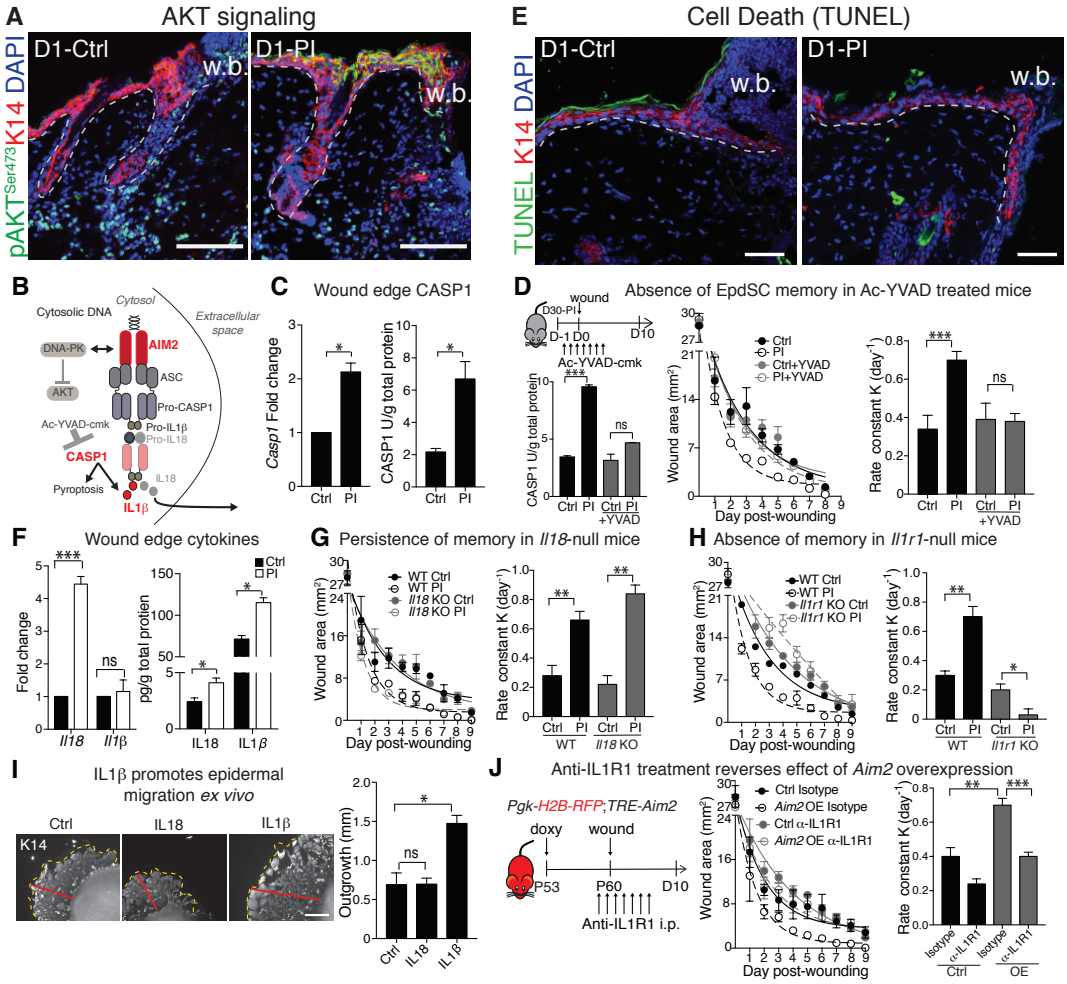

Figure 2.16: CASP1 and IL-1β downstream of the AIM2 inflammasome enhance wound re-epithelialization in inflammation-experienced skin. **A** pAKT^{S473} expression in D1 wounds in PI and naive skin, scale bars (sb) = 100μm. **B** Diagram of AIM2 and its downstream effectors. **(**C) TUNEL labeling of D1 wounds in PI and naive skin, sb = 50μm. **D** Elevated levels of *Casp1* transcript (***P*=0.0025) and CASP1 activity (***P*=0.0014) in PI skin 12hr after wounding, *n*=3. **D** Schematic depicts experimental design. Ac-YVAD-cmk reduced CASP1 activity and re-epithelialization rates of wounded, PI skin to naive, vehicle control levels (***P*=0.0018). **E** Increased levels of *Il18* transcipts (***P*=0.0014) and also IL-18 (**P*=0.0202) and IL-1β (***P*=0.0073) protein in PI skin post-wounding, *n*=3. **F** Loss of *Il18* does not effect the injury response of PI skin, *n*=3 (WT, **P*=0.0146; KO, ***P*=0.0019). G Loss of *Il1r1* abrogates the enhanced injury response of PI skin *n*=4 (WT, **P*=0.0155; KO, *P*=0.0086). *H* IL-1β, but not IL-18 (50 ng/ml ea), accelerated outgrowth of Krt14$^+$ keratinocytes in D5 *ex vivo* explants. Dotted lines mark borders of outgrowths; red lines denote migration distance, *n*=3; 3 technical reps per mouse (**P*=0.00128). Quantification at right, sb 500 μm. **I** Anti-IL1R1 treatment reverses the wound repair advantage conferred by epidermal *Aim2* overexpression in naive mice, *n*=4 (IgG, ***P*=0.0055, anti-IL1R1 ****P*=0.0007). All plots represent mean $\pm$ s.e.m. All experiments, except H, repeated at least 2X. Significance: two-tailed *t*-test (95% confidence).

AIM2 is a cytosolic double-stranded (ds) DNA sensor. When AIM2's HIN domain binds dsDNA, the inflammasome complex is oligomerized and a complex member protein, ASC, subsequently recruits procaspase-1 to the complex resulting in autoactivation of caspase-1 (CASP1) (Figure 2.16 B). CASP1 is a central downstream effector of AIM2, and both its transcription and enzymatic activity were rapidly initiated within 12 hours after injury in post-inflamed skin relative to naive controls (Figure 2.16 C). Moreover when the ability of CASP1 to process the pro-forms of cytokines IL-1β and IL-18 was blocked by the inhibitor AC-YVAD-cmk, rates of wound healing were reduced to naive levels in inflammation-experienced skin, while remaining unaffected in naive control skin (Figure 2.16 D). This loss of the inflammation-induced wound healing advantage was not attributable to CASP-1 dependent pyroptosis, as both control and post-inflamed wound edge EpSCs exhibited minimal and equal levels of cell death (Figure 2.16 E).

After determining that CASP1 was also a downstream effector of inflammatory memory, we decided to work further down the pathway and assess the contribution of pro-inflammatory cytokines IL-18 and IL-1β. Indeed, post-inflamed skin displayed increased *Il18* transcription and levels of IL-18 and IL-1β proteins compared to naive skin (Figure 2.16 F). To determine whether AIM2 acts through cytokine production to accelerate wound repair, we repeated our experiments with *Il18* and *Il1r1*-null mice. We found that while IL-18 was dispensable, without IL-1R1, which is required for IL-1β signaling, inflammation-experienced skin failed to enhance wound repair (Figure 2.16 G, H). To further confirm these results, we returned to the *ex vivo* wound healing model of the explant migrant assay, whereby we added recombinant cytokine to control explants and assess outgrowth. Consistent with our *in vivo* findings, the addition of recombinant IL-1β, but not IL-18, enhanced the migration of keratinocytes from naive skin explants (Figure 2.16 I). We next hypothesized that if AIM2-mediated IL-1β secretion was responsible for acclerated re-epithelialization of post-inflamed wounds,

then blocking IL-1β signaling should counteract inducing overexpression of *Aim2*. To this end, we injected IL-1R1-blocking antibodies into doxycycline-treated *TRE-Aim2* mice, and observed the rate of wound closure was comparable to that of untreated naive control mice (Figure 2.16 J). Taken together, these data point to AIM2 and its downstream effectors CASP1 and IL-1β as central regulators of the heightened wound-repair response observed in inflammation-experienced skin.

2.2.8 Chromatin rearrangements in the absence of AIM2

Genetic ablation of AIM2 resulted in loss of the post-inflamed accelerated wound-healing phenotype. However, it remained to be determined whether loss of augmented tissue repair was a failure of *Aim2* null mice to remodel their chromatin to establish memory or if upregulation of AIM2 following inflammation was necessary for rapid release of pro-wound healing cytokines such as IL-1β. First to address this question, I confirmed that AIM2KO mice elicited an IMQ inflammatory response that paralleled WT mice. Second, I performed ATAC-Seq on *Aim2* null (AIM2KO) mice at the peak of inflammation and after resolution to address what may have accounted for the loss of the post-inflamed wound healing advantage.

In the absence of *Aim2*, mice were capable of mounting a full inflammatory response with infiltration of CD45$^+$ immune cells and CD3ϵ^+ T cells (Figure 2.17 A). EpSCs responded to the immune cell infiltrate and resulting proinflammatory cytokine storm by ramping up proliferation as indicated by EdU incorpation after a 1 hour pulse (Figure 2.17 B). The basal proliferation rate of EpSCs in both WT and AIM2KO shifted from approximately 5$\%$ EdU incorporation within the hour to greater than 40$\%$. As a result, there was severe epidermal hyperthickening and hyperdifferentiation in both WT and KO inflammatory responses (Figure 2.17 C). Importantly, mice were able to resolve this inflammation in the absence of *Aim2* indicated by a return to basal proliferation rates, homeostatic epidermal thickness, and recession of the immune infiltrate

(Figure 2.17 A-C).

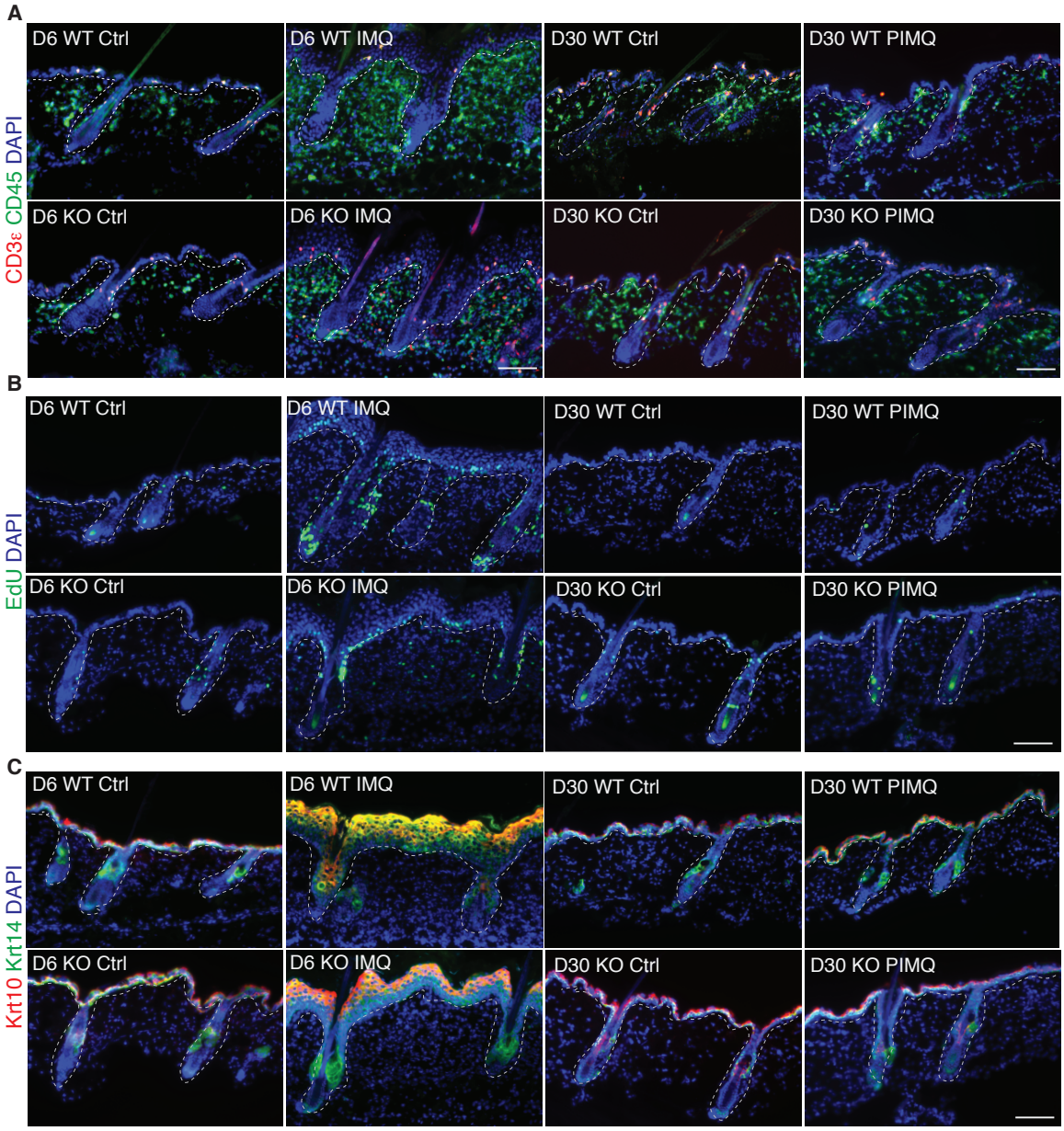

Figure 2.17: AIM2KO mice mount a robust inflammatory response that resolves 30 days later. **A** Immunoflourescence of $CD45^{+}$ immune cells and $CD3\epsilon^{+}$ T cells in WT and AIM2KO mice peak and post inflammation. **B** Immunofluorescence of EdU incorporation after a 1 hour pulse in WT and AIM2KO mice peak and post inflammation. **C** Immunofluorescence of Keratin 10 (Krt10, marker of differentiated keratinocytes) and Keratin 14 (Krt14, marker of basal keratinocytes) in WT and AIM2KO mice peak and post inflammation. Scale bars = 100μm.

As described previously, epithelial stem cells were purified from tissue at the peak

of inflammation and after resolution. Two independent biological replicates were performed for each AIM2KO condition and sequenced on the Illumina HiSeq2500 platform for comparison to the previously acquired WT ATAC-seq data set. All replicates with the exception of the D30 AIM2KO Ctrl, where Replicate 2 had a low read count, were highly correlated with R^2 values 0.81 (Figure 2.18 A). AIM2KO ATAC-signals were similarly distributed over various genomic and intergenic regions for all conditions. Additionally, there was no difference in ATAC-signal distribution between WT and AIM2KO samples (Figure 2.18 B).

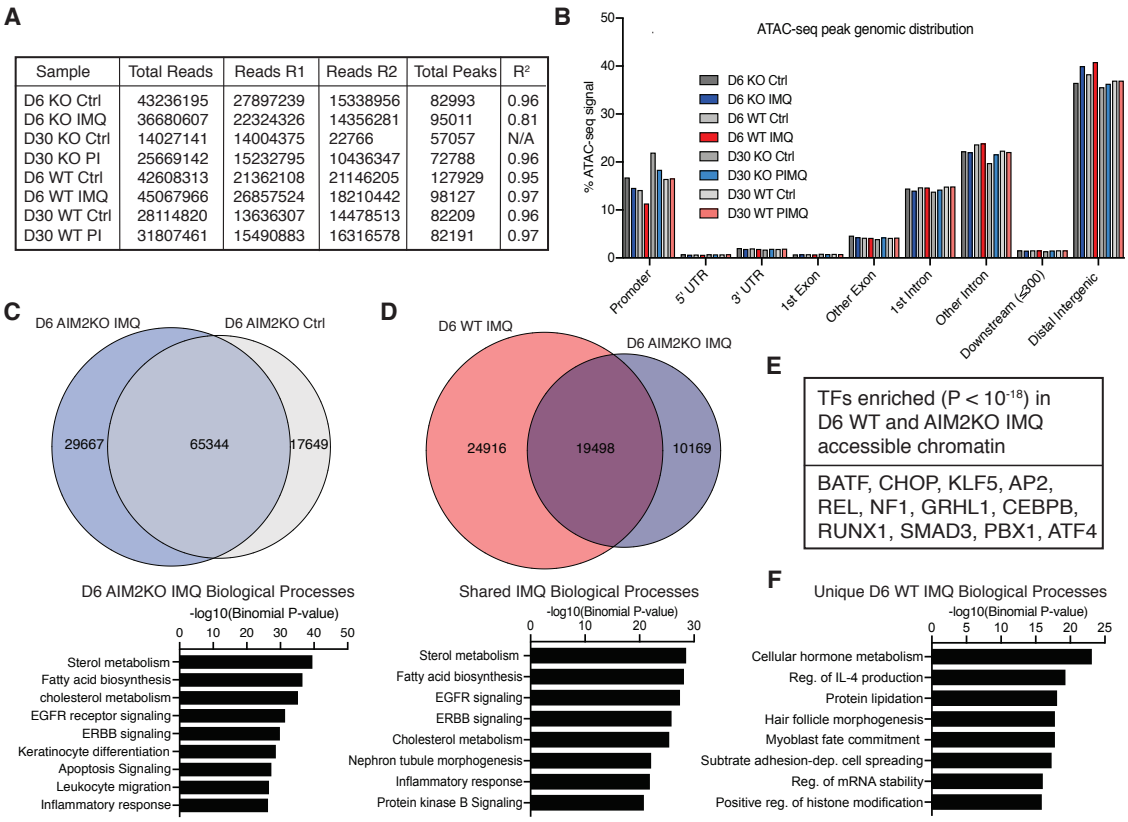

Sample	Total Reads	Reads R1	Reads R2	Total Peaks	R^2
D6 KO Ctrl	43236195	27897239	15338956	82993	0.96
D6 KO IMQ	36680607	22324326	14356281	95011	0.81
D30 KO Ctrl	14027141	14004375	22766	57057	N/A
D30 KO PI	25669142	15232795	10436347	72788	0.96
D6 WT Ctrl	42608313	21362108	21146205	127929	0.95
D6 WT IMQ	45067966	26857524	18210442	98127	0.97
D30 WT Ctrl	28114820	13636307	14478513	82209	0.96
D30 WT PI	31807461	15490883	16316578	82191	0.97

Figure 2.18: Chromatin remodeling occurs in the absence of AIM2. **A** Table depicts total reads, reads per replicate (R), peaks called, and replicate correlation coefficients for WT and AIM2KO ATAC-Seq (*n*= 3 pooled mice per group). **B** Distribution of ATAC-seq peaks within defined genomic regions. UTR, untranslated regions of predicted mRNAs. **C** Venn diagram depicting the intersect between D6 AIM2KO IMQ ATAC peaks and D6 AIM2KO Ctrl peaks. Plot below is top 8 GO Biological Processes enriched for 29667 D6 AIM2KO IMQ unique chromatin domains. **D** Venn diagram of overlap between WT and AIM2KO unique IMQ ATAC peaks. Plot below depicts top 8 GO Biological Processes enriched for 19498 shared peaks. **E** Transcription factor (TF) motif enrichment within shared WT and AIM2KO D6 IMQ peaks. **F** Top 8 GO Biological Processes enriched in ATAC peaks unique to the WT IMQ response. *n* denotes the number of biologically independent animals. Experiments replicated at least twice.

As in WT EpSCs, there was an appreciable difference in chromatin accessibility patterns between D6 IMQ EpSCs and control EpSCs. There was an increase in accessibility at the peak of inflammation with a total of 29,667 (31% of total) unique regions emerging (Figure 2.18 C). These unique chromatin domains were associated with pathways involved in cholesterol and fatty acid metabolism, the inflamma-

tory response, apoptotic signaling among others. To address whether the loss of *Aim2* impacted the inflammatory response at the chromatin level, I compared the AIM2KO data to the WT data. While there were more peaks called in D6 IMQ WT EpSCs (44,414), this still represented 31% of the total peaks called; the same ratio as for AIM2KO. Of the unique WT and AIM2KO IMQ chromatin regions, 19,498 were common between the two samples (Figure 2.18 D). Shared chromatin domains corresponded to biological processes such as cholesterol metabolism, EGFR signaling, and the inflammatory response. Additionally, these domains were enriched for transcription factors both associated with inflammation and EpSC homeostasis including BATF, KLF5, AP2, CEBPB, RUNX1, and ATF4 among others (Figure 2.18 E). To determine what was unique to the WT response, we assessed the 24916 unique chromatin regions and determined that the domains were associated unique processes such as cellular hormone metabolism, IL-4 production, protein lipidation, and positive regulation of histone modification among others (Figure 2.18 F). It remains to be determined if these differences at the peak of the inflammatory response are responsible for the loss of accelerated wound healing post inflammation.

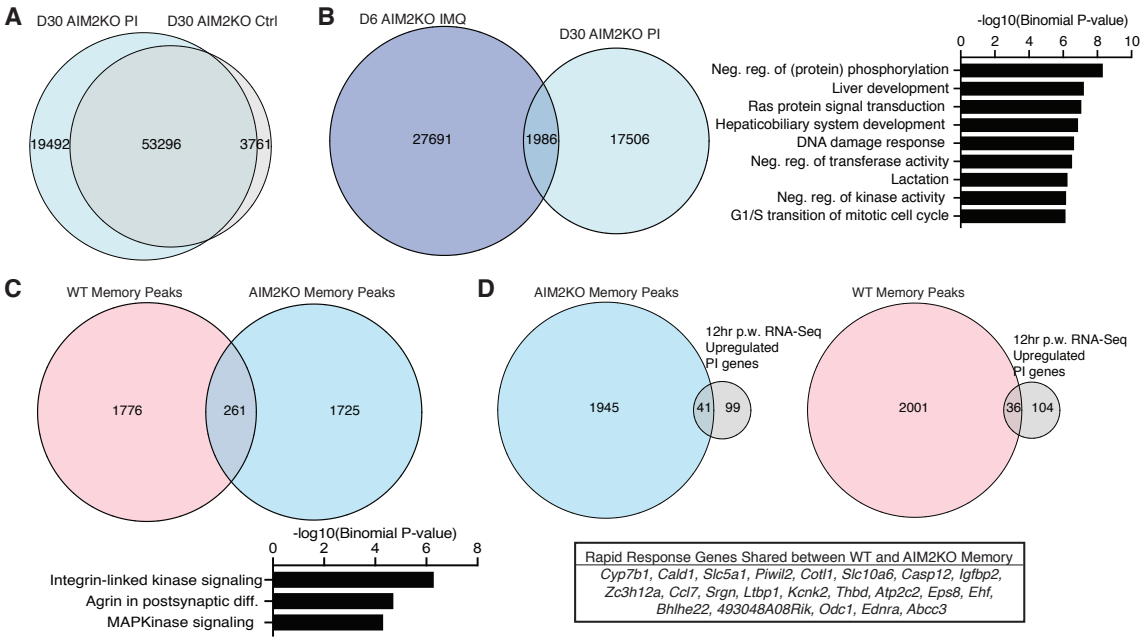

Figure 2.19: Chromatin rearrangements retained post-inflammation in absence of AIM2. **A** Venn diagram depicting overlap between D30 PIMQ AIM2KO and control ATAC peaks. **B** Venn diagram depicting chromatin accessibility gained at the peak of the AIM2KO inflammatory response and retained at D30. Adjacent plot of top 8 GO Biological Processes for AIM2KO memory domains. **C** Comparison between WT and AIM2KO memory domains. Significant GO Biological Processes indicated below. **D** Venn diagrams of intersect between AIM2KO (left) and WT (right) memory domains with 12 hour rapidly upregulated genes post-wounding. Table below of 22 common rapid response genes with a memory ATAC peak between WT and AIM2KO.

After establishing that inflammation-induced chromatin rearrangements occurred at the peak of inflammation in the absence of *Aim2*, I next wanted to determine if these changes were retained after resolution of inflammation. At D30, there were 19,492 (26% of total) unique peaks compared to control (Figure 2.19 A). This difference was larger than what was observed for WT (9,561 peaks). However, when I looked specifically at the memory domains or chromatin regions that became accessible at the peak of inflammation and then retained an open state after resolution, there were 1,986 regions (Figure 2.19 B). These AIM2KO memory domains were associated with distinct pathways from the WT such as negative regulation of protein phosphorylation, Ras protein signaling, DNA damage response, and negative reg-

ulation of transferase activity. These difference in pathways was supported by the small degree of overlap (261 chromatin regions) between the two sets of memory domains (Figure 2.19 C). Next, I wanted to determine if AIM2KO memory domains were associated with the previously identified 140 rapid response post-inflamed genes 12 hours after wounding. 29% (41) of the rapid response genes did have an associated AIM2KO memory domain. 22 of these 41 were shared with the wild type response (Figure 2.19 D). It remains to be determined whether the loss of the post-inflamed wound healing advantage in AIKM2KO mice is due to the identified differences in the memory domains, rapid response genes, or that upregulation and maintenance of AIM2 in the interim is required for rapid release of IL-1B.

2.2.9 Inflammatory memory can be maladaptive

Thus far, we have demonstrated that inflammatory memory is largely an adaptive mechanism adopted by stem cells to cope with and better prepare for inflammatory stress. We determined that retained chromatin accessibility at key inflammatory response pathways enabled accelerated tissue repair in post-inflamed mice. While this accelerated wound healing is largely beneficial, we wanted to understand whether inflammatory memory's advantage is context specific. We therefore addressed if in a tumor susceptible environment, these same pathways would potentially augment tumorigenesis.

To address this problem, we implemented the two-step skin carcinogenesis model [71]. Briefly, a subcarcinogenic dose of the carcinogen, 7,12-Dimethylbenz(a)anthracene (DMBA), was applied topically to the back skin of both post-inflamed and inflammation-naive mice. DMBA is a mutagen causing EpSCs and keratinocytes to acquire mutations. A primary target of DMBA is *Hras1*, which acquires activating mutations predominantly an A to T (182) transversion [72]. DMBA treatment serves as the tumor initiation step. Mice are then subsequently treated with a tumor-promoting agent, 12-

O-Tetradecanoylphorbol-13-acetate (TPA), which promotes clonal expansion of mutated EpSCs via increasing proliferation and inducing epidermal hyperplasia. It is thought that initiated cells have a growth advantage over their neighbors resulting in their selective expansion leading ultimately to tumor development [73]. The two-step skin carcinogenesis model results in papillomas that have the potential to progress to full blown squamous cell carcinomas.

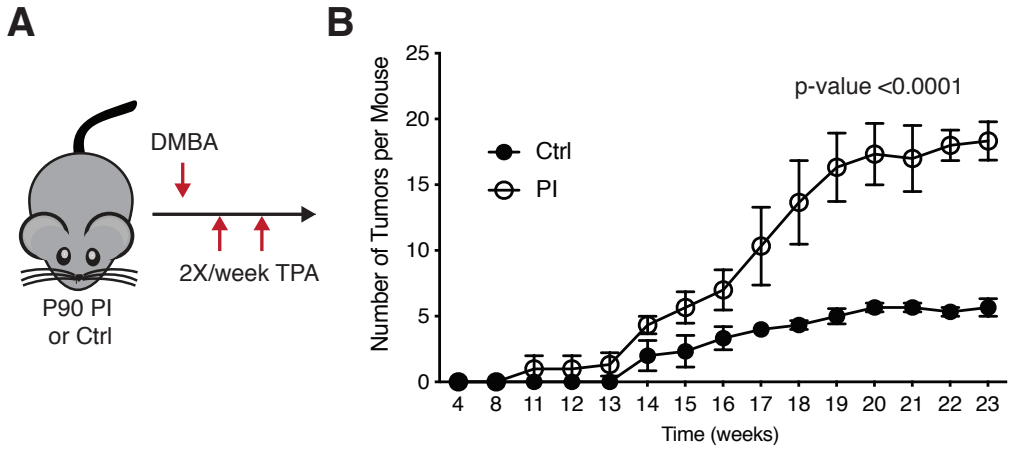

Figure 2.20: Post-inflamed mice are more susceptible to two-step carcinogenesis. **A** Schematic of DMBA-TPA model of skin carcinogenesis. **B** Plot depicts the number of tumors (papillomas) per mouse over time. *n*=3. *P*-value0.0001. Experiment included three mice per group. Statistical analysis for B performed with an ANOVA. GPower software used to determine that N=3 in each group with an observed effect size of 6.467 and a significance level set at 0.05 achieved 0.9998517 power.

After resolution of inflammation (D30), post-inflamed mice and inflammation-naive mice were topically treated with DMBA. One week after tumor initiation, mice were treated two times per week with topical TPA (Figure 2.20 A). Tumors began to appear 11 weeks after the initial exposure to DMBA in post-inflamed mice, 3 weeks earlier than in controls (Figure 2.20 B). Over the duration of the experiment, post-inflamed mice had a significantly higher tumor burden with an average of roughly 17 papillomas per mouse compared to the 5 in control mice. To determine the possibility that this observation was due to a false negative, the GPower software was used to calculate

the power achieved by this study. At week 23, the final time point collected, the mean number of tumors for the control group was 5.67 and 18.33 for the post-inflamed, with a standard deviation of 1.16 and 2.52, respectively. The observed effect size for this experiment was 6.47 with 3 mice in each group. With a significance level set at 0.05, the achieved power from this experiment was 0.9998517 indicating that the observations are not due to a false negative.

These initial observations indicate that inflammatory memory can be maladatpive leaving the mouse more susceptible to carcinogenesis in an inflammatory microenvironment. More work is needed to determine the potential contribution of the altered skin niche (i.e. increased frequency of $RORC^{+}$ cells) to tumorigenesis. Additionally, we need to elucidate the retained accessible chromatin domains in post-inflamed mice that contribute to increased susceptibility to tumorigenesis. These observations beg the question of whether the adaptive features of inflammatory memory can be distinguished from the maladaptive ones.

2.3 Discussion

Tissue adaptation to inflammation has largely been attributed to innate immune memory within macrophages and natural killer cells, or to the persistence of memory in tissue resident T cells. Recent studies suggest that immune cells 'remember' a primary inflammatory stimulus by maintaining certain chromosomal and/or transcriptional features that were induced at the time of the assault. Here we provide powerful evidence that in contrast to prevailing notions, inflammatory memory is not merely a specialized property of immune cells, but rather also a feature of long-lived epithelial stem cells. Building upon the paradigm set for memory T cells, we now find that unexpectedly, EpSCs induce and sustain long-term changes to their chromosomal landscape in response to inflammation. Moreover, these changes endow EpSCs with the ability to accelerate their response to subsequent stressors. Analysis of the

myriad of potential contributing factors offers areas for future research. For instance, although the overall numbers of basal skin cells remained unchanged, distinct pools of EpSC that do not participate in naive skin responses might become sensitized to do so as a result of inflammation.

The majority of EpSC chromatin changes sustained long-term after the primary inflammatory exposure were not accompanied by sustained transcription of their associated genes, nor did inflammation-induced transcription factors remain active. The paradoxical issue is how then do these chromatin regions remain accessible in EpSCs long-after the return to normal epidermal homeostasis. Our existing evidence indicates and working hypothesis suggests EpSC transcription factors and other chromatin modifiers present in normal homeostasis can propagate these chromatin sites made accessible during inflammation.

Although the underlying mechanisms are complex, our *in vivo* reporter analyses indicate that sustained open-chromatin domains possess the information needed to sense tissue damage. Moreover, by remaining open long after inflammation resolves, these sensors seem to have functional relevance to the secondary assault. Consistent with this notion, greater tahn 50$\%$ of genes induced early and selectively at the wound edge of inflammation-experienced skin were associated with these sustained open-chromatin domains.

The active transcription of *Aim2* post-inflammation along with other components of the inflammasome pathway in the rapid responders gene list provided a clue to the downstream mediators of inflammatory memory. Our loss- and gain-of-function studies with AIM2, CASP1, IL-1β, and IL1-R1 underscore the importance of this pathway in conferring a wound repair advantage to inflammation-experienced EpSCs.

As beneficial as it may seem, heightened sensitivity to tissue damage may not always be a blessing: genetic alterations that mobilize stem cells more rapidly are often associated not only with accelerated wound repair, but also increased cancer

susceptibility. Indeed, individuals with gain-of-function mutations in inflammasome components are known to have increased risk of epidermal hyperplasia and cancers. Our findings suggest that the inflammation-induced memory imparted to EpSCs may also underlie the recurrent and exacerbated skin inflammation displayed by patients with autoimmune disorders such as psoriasis and atopic dermatitis. Overall, the inflammation-induced rewiring of EpSCs that we have unearthed here is likely to have major implications for future therapeutics aimed at enhancing adaptive features and counteracting maladaptive ones.

CHAPTER 3

RETAINED HISTONE MODIFICATIONS DEFINE INFLAMMATORY MEMORY

3.1 Introduction

Inflammatory memory endows stem cells with enhanced responsiveness to subsequent challenges. This memory is a result of chromatin rearrangements that open and maintain accessibility at key immune response pathways long-term. These memory domains enable rapid upregulation of key genes that enable accelerated tissue repair and heightened stem cell sensitivity [74]. How this memory forms and more importantly why only a subset of these chromatin domains stay accessible remains to be elucidated.

Gene expression patterns can be predicted by the histone code, which consists of post-translational modifications to histone tails that facilitate recruitment of chromatin remodelers and transcriptional machinery [41]. By assessing histone modifications over these memory domains and the genome at large, we can glean what is unique about these chromatin regions. Based on the marks deposited during the peak of the inflammatory response and retained afterwards, we can hope to both elucidate the initial chromatin rearrangements that lead to establishment of inflammatory memory and identify potential mechanisms for its retention. While this work remains ongoing, we thus far have identified that identified specific retention of monomethylation of Histone 3 lysine 4 (H3K4me1) at these memory chromatin domains.

3.2 Results

3.2.1 Increase in active chromatin detected at the peak of inflammation with global histone modification patterns restored after resolution

To address changes to the chromatin landscape during and after resolution of inflammation, we returned to the self-resolving model of acute Imiquimod (IMQ)-induced skin inflammation. The peak of the inflammatory response occurs 6 days after consecutive daily treatment, and resolves 30 days later (post-inflamed). EpSCs were collected from the skin as described previously, excluding potential contaminating cell populations. EpSCs were then prepared for multiplexed indexed T7 chromatin immunoprecipitation with high throughput sequencing (MINT ChIP) [**?**]. This assay enables both individual samples and antibodies to be barcoded enabling submission of one pooled library containing all samples with multiple histone ChIPs (Figure 3.1). Briefly, chromatin from each sample was digested with micrococcal nuclease (MNase) and barcoded with a T7 adaptor. Next, samples were pooled together and redistributed for incubation with individual histone antibodies. Each antibody pool then received an individual Illumina barcode, after which each pool was combined at equal concentrations and submitted for sequencing. The major advantages of this technique is it requires small cell numbers (200K), is cost-effective (20 ChIPs in one go), and is quantitative. Total histone 3 (TH3) is included as one of the antibodies, and enables signal normalization of modified histone 3 antibodies to the total H3 input. The histone modifications assessed using MINT ChIP included: H3K27ac, H3K4me1, and H3K27me3.

The histone modifications assayed were selected to distinguish active from poised, primed, and repressed chromatin [75] [76]. H3K27ac marks active enhancer regions. H3K4me1 marks primed chromatin, likely once active and left accessible for reactivation [49]. H3K27me3 is associated with repressed promoter regions; however, is also

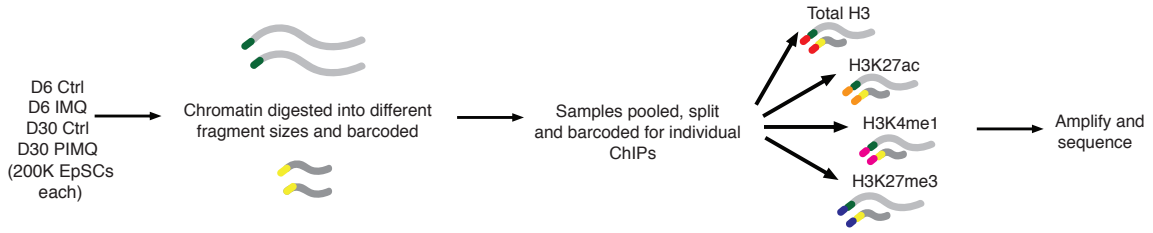

Figure 3.1: Multiplexed indexed T7 ChIP-Seq enables quantitative comparisons of histone modifications on small cell numbers. Schematic of MINT ChIP experimental design.

found in bivalent chromatin domains containing active marks such as H3K4me3 [77]. Bivalent chromatin is poised for activation, but has a repressive mark that prevents active transcription until the necessary activation signal is present.

A total of three replicates were completed for MINT ChIP. Across samples we observed similar frequencies of reads mapped, multimapped, unmapped, and duplicates (Figure 3.2 A). Replicates 2 and 3 were run on the Illumina HISeq2500, which achieves a sequencing depth of approximately 160 million. Replicate 1 (R1) was run on the Illumina NextSeq, which can achieve greater sequencing depth with closer to 400 million total reads. Samples from R1 therefore have more total reads than R2 and R3 (Figure 3.2 B).

At first, MINT ChIP was performed separately for day 6 and day 30 samples. However, we observed a batch effect that made quantitative temporal comparisons difficult. Therefore, for the last replicate (R1) we simultaneously ran D6 and D30 samples for each condition. This facilitated normalization both to total H3 and to total reads. Normalization ratios of modified histones over total H3 revealed subtle differences at the peak of inflammation such as increased H3K27ac and reduced H3K27me3. However, these differences were not sustained post-inflammation. (Figure 3.3 A). Globally histone modifications largely looked similar across time and conditions. This observation is confirmed by western blots of whole cell lysates, where there is no overt difference in global histone modifications (Figure 3.3 B).

A

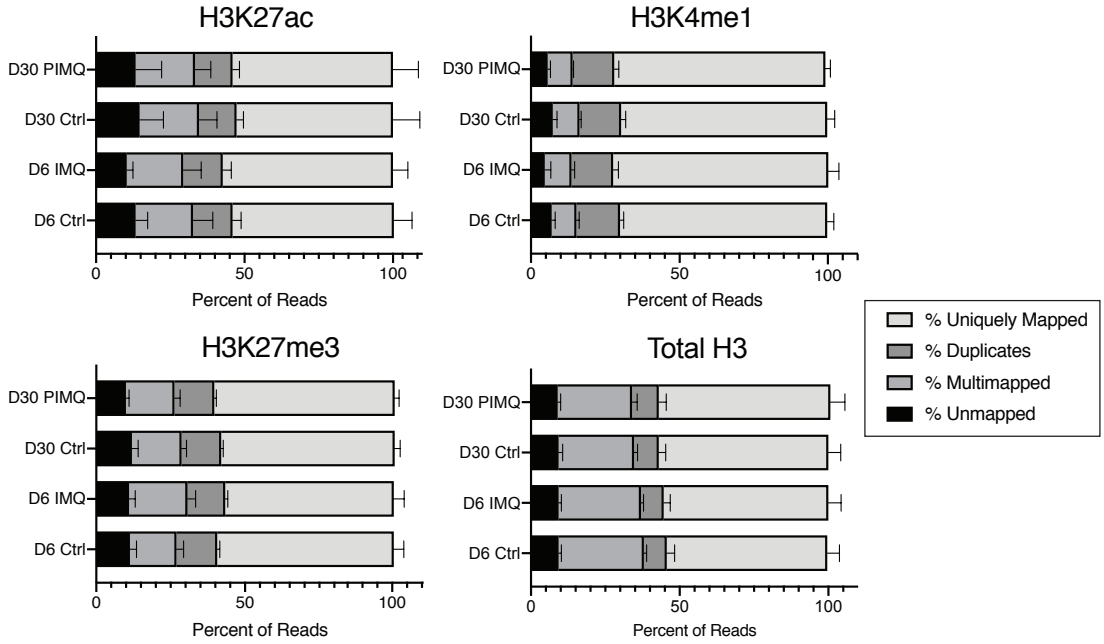

B

	H3K27ac		H3K4me1		H3K27me3		Total H3	
	Total Reads	Unique Aligned	Total Reads	Unique Aligned	Total Reads	Unique Aligned	Total Reads	Unique Aligned
D6 Ctrl R1	34018842	16766940	50854472	33343814	32995150	17654962	75180336	34774017
D6 Ctrl R2	22456186	13765937	31486768	23199012	22952202	15303171	33438604	19736235
D6 Ctrl R3	14465148	7602548	19824526	13755078	19113604	10875315	25778166	14789410
D6 IMQ R1	42686242	22177338	34456908	22385608	19879424	9866410	58876240	27614789
D6 IMQ R2	17588088	10892456	14570982	10963675	9293648	5972439	21561688	13224574
D6 IMQ R3	20647432	11893186	19496720	14975899	17857516	9925504	32700530	18818176
D30 Ctrl R1	32485048	15933195	49659380	32454066	32772958	18204240	75076830	36649997
D30 Ctrl R2	26807792	16861048	21927136	16162114	27281610	17167412	39407626	23245907
D30 Ctrl R3	12168926	5642990	20932354	14406824	21318572	12030890	36630260	23055856
D30 PIMQ R1	52719234	27709065	79721090	53259868	47759406	27305432	113447184	53934979
D30 PIMQ R2	16467850	10292990	14183052	10681200	16703858	10712011	25290934	15501025
D30 PIMQ R3	10953464	6090325	22232798	15869409	20282476	12361534	39629134	25251115

Figure 3.2: Alignment metrics for MINT ChIP on EpSCs peak and post inflammation. **A** Average frequencies of reads mapped, unmapped, duplicates, and uniquely aligned. **B** Table depicting total reads and reads uniquely aligned to the mouse mm10 genome after filtering out T7 duplicates, PCR duplicates, unmapped and multimapped reads. MINT ChIP was performed in triplicate with 3 mice per group.

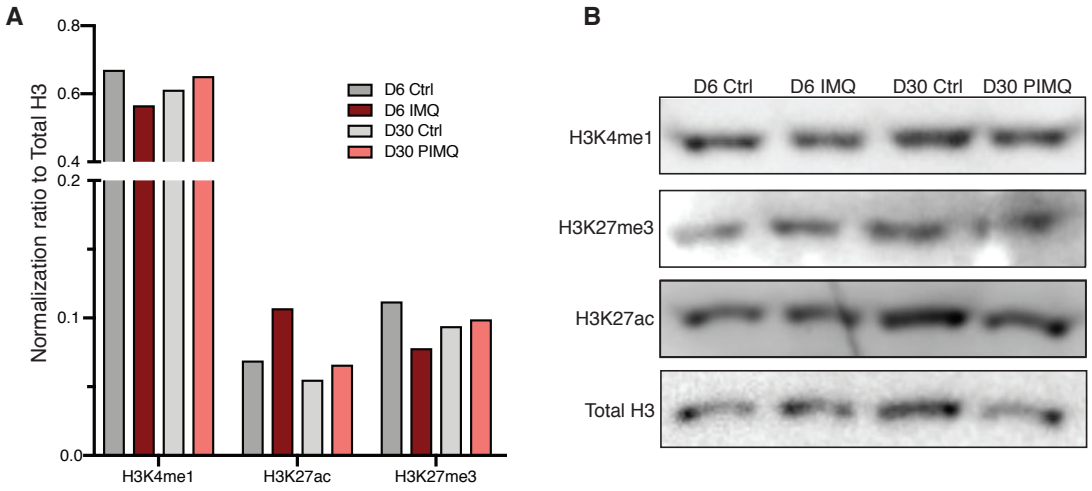

Figure 3.3: Normalization ratios of histone modifications over total H3. **A** Normalization ratios for each sample from replicate 1. **B** Western blot images of histone modifications from whole cell lysates of 10K cells.

Principal component analyses for each histone modification also identifies D6 IMQ as unique, and D30 post-inflamed (PIMQ) as more closely correlated with the controls (Figure 3.4). Specifically for H3K27ac, H3K4me1, and H3K27me3, D6 IMQ clusters distinctly from the other samples. Intriguingly, the D30 PIMQ samples appeared further along PC1 in the direction of D6 IMQ for H3K4me1 than the controls indicating more similarity and potential biological meaning.

All in all these global histone patterns matched our expectations: minimal sustained global differences in the histone code post-inflammation in accordance with our prior ATAC-Seq data where a majority of the inflammation-induced chromatin accessibility resolved by D30 PIMQ.

3.2.2 Maintenance of inflammation-induced histone modifications over memory domains

An important question following the establishment of inflammatory memory is why only a small subset of chromatin domains remain accessible after resolution of inflammation. At the peak of the inflammatory response, there were 44,414 uniquely

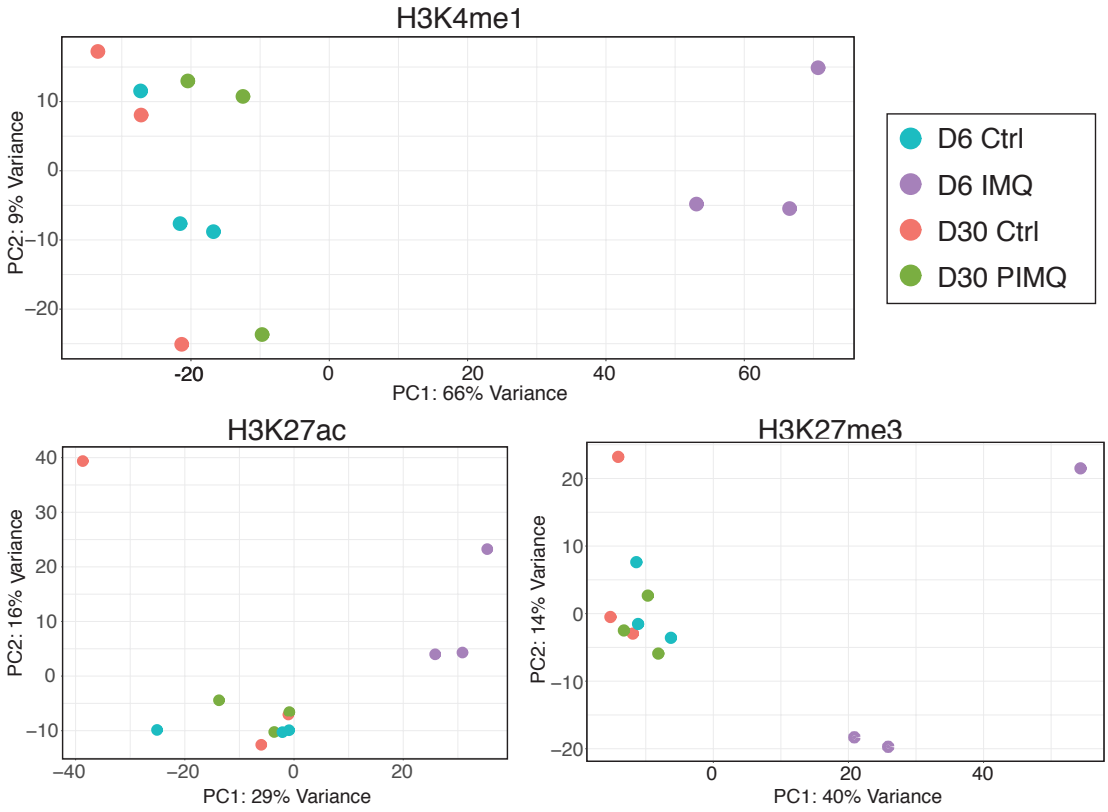

Figure 3.4: PCA confirms majority of inflammation-induced histone modifications resolve. PCA plot broken down by individual histone modification. Each MINT ChIP replicate is plotted as an individual dot.

ATAC peaks that had emerged, but only a small fraction, specifically 2,037 (roughly 4.5%) remained accessible. These peaks were functionally significant in that they were associated with genes that were rapidly upregulated upon a secondary injury contributing to EpSCs enhanced responsiveness. The question remains what is special or unique about these memory ATAC domains that keep them accessible?

To address this question, we returned to our MINT ChIP data and took the 2,037 memory ATAC domains and assessed histone ChIP signal specifically over these regions (Figure 3.5 A, B). As expected at the peak of the inflammatory response, we see a sharp increase in H3K27ac signal indicating active chromatin. The peak of inflammation is where we observed robust transcriptional changes, and it is therefore

apt that the associated chromatin would be active. H3K27ac is not retained post-inflammation, which fits considering that resolved EpSCs differentially express only a handful of genes. These sites uniquely retain H3K4me1 post-inflammation suggesting the chromatin is accessible and primed for reactivation. As the above projects are ongoing and for the purpose of this dissertation, the remainder of this chapter will discuss H3K4me1 and enhancer regions.

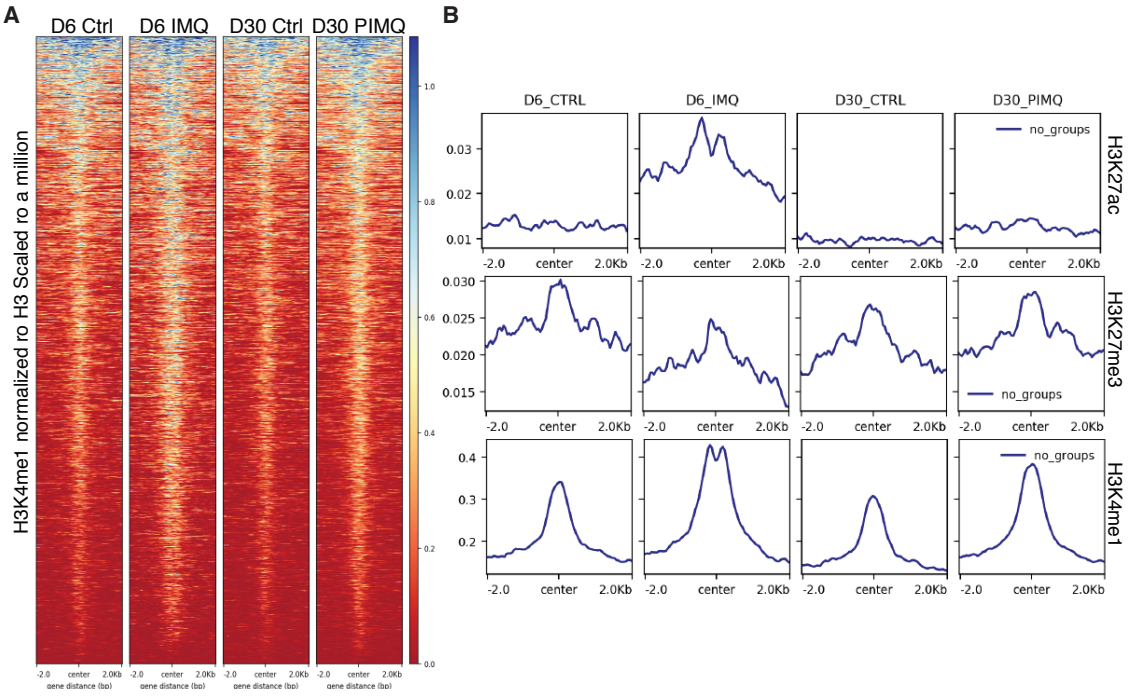

Figure 3.5: Post-inflamed EpSCs retain H3K4me1 in memory domains. **A** Heat map of H3K4me1 ChIP signal normalized to total H3 and scaled to a million over ATAC memory domains for each sample. **B** Plots depict signal intensity for each ChIP normalized to total H3 and scaled to a million centered over the ATAC memory domains. Data presented from replicate 1 of MINT ChIP data set.

H3K4me1 marks active and primed enhancers, which are distinguishable by the presence of H3K27ac [51]. Recent work suggests that H3K4me1 is involved in fine tuning enhancer activity through recruitment of chromatin remodelers such as the BAF complex and inhibition of *de novo* methylation machinery [78] [79] [80]. The lack of DNA methylation at these enhancer regions in addition to their ability to recruit chromatin remodelers enables H3K4me1 marked enhancers to rapidly respond to

environmental cues to influence expression of their associated genes [75]. The rapid response nature of H3K4me1 marked enhancers makes them an enticing subset of chromatin to explore for insights into the nature of inflammatory memory.

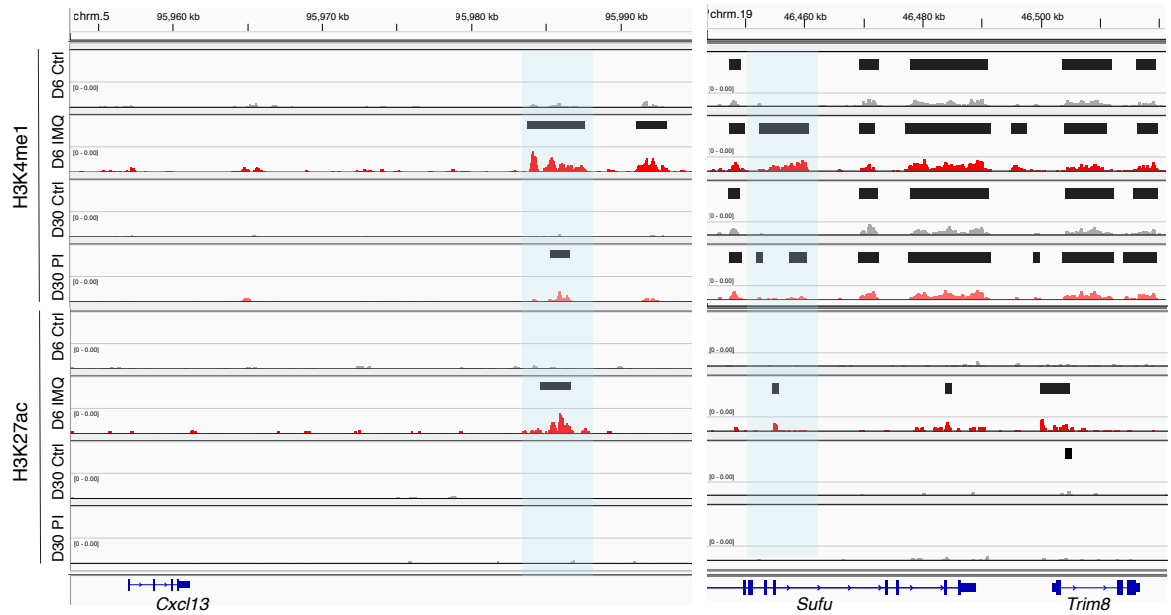

Figure 3.6: De novo enhancers emerge at the peak of inflammation and are retained. Genomic browser views of two emergent enhancer regions within memory ATAC domains that gain H3K4me1 and H3K27ac at the peak of inflammation, and remain primed in the interim by retaining H3K4me1. These enhancer regions are associated with immune response genes left, *Cxcl13* and right, *Trim8*.

As the heatmap in Figure 3.5 A shows many of the memory domains possess H3K4me1 across conditions. However, a subset of these regions gained H3K4me1 uniquely at the peak of inflammation. The development of ”de novo” enhancers or reactivation of latent enhancers was recently described in macrophages, where upon activation sequential binding of stimulus-activated and lineage-specific TFs facilitated deposition of enhancer marks [75]. After withdrawal of the stimulant, these latent enhancers remained primed with H3K4me1. Here we find that our de novo H3K4me1 enhancers are active at the peak of inflammation as they are simultaneously marked by H3K27ac, and after resolution they retain the H3K4me1 mark but lose the active marks (Figure 3.6). Furthermore, HOMER Motif analysis of these 2037 memory

domains reveals enrichment of both inflammatory and EpSC-specific TFs specifically FRA1 (member of AP-1 family), ELF3, CEBPB, SMAD2, and KLF5. It is plausible that a similar mechanism as identified in macrophages is at play in EpSCs.

3.3 Discussion and Future Directions

Inflammatory memory is an intrinsic feature of EpSCs, but how it is formed and more importantly retained remain works in progress. To understand retention of memory domains, we plan to interrogate which inflammatory and EpSC-specific TFs are enriched and bound to these regions through ChIP-Seq experiments. While Otsuni *et al.,* found that in macrophages the lineage-specific TF PU.1 did not remain bound in the absence of an inflammatory stimulus, others have identified more active role for TFs in orchestrating and sustaining chromatin rearrangements [75] [81] [82]. With consideration to H3K4me1, we are interested in histone methyltransferases (Mll3/4) that generate the mono-methyl mark on H3K4: how are Mll3/4 recruited to these chromatin domains and conversely, which histone demethylases do not subsequently remove these marks? Additionally, H3K4me1 inhibits binding of DNMT3L which could result in a reduction of *de novo* DNA methylation thereby preventing enhancer repression. To assess the DNA methylation status of EpSCs, we are collaborating with Alexander Meissner's group at the Max Planck Institute for Molecular Genetics to perform whole genome bisulfite sequencing on cells collected from the same skin preps from which the MINT ChIP EpSCs were derived.

CHAPTER 4

SUMMARY AND PERSPECTIVES

4.1 More than just the skin: adult tissue stem cells remember inflammation

Tissue stem cells sense and respond to environmental cues, which influences their decision between quiescence and activation, self-renewal and differentiation. Beyond simply influencing the immediate outcome of a round of division, these environmental cues educate stem cells so they are primed to respond to future encounters. This concept was first developed in innate immune cells and termed trained immunity, but recently this is a phenomenon found to occur within tissue stem cells. Trained immunity is a nonspecific memory that is coded epigenetically or metabolically within a cell after an inflammatory event that primes the cell to respond quicker and more efficiently to secondary inflammatory assaults or infection. This epigenetic memory can be established through a myriad of alterations including but not limited to changes in chromatin accessibility, DNA methylation, histone modifications, modulation of miRNA, and long-noncoding RNA expression [66]. Upon secondary challenges, this education results in expeditious transcriptional activation of key genes that function to defend against infection to either protect the stem cells or bias their lineage determination.

The ability of stem cells to both self-renew and differentiate means that alterations to their epigenome will be sustained and propagated within a tissue throughout an organism's lifetime. In the case of fighting off future infection, these changes are

highly beneficial. Recent work highlights that administration of Bacillus Calmette-Guérin (BCG), a vaccine used against Mycobacterium tuberculosis(Mtb), to bone marrow results in reprogramming of hematopoietic stem cells (HSCs). Following exposure to BCG, these HSCs alter their transcriptome resulting in lineage bias towards myelopoiesis over lymphopoiesis. Resulting bone marrow-derived macrophages (BMDMs) from BCG-educated HSCs are epigenetically modified, with more H3K27ac in putative enhancer regions leading to significantly higher expression of immune-related genes including Ifng, Tnf, and Il1b during Mtb infection. Rapid transcription of these antimycobacterial immunity genes enables trained macrophages to confer significantly better protection against Mtb than naïve macrophages. Subsequent bone marrow transplant experiments demonstrate that HSC reprogramming is sustainable in the absence of BCG, substantiating that these HSCs are bona fide memory HSCs [83].

As a proof of concept that HSCs and their progenitors (HSPCs) can indeed be trained and develop a long lasting memory, β-glucan considered to be the prototypical trained-immunity agonist was intraperitoneally injected into mice, which resulted in a long term sustained increase in myelopoiesis. While, HSCs do not express the β-glucan receptor Dectin-1, it was found that β-glucan triggered IL-1B related bone marrow inflammation mediated trained immunity of HSPCs. Trained HSPCs were significantly better at protecting against systemic LPS, and ameliorating the effect of replication stress and DNA damage in long term HSCs over naïve progenitors. Furthermore, β-glucan-trained HSPCs confer a protective hematopoiesis response to myeloablative chemotherapy via cyclophosphamide or 5-fluoracil. Metabolic and lipidomic experiments find a reduction in linoleic and arachidonic acid metabolism as well as broad changes in the lipidome specifically more lipids with shorter (34-36 carbon atoms) and more saturated acyl chains in trained HSPCs over naïve cells. Taken together IL-1β signaling in conjunction with key metabolic changes results in

training of HSPCs that confer protection against subsequent infections as well as an enhanced hematopoiesis response [84].

Trained immunity can also develop after sterile triggers of inflammation such as feeding low-density lipoprotein receptor (ldlr) null mice a Western diet (WD). The calorically rich WD is considered to have an inflammatory nature and is tightly linked to the development of diseases such as type II diabetes, obesity, and cardiovascular disease. Mice fed with WD for four weeks and then shifted back to a classical diet (CD) experienced transient hypercholesterolemia and a systemic inflammatory response with circulating growth factors, cytokines, and chemokines. WD induced an expansion of HSPCs, myeloid progenitor cells (MPPs) and granulocyte-monocyte progenitor cells (GMPs). GMPs were functionally distinct with enhanced responsiveness to LPS via differentially expressing key type I interferon response genes indicating that they and MPPs were reprogrammed. Assessing chromatin accessibility in GMPs from WD fed mice reveals enrichment of peaks associated with IL-6 production and the JAK/STAT pathway. Furthermore, key enhancer regions including *Tet2* and *Tlr4* remained more accessible even after mice were switched back to a CD. WD is sensed by the NLRP3 inflammasome resulting in release of IL-1β. IL1R1 blockade abrogates WD-induced systemic inflammation, and results in weaker responses upon secondary LPS challenge following the training period. Altogether transcriptional and epigenetic data reveal that exposure to WD can sustainably reprogram GMPs as many of the noted changes persist after return to a CD and that IL-1β is significant to cellular reprogramming [85].

As previously discussed in this dissertation, the link between inflammation, inflammasomes, IL-1B and reprogramming of stem cells is not unique to the hematopoietic compartment as the AIM2 inflammasome and IL-1B were identified as essential downstream mediators of EpSC inflammatory memory in contributing to augmented wound healing post-inflammation. Here I discuss cases where the establishment of

trained immunity or memory in stem cells has been a positive adaptation resulting in more efficacious protection against infection and enhanced tissue repair capacity. However, as previously discussed in Chapter 2 of this dissertation, in a tumor-prone environment EpSC inflammatory memory leads to accelerated tumorigenesis. Another recent study describes an inflammatory memory phenomenon in respiratory epithelial progenitors in human allergic inflammatory disease, where polyp cells exhibited a heightened transcriptional response and reinforcement of progenitor programs upon restimulation with pro-inflammatory type 2 cytokines. This rapid recall and augmented response, after weeks in culture, may offer insights into epithelial pathology and the chronic nature of allergic disease [86]. Stem cells are superlative at balancing acts, and memory will be another one: a fine-tuned tipping scale between 'good' and 'bad' memories resulting in enhanced tissue fitness or pathogenesis.

4.2 Insights from innate immune cells on stem cell inflammatory memory

Innate immune cells including monocytes, macrophages, and natural killer cells can recollect prior exposure to a pathogen or damage associated molecular pattern and mount immunological memory. This memory results in an augmented and non-specific response to future encounters with either a similar or unrelated inflammatory stimulus. Work in innate immune cells has elucidated the metabolic reprogramming and epigenetic rewiring that take place to establish immunological memory. Here, I will discuss the recent work in this space and comment on how it relates to the work presented in this dissertation.

4.2.1 Insights into metabolic reprogramming

Training of monocytes with β-glucan identified an important metabolic shift sustained in educated monocytes. These monocytes ramped up glycolysis in an AKT/mTOR/HIF1α

dependent manner resulting in increased glucose consumption and pyruvate to lactate conversion [87]. Training with BCG resulted in a similar metabolic shift with the addition of increased oxygen consumption [88]. Despite the shift towards glycolysis, trained macrophages possessed elevated levels of TCA metabolites including citrate, succinate, malate, fumarate, and 2-hydroxyglutarate fueled instead by glutaminolysis. These TCA intermediates likely played an important role in the training process as inhibiton of glutaminolysis via BPTES is sufficient to prevent formation of trained immunity by either β-glucan or BCG [88] [89]. Arts *et al.,* also find upregulation of a large number of cholesterol biosynthesis genes during induction of trained immunity. Atorvastatin-mediated inhibition of HMG-CoA-reductase, the rate-controlling enzyme in the mevalonate pathway that leads to production of cholesterol, resulted in diminished induction of trained immunity [89] highlighting the importance of sterol synthesis.

Reliable *ex vivo* metabolomics has proved a challenge for the field as a whole, and renders assessing individual metabolites in isolated EpSCs presently an unattainable goal. However, our current work suggests that many of the same players are essential to EpSC inflammatory memory. For instance, our MINT-ChIP data led us to HIF1α and mTOR signaling as important signaling pathways during the primary response in contributing to formation of inflammatory memory. Additionally, the D6 IMQ ATAC-Seq data set reveals cholesterol biosynthesis and sterol metabolism as the most significantly enriched pathways. As a rudimentary read out for an increase in glycolysis, we see an abundance of phosphorylated pyruvate dehydrogenase, which suggests pyruvate is not entering the mitochondria and instead may be converted to lactate. To more rigorously address the metabolic status of these EpSCs both during the primary response and after resolution of inflammation, we are establishing an *ex vivo* human skin raft culture system, where primary normal human epidermal keratinocytes stratify to form each epidermal layer when exposed to an air-liquid interface (Figure 4.1

A). After stratification, administration of proinflammatory cytokines IL-17A, IL-22, and TNF-α recapitulates a psoriatic inflammatory response as indicated by phosphorylation of Stat3^{Tyr705} (Figure 4.1 B). This system will enable us to profile individual metabolites, lactate production, and oxygen consumption in each condition.

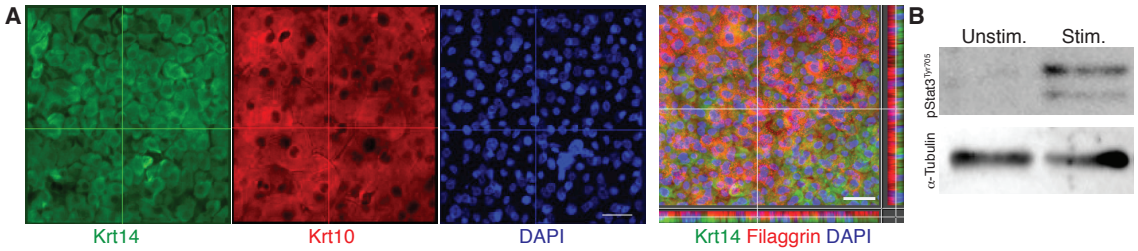

Figure 4.1: Primary normal human epidermal keratinocytes stratify to form skin equivalents and are responsive to pro-inflammatory cytokines. **A** Top-down view of immunofluorescence images of human skin rafts depicting basal epidermal layer (Krt14), differentiated layer (Krt10 or Filaggrin), and nuclei. Right most image includes sagittal view (below and right side) depicting basal layer (green) on bottom with differentiated suprabasal layers (red) on top. **B** Western Blot for phosphorylated Stat3 on Tyr705 and α-tubulin in human skin rafts that were unstimulated or stimulated for 3 days with 3 ng/mL each of IL-17, IL-22, and TNF-α. Courtesy of Christopher Cowley.

4.2.2 Insights into epigenetic rewiring

Induction of trained immunity requires large scale epigenetic rewiring involving histone modifications, changes in DNA methylation, and recruitment of transcription factors/ chromatin remodelers [90] [91] [92] [93] [94]. Seminal work by Ostuni et al., demonstrated the dynamism of epigenetic reprogramming through identification of the expansion of the cis-regulatory repertoire upon macrophage stimulation. They identified that upon stimulation, macrophages recommissioned latent enhancers, which prior were unmarked and lacked transcription factor (TF) occupancy. After withdrawal of the stimulant, macrophages rapidly lost H3K27ac (active) and PU.1 (master regulator), but retained H3K4me1 long term, which enabled faster and stronger induction of the associated genes [75]. Regarding DNA methylation, differential methylation was stimulant dependent, where LPS-treated cells resulted in

a distinct methylation pattern but β-glucan had minimal effect. In LPS-treated cells, most of the differentially methylated regions occurred at distal enhancers [95].

These epigenetic marks require a series of writers, erasers, and readers, which upon stimulation are activated to modify the chromatin and interpret the resultant change. For instance, TLR4 signaling results in the establishment of *de novo* enhancers through activation of lysine methyltransferases, specifically Mll1, Mll2/4, and Mll3, mediated deposition of H3K4 methylation [52]. The activation of these modifying proteins provides a link between the metabolic status of the cell and the regulation of chromatin modifications. Metabolites serve as cofactors and/or substrates for these writers, erasers, and readers making them sensitive to changes in metabolite pools [96]. For instance, NAD^+ and acetyl-CoA influence histone deacetylases and histone acetyltransferases, respectively; succinate and fumarate can inhibit certain demethylation reactions; and α-ketoglutarate is an essential cofactor for several lysine and cytosine demethylating enzymes. A specific example of how the integration of these pathways influences trained immunity was demonstrated via the accumulation of fumarate inhibiting lysine demethylase (KDM5), resulting in increased H3K4me3 at the promoters of genes encoding pro-inflammatory cytokines [89].

The contribution of dynamic transcription factor binding to trained immunity has not been as thoroughly fleshed out as have other epigenetic modifications. Studies thus far have identified distinct TF binding motifs within stimulant-specific accessible chromatin regions, which contribute to the distinction of trained from tolerized transcriptional programs in macrophages [95]. Additionally, recent work found that upon LPS-stimulation, the stress-responsive TF ATF7, which normally binds to and causes repression of immune-response related genes, is phosphorylated resulting in its release from chromatin and the concomitant decrease in the repressive histone marks [97].

4.3 Future Directions and Clinical Significance

Thus far, I have demonstrated an adaptive mechanism used by epithelial stem cells to retain epigenetic memory of inflammatory exposure that functions to heighten sensitivity to future tissue damage. While much of this dissertation discussed the tissue repair advantage conferred by inflammatory memory, I also discussed how the same features can be maladaptive and contribute to tumorigenesis. Along these lines, this dissertation began with a discussion of remitting and relapsing inflammatory skin disorders namely psoriasis and addressed the need for novel therapies. To this end, we have addressed some of the outstanding questions in this space including EpSC participation in an active inflammatory response leading to epidermal hyperthickening and their epigenetic rewiring, but most importantly their survival and retention in the basal compartment long-term post-inflammation. These observations beg the question of inflammatory memory's role in psoriatic flares. If inflammatory memory is inadequately regulated then these chromatin domains could sustain an inflammatory response. Does inflammatory memory address in part why the disease relapses in the same skin location over and over again? Could modulating memory and retention of these chromatin domains make the EpSCs refractory to aberrant immune cell signaling or alleviate EpSC feed-forward communication with infiltrating immune cells? The current findings identify EpSCs an interesting avenue to explore for the development of novel therapeutic interventions to treat inflammatory skin diseases.

To understand whether we can modulate inflammation-induced chromatin rearrangements either positively to augment wound healing or negatively to wipe clean a slate of inflammatory exposures that potentially contribute to disease pathogenesis, we need to have a better understanding of the underlying mechanisms. How is inflammatory memory established and why do only a small subset of domains re-

main primed? To this end, our genomic approaches have identified unique features of the memory chromatin domains namely the unique retention of H3K4me1. Probing for deposition and maintenance of these marks will elucidate how select chromatin domains remain accessible.

All together, this work highlights EpSCs commitment to maintaining tissue integrity. Their ability to respond to inflammatory stress and retain rapid response chromatin domains make EpSCs formidable masons that generate and maintain the skin barrier.

CHAPTER 5

MATERIALS AND METHODS

Animals

The following mouse strains were purchased from the Jackson Laboratories: C57BL/6, B6.FVB-Tg(*Rorc-Cre*)1Litt/J (*Rorc-Cre*), C57BL/6-Gt(ROSA), 26Sortm1(HBEGF)Awai/J B6-*Rosa26iDTR*, B6.129P2-Aim2Gt(CSG445)Byg/J, B6.129S7-Il1r1tm1Imx/J, and B6.129P2-Il18tm1Aki/J. Tg(*Rorc-EGFP*Ebemice were a gift from Dr. Gerard Eberl (Institut Pasteur). Tg(*Ly6a-Cre*)1Isg mice were a gift from Dr. Isidro Sanchez-Garcia (Universidad de Salamanca). Krt14CreER and *Krt14rtTA* mice were previously generated in the Fuchs' lab. *Krt10CreER* transgenic mice were generated by retrieving the murine *Krt10* promoter region (8416 bp fragment upstream of *Krt10* start codon) from bacterial articial chromatin DNA (CHORI clone ID:RP23-336D20) and then inserting it upstream of the *Beta-Globin Intron-CreER–polyA*, analogous to our Krt14CreER transgene. All keratin promoter driven CreER mice were then each crossed to *Rosa26Flox-Stop-Flox-YFP mice*. Mice were bred and maintained under pathogen-free conditions at an American Association for the Accreditation of Laboratory Animal Care (AAALAC)-accredited animal facility at the Rockefeller University and housed in accordance with the procedures outlined in the Guide for the Care and Use of Laboratory Animals. When possible, preliminary experiments were performed to determine requirements for sample size, taking into account resources available and ethical, reductionist animal use. Animal studies were not performed in a blinded

fashion. Animals were assigned randomly to experimental groups.

Skin inflammation models

The dorsal skin of 8 week old mice in the telogen (resting) phase of the hair cycle were shaved with clippers and then subjected to topical application or treatment of the skin as below:

Imiquimod: Mice were treated with either 1 mg/cm2 skin of 5% imiquimod cream (Perrigo) or control Vanicream (Pharmaceutical Specialties Inc.) for six consecutive days as previously described.

Epidermal abrasion wounds: Mice were treated with depilatory agent Nair (Church and Dwight). A 2 cm^2 area was then wounded shallowly with a rotary drill (Model 520 Dremel) as previously described to remove the epidermis and induce re-epithelialization of the wounded skin.

TPA: Mice were topically treated with 40 nM/3cm2 skin 12-O-tetradecanoylphorbol 13-acetate (TPA) (Sigma-Aldrich) in acetone or acetone alone daily for five consecutive days.

MC903: Mice were topically treated with 2 nM/3cm^2 skin of vitamin D analog Calcipotriol (MC903) (Tocris Bioscience) in EtOH or EtOH alone for 14 consecutive days as previously described.

Candida albicans (Fungi) infection: Mice were infected with 10^6 *Candida albicans* (ATCC36801) as previously described.

Lineage tracing

At 8 weeks of age during the telogen (resting) phase of the hair cycle, mice were treated with 10 μ/ml of 4-hydroxytamoxifen (TAM) in corn oil (Sigma-Aldrich) by intraperitoneal (i.p.) injection for 3 consecutive days at the following doses: *Krt14CreER;RosaYFP* treated with 10 μg of TAM, and *K10CreER;RosaYFP* treated with 100 μg of TAM. Two days after the last tamoxifen treatment, the dorsal skin of a cohort of mice was analyzed for YFP expression by flow cytometry and immunofluorescence (Day 0 time

point). Upon confirmation of YFP expression the remaining cohort mice were treated with the aforementioned IMQ regimen and analyzed at days 6, 30, and 180 post-treatment.

EdU pulse

For 5'-ethynyl-2'-deoxyuridine (EdU) pulse experiments, mice were injected intraperitoneally (50 μg/g) (Sigma-Aldrich) at specified intervals (typically 1-4 hrs) before analysis.

Punch biopsy and splint wounds

The dorsal skin of mice was shaved at indicated time points after imiquimod treatment. After visually confirming that hair follicles in the shaved area were in telogen (resting) phase of the hair cycle, 6 mm biopsy punches (Miltex) were used to make full-thickness wounds. Wound closure was assessed macroscopically with an engineer's caliper daily. 3 mm wounds were splinted with 8 mm silicone splints as previously described. Wound closure was assessed macroscopically with an engineer's caliper daily. Wound area was calculated by applying the area of an ellipse (π*r1*r2) to the two diameter measurements on the y-axis, and x-axis of the wound. One-, two- and three-phase decay model of curve fitting was performed for wound healing assays. The two- and three-phase decay analyses showed minimal contributions from second (K_{slow} Ctrl=0.00015 PI=0.0017) phase and generated an "ambiguous fit" error indicating wide confidence intervals and that the software (PRISM GraphPad) is unable to find a unique curve to fit the data. Therefore, wound healing rate constants were calculated using a One-Phase Decay Model (PRISM GraphPad).

Diptheria toxin administration

Mice were intraperitonially (i.p.) injected with 200 ng of Diptheria Toxin (Sigma Aldrich) twice daily for 5 consecutive days. Mice were maintained on a sulfatrim diet and 0.5 mg/ml oral fluconazole (Citron Pharma) supplemented in drinking water throughout the course of treatment and subsequent wounding experiment.

Caspase inhibitor administration

Mice were i.p. injected with 0.6 mM of Ac-YVAD-cmk (Caymon Chemicals) 1 day prior to wounding and then daily for the first five days of the wound response.

Clodronate liposome administration

Mice were i.p. injected with either 200 μl clodronate or control liposomes 8 days prior to and then every two days until wounding.

Anti-IL1R1 administration

Mice were i.p. injected with 0.2 μg of Anti-IL1R1 antibody (JAMA-147) or Armenian Hamster Isotype control (BioXCell) 1 day prior to wounding and then daily for the first five days of the wound response.

***In utero* lentiviral (LV) transduction**

Transductions were achieved by *in utero* injection of lentivirus into the amniotic sacs of E9.5 mice. At E9.5, the surface ectoderm exists as a single layer of unspecified Krt14$^+$ EpSC progenitors, which become stably transduced by LV within 24 hrs. High LV titers enable highly efficient and selective transduction of the entire embryonic skin epithelium, without affecting other skin cell types. *In utero* injections are non-invasive and do not alter embryonic development or elicit inflammatory responses in the skin. The DNA carried by the lentivirus is stably propagated into adulthood within the skin epithelium, including the epidermis and hair follicles. *In utero* LV deliveries were used for all ATAC-peak reporters and for delivery of *TRE-Aim2* expression.

Doxycycline Feed Administration

Mice transduced with *LV-TRE-Aim2* were placed on 2 mg/kg doxycycline feed (Bioserv) at postnatal day 53 and maintained on doxycycline diet throughout the course of wound repair.

Cell Isolation and Tissue Processing

Keratinocyte isolation was adapted from a previously described protocol. Briefly, dorsal skin was shaved and digested using either 0.25% Trypsin/EDTA (Gibco) or

Collagenase (Sigma) to obtain a single cell suspension. Immune cells from 1 cm^+ pieces of skin were isoplated after digestion with Liberase TM (Roche) based on an adapted procol. To isolate wound edge epithelial stem cells, 0.5 mm^2 of skin adjacent to the wound was excised and digested in collagenase.

***Ex vivo* explant migration assay**

The *ex vivo* explant migration assay was performed as previously described. 2 mm punch biopsies (Miltex) were taken from the back skin after hair depilation. The skin was adhered to the bottom of a fibronectin-coated plate with matrigel (Corning) and cultured in 300 μM Ca^{2+} keratinocyte growth media made as previously described. Explants supplemented with recombinant IL-18 and IL-1β (Peprotech) received 50 ng/ml of the cytokine daily. Outgrowth of $Krt14^+$ cells from explants was imaged at indicated time-points using the 10X objective of a Nikon Eclipse TS100 microscope equipped with an Exfo X-Cite Series 120 and a Hamamatsu ORCA-ER Digital Camera. Images were analyzed with ImageJ software.

Flow cytometry and cell sorting

Female mice were used for sorting experiments at all time points and conditions to obtain maximal cell numbers. Single cell suspensions were stained with antibodies (Extended Data Table 1) at predetermined concentrations in a 100 μl staining buffer (PBS containing 5$\%$FBS and 1$\%$ HEPES) per 10^6 cells. Stained cells were resuspended in 4',6-diamidino-2-phenylindole (DAPI) in FACS buffer (Sigma-Aldrich) prior to analysis. Data were acquired on LSRII Analyzers (BD Biosciences) and then analyzed with FlowJo program. Fluorescence-activated cell sorting (FACS) was conducted using Aria Cell Sorters (BD Biosciences) into either staining buffer or Trizol LS (Invitrogen).

Immunofluorescence and image analysis

Immunofluorescence staining protocols were adapted from [22]. Briefly tissue was fixed in 4$\%$ paraformaldehyde in PBS for 20 min at room temperature or 4 hours

at 4°C. Tissue was washed 3X with PBS and switched to 20% sucrose overnight and subsequently washed. Tissue was then embedded in OCT (Tissue Tek), frozen, cryosectioned (14-20 μm). Sections were permeabilized, blocked and stained with primary and then secondary fluorescence conjugated antibody. Nuclei were stained using 4'6'-diamidino-2-phenylindole (DAPI). EdU and TUNEL Click-It reaction were performed according to manufacturer's directions (Life Technologies). For pSTAT3 immunofluorescence, sections were fixed in methanol for 20 minutes at -20°C before primary and secondary antibody labeling. For complete list of antibodies see Extended Data Table 2. Migrating tongue was determined by measuring the length of Keratin14$^+$ Integrin-α5$^+$ cells. Percentage of wound-edge proliferating EpSCs was determined by counting EdU$^+$ Keratin14$^+$ cells per total number of Keratin17$^+$ cells. Data were analyzed using ImageJ Software.

Confocal microscopy and image processing

Images were acquired with an AxioOberver.Z1 epifluorescence microscope equipped with a Hamamatsu ORCA-ER camera and an ApoTome.2 (Carl Zeiss) slider. Tiled and stitched images of sagittal sections were collected using a 20X or 40X objective, controlled by Zen software (Carl Zeiss). Maximal projection Z-stacks are presented and co-localizations were interpreted only in single Z-stacks. Z-stacks were projected using ImageJ software. RGB images were assembled in Adobe Illustrator CC2015.3.

Histology

Skin tissue was fixed in PBS containing 10% formalin, paraffin embedded, sectioned (0.8 mm) and stained with hematoxylin and eosin by Histowiz Inc. Stained slides were scanned at 40X magnification using Aperio AT2. Slides were visualized and epidermal thickness was analyzed using Aperio Image Scope software.

Gross images

Animals were imaged using a Leica DFC310 FX fitted with a Schott Fostec Ace fiber optic light source and a Leica microscope video lens objective 0.63x no. 10447367.

RNA purification, quantitative PCR and RNA-sequencing

Quantitative PCR: Individual animals were used for qPCR experiments. Total RNA was purified from either whole skin biopsies, flash frozen and then homogenized with a Bessman Tissue Pulverizer (SpectrumTM) or FACS purified keratinocyte populations using Direct-zol RNA MiniPrep kit (Zymo Research) per manufacturer's instructions. Equal amounts of RNA were reverse-transcribed using the superscript VILO cDNA synthesis kit (Invitrogen). cDNAs for each sample were normalized to equal amounts using primers against *Actb*. XpressRef Universal Total RNA (Qiagen) was used as a negative control to assess FACS population purity. For complete list of qPCR primers refer to Data Table 1.

RNA-seq: 3-4 animals were pooled per condition for each RNA-seq experiment. Total RNA was isolated from FACS purified keratinocyte populations using Direct-zol RNA MiniPrep kit (Zymo Research) per manufacturer's instructions. Quality of the RNA for sequencing was determined using Agilent 2100 Bioanalyzer, all samples used had RNA integrin numbers (RIN) 9. Poly-A selection and library preparation using Illumina TrueSeq mRNA sample preparation kit and sequencing on Illumina HiSeq 2500 or HiSeq 4000 machines was performed by Weill Cornell Medical College Genomic Core facility, 50 bp Single-end FASTQ sequences were aligned to mouse genome (GRCm38/mm10) using STAR41 and transcripts were annotated using Gencode release M9. Differential gene expression analysis was performed using DESeq2 package using the gene counts output from STAR read aligner.

Ingenuity pathways analyses were performed on differentially expressed genes 12 hours post-wounding.

ATAC-Seq

Assay was performed on 100K FACS purified cells as previously described. Briefly, cells were lysed in ATAC lysis buffer for 5 minutes and then transposed with TN5 transposase (Illumina) for 30 minutes. Samples were barcoded and sequencing li-

Table 5.1: qPCR Primer List

Gene Name	Forward Primer	Reverse Primer
β-actin	ccaaccgtgaaaagatgacc	accagaggcatacgggaca
Aim2	caggcaattgcatctgagag	cgcctcacaaagattttcact
H2-M2	tgtactttcagaaactgcgagact	tcatcctttggatggtgtga
Trp63	cactctccatgccctcca	gcccaaccttgctaagaaact
Klf5	gattcacaacccaaatttacctg	ctttgtataaacttttgtgcaacca
Lhx2	cagcttgcgcaaaagacc	taaaaggttgcgcctgaact
Cd34	gaaccgtcgcagttggag	tccaccattctccgtgtaataa
Sox10	atgtcagatgggaacccaga	gtgtttggggtggttggag
Pdgfra	aagacctgggcaagaggaac	gaacctgtctcgatggcact
Ptprc(CD45)	ttcagaaaatgcaacagtgaca	ccaactgacatctttcaggtatga
Vcam1	tggtgaaatggaatctgaacc	gacccagatggtggtttcc

brary was prepared according to manufacturer's guidelines (Illumina) and sequenced on an Illumina HiSeq 2500.

For sequencing data analysis 50 bp paired-end FASTQs were aligned to mouse genome (GRCm38/mm10) as previously described. Correlation between replicates was measured by first calling peaks in each replicate, merging the peak sets, followed by plotting Log2 transformed signal against individual replicates. Aligned reads for the two replicates were then merged and peaks called on the merged dataset. Genomic annotation of peaks was performed using the Cis-regulatory Element Annotation System (CEAS).

Average ATAC signals for transcription start sites (TSS, +/- 3000 bp) and for chromatin insulator protein CTCF sites (+/- 1000 bp) were plotted for each sample CTCF sites were derived from CTCF peaks called in E14.5 C57BL/6 limb embryo from ENCODE (Accession: ENCFF001YAK) and converted to mm10 coordinates using liftOver. Average tag count is calculated by averaging the number of reads overlapping each base pair per million mapped reads. (Number of reads at each base pair)/(Total readcounts x10^6). X-axis is distance from either the CTCF of TSS site.

ATAC-Seq peaks were determined algorithmically using Model-based Analysis of ChIP-Seq 2 (MACS2) algorithm with the option "–keep-dup all" to keep duplicates

generated by combining experimental replicates. Each peak is of varying size representing regions of signal enrichment over background. Shared peaks were defined as regions that had 1base pair overlap between the two datasets. Unique peaks were then defined as regions that had no overlap. Regions where signal intensity did not meet the threshold (FDR 0.01) for statistical significance over background were considered “closed”.

Z-score transformations were performed to normalize data across various samples and time points. ATAC signals per base-pair over the mouse genome (GRCm38/mm10), excluding the mitochondrial and Y chromosome, were scored and then averaged over 500 bp non-overlapping genomic windows. Background signal was then filtered out by excluding genomic windows that averaged less than 1 in any replicates. Data was clustered using Cluster 3.0 and visualized using GENE-E software46. Significantly different windows were assayed between samples by t-test (p-value 0.05).

Sequencing data tracks were presented using University of California Santa Cruz genome browser. Unique peaks at from day 6 and day 30 control and IMQ treated EpSCs, and overlapping peaking from day 6 and day 30 IMQ treated EpSCs were subject to ontology analysis using Genomic Regions Enrichment of Annotation Tool (GREAT) with whole mouse genome (GRCm38/mm10) as the background. PANTHER pathways analysis was used to compare peak-associated genes with known pathways. Motif analysis of these regions was performed using HOMER software. Selected ontologies and MOTIFS are displayed. Values below the false positive range (1e-10 to 1e-12) for this algorithm were considered statistically significant.

Peak reporters

Genomic regions with enriched signal in post-inflamed EpSCs associated with *Aim2* (Peak1 - Chr1:173,420,163-173,420,883, Peak 2 - Chr1:173,422,670-173,423,721) *Armc6* (Chr8:70,221,668-70,222,912), *Aoah* (Chr13:20,935,623-20,936,830), and Cotl1 (Chr8:119,810,704-119,812,768) were PCR amplified from keratinocyte genomic DNA

and cloned into a *pLKO-PGK-H2B-mRFP1-"Peak"-minSV40-EGFP* vector. After sequence verification individual plasmids were packaged into a lentivirus injected *in utero* into the amniotic sacs of E9.5 C57BL/6 embryos, as described above.

Inducible *Aim2* mice

Murine *Aim2* cDNA was amplified from FACS purified EpSCs and cloned downstream of the *TRE* and minimal promoter of the *pLKO-TRE-PGK-H2BmRFP1* vector.After sequence verification the plasmid was packaged into a lentivirus for *in utero* injection into the amniotic sac of *K14rtTA* E9.5 embryos. *Aim2* induction was verified by qPCR 7 days after doxycycline administration to activate rtTA, which in turn binds to the TRE element.

CASPASE 1 fluorometric and cytokine enzyme-linked immunosorbent assay (ELISAs)

Tissue lysates from 0.5 mm^2 wound edge skin 12 hours post-injury were prepared by freeze thawing and then dissociating tissue with a tissue lyser (Qiagen). Lysates were assayed for CASP1 activity and cytokine levels. CASPASE-1/ICE flourometric assay (RD) and IL-1β (eBioscience) and IL-18 (MBL international) ELISAs were performed according to manufacturer's instructions. Recombinant human CASP1 (Sigma-Aldrich) was used a standard to determine CASP1 activity. All assays were normalized to total protein levels in lysate as measured by Pierce™ BCA Protein Assay Kit (ThermoFisher).

Two-step carniogenesis model

Topical 7,12-Dimebthylbenz(a)anthracene (DMBA)/ 12-O-Tetradecanoylphorbo-13-acetate (TPA) was performed as previously described [98]. Briefly, the back skin of post-inflamed or inflammation naive mice (P90) was shaved and treated with 400 nM DMBA in 100 μl acetone. Thereafter mice were treated with 17 nM TPA in 100 μl acetone twice weekly for the duration of the experiment. Tumors were measured weekly with an engineer's caliper.

GPower software was used to determine the achieved power of the study. Using the observed mean and standard deviation of each group, the observed effect size was calculated. With 3 mice in each group and setting the desired significance level to 0.05, the software can determine the power achieved.

Multiplexed indexed T7 ChIP-seq (MINT-ChIP)

200K EpSCs from each condition were collected from 2-3 mice as previously described. Cells were split into 2 groups (100K each) low MNase (to capture large fragments) and high Mnase (to capture small fragments). After digestion each sample received an individual T7 adapter, after which each sample was pooled and divided into groups based on histone antibody ChIP (either Total H3, H3K27ac, H3K4me1, or H3K27me3). After immunoprecipitation each ChIP received an Illumina barcode. Samples could then be pooled together in equal concentration and submitted for sequencing. Replicates 2 and 3 were sequenced on the Illumina HiSeq 2500. Replicate 1 was sequenced on Illumina NextSeq 4000. All sequencing was paired-end.

Data processing was done in accordance with the methods outlined by Bradley Bernstein's group [99]. Briefly, files were de-multiplexed using bcl2fastq algorithms. Read1 was demuliplexed further based on the T7-adapter barcode (first 6 bases of the read). Glimpse package allowed for 1 mismatch. Corresponding reads based on the identifier were extracted from Read2 fastq files, and the files trimmed to remove the barcodes. Burrows-Wheeler Aligner was used for paired-end alignment to mm10 genome.

Resulting bam files were then filtered in three stages to: remove multimapped and unmapped reads, PCR duplicates (using Picard Tools option MarkDuplicates), and T7 duplicates (have identical Read1 but variable Read2). Filtered bam files could be views as tiled data files in IGV and peaks were called using the Homer package. Pos2bed.pl and bedtools merge were used to generate bed files. Quantitative normalization was achieved by dividing the peak signal values by the number of Total H3

reads in the corresponding data set.

Data processing for this data set was performed by Thomas Carroll, and I would again like to thank him for the tremendous help he has provided.

Statistics

Data are presented as mean standard error of the mean, mean $\pm$ standard deviation, or mean $\pm$ 95$\%$ confidence interval. Group sizes were determined based on the results of preliminary experiments. Mice were assigned at random to groups. Experiments were not performed in a blinded fashion. Statistical significance was determined with the two-tailed unpaired Student's t-test, under the untested assumption of normality. Within each group there was an estimate of variation, and the variance between groups was similar. Statistical significance of ATAC-seq peak gene comparisons was calculated using a Mann-Whitney test). Statistical analysis was calculated using either Prism software (GraphPad), DESeq2 or in R.

Data availability

Datasets generated and/or analyzed during the current study are presented in the published article [74] or the accompanying Source Data or Supplementary Information files. Genomic datasets generated during and/or analyzed during the current study are available in the Gene Expression Omnbibus (GEO) repository under accession GSE92967. AI2KO ATAC-Seq and MINT ChIP data sets will be released upon publication.

Antibodies

Table 5.2: Antibody List

Begin of Table 5.2		
Antibody	Source	Identifier
Chicken Anti-Mouse GFP	Abcam	Cat ab13970
Rabbit Anti-Mouse Keratin 14	Fuchs Lab	N/A
Rabbit Anti-Mouse Keratin 10	Fuchs Lab	N/A

Continuation of Table 5.2		
Antibody	Source	Identifier
Rabbit Anti-Mouse Keratin 24	Fuchs Lab	N/A
Rat Anti-Mouse CD49e (integrin-a5) clone: 5H10-27	BD Pharmingen	Cat 553319
Rat Anti-Mouse CD3e clone: 17A2	Biolegend	Cat 100212
Armenian Hamster Anti-Mouse gdTCR clone: GL3	Biolegend	Cat 1181011
Armenian Hamster Anti-Mouse TCRb Clone: H57-597 PerCp/Cy5.5	Biolegend	Cat 109227
Armenian Hamster Anti-Mouse gdTCR clone: GL3 AF647	Biolegend	Cat 118133
Anti-Mouse CD24 Clone: M1/69 PerCP/Cy5.5	eBiosciences	Cat 45-0242-80
Anti-Mouse CD11b-PacBlue Clone: M1/70	Biolegend	Cat 101223
Anti-Mouse CD64-PerCP-Cy5 Clone: X54-5/7.1	Biolegend	Cat 139307
Anti-Mouse CD11c-PECy7Clone: N418 Biolegend Cat 117317		
Anti-Mouse I-A/I-E (MHCII) PerCp/Cy5.5 Clone: 107625	Biolegend	Cat 107625
Rat Anti-Mouse Siglec-F Clone: E50-2440 PE	BD Pharmingen	Cat 552128
Anti-Mouse Ly6c-FITC Clone: HK1.4	Biolegend	Cat 128005
Anti-Mouse CD34 eFluor 660 Clone: RAM34	eBiosciences	Cat 50-0341-82

Continuation of Table 5.2		
Antibody	Source	Identifier
Anti-Mouse Ly-6A/E (Sca-1) Clone D7 APC/Cy7	Biolegend	Cat 108126
Purified Anti-Human/Mouse CD49f Clone: GoH3	Biolegend	Cat 313602
Anti Human/Mouse Cd49f PE Clone: GoH3	eBiosciences	Cat 12-0495-81
APC/Cy7 Anti-Mouse CD45 Clone: 30-F11	Biolegend	Cat 103116
Biotin Anti-Mouse CD45 Clone: 30-F11	Biolegend	Cat 103104
Biotin Anti Mouse CD117 (c-kit) Clone: 2B8	Biolegend	Cat 105804
Biotin Anti-Mouse CD140a Clone: APA5	Biolegend	Cat 135910
Biotin Anti-Mouse CD31 Clone: 390	Biolegend	Cat 102404
Rabbit Anti-pStat3 (Tyr705) Clone: D3A7	Cell Signaling	Cat 9145
Anti-Mouse/Rat CD29 Clone: HMB1-1	Biolegend	Cat 102214
Purified Anti-Mouse/Rat CD29 Clone: HMB1-1	Biolegend	Cat 102201
Anti-Mouse Total H3 Clone: MABI 0301	Active Motif	39763
Anti-Mouse H3K27ac (for ChIP)	Active Motif	39133
Anti-Mouse H3K27ac (for Western)	Abcam	ab4729

Continuation of Table 5.2		
Antibody	Source	Identifier
Anti-Mouse H3K27me3	Abcam	ab6002
Anti-Mouse H3K4me1 Clone: D1A9 XP	Cell Signaling	5326S
FITC Streptavidin	Biolegend	Cat 405202
Donkey Anti-Rabbit AF488 conjugated secondary	Jackson ImmunoResearch	Cat 711-545-152
Donkey Anti-Rabbit AF546, conjugated secondary	Jackson ImmunoResearch	Cat 711-165-152
Donkey Anti-Rabbit AF647, conjugated secondary	Jackson ImmunoResearch	Cat 711-605-152
Donkey Anti-Rat AF488, conjugated secondary	Jackson ImmunoResearch	Cat 712-545-150
Donkey Anti-Rat AF647, conjugated secondary	Jackson ImmunoResearch	Cat 712-605-150
DyLight 594 Goat Anti-Ar. Hamster AF594 Clone: Poly4055	Biolegend	Cat 405504
End of Table		

BIBLIOGRAPHY

[1] E. Christophers, "Psoriasis–epidemiology and clinical spectrum.," *Clinical and experimental dermatology*, vol. 26, pp. 314–320, June 2001. 1

[2] F. O. Nestle, D. H. Kaplan, and J. Barker, "Psoriasis.," *The New England journal of medicine*, vol. 361, pp. 496–509, July 2009. 2

[3] M. A. Lowes, M. Suárez-Fariñas, and J. G. Krueger, "Immunology of psoriasis.," *Annual review of immunology*, vol. 32, no. 1, pp. 227–255, 2014. 2

[4] K. E. Nograles, L. C. Zaba, E. Guttman-Yassky, J. Fuentes-Duculan, M. Suárez-Fariñas, I. Cardinale, A. Khatcherian, J. Gonzalez, K. C. Pierson, T. R. White, C. Pensabene, I. Coats, I. Novitskaya, M. A. Lowes, and J. G. Krueger, "Th17 cytokines interleukin (IL)-17 and IL-22 modulate distinct inflammatory and keratinocyte-response pathways.," *The British journal of dermatology*, vol. 159, pp. 1092–1102, Nov. 2008. 2

[5] C. Albanesi, S. Madonna, P. Gisondi, and G. Girolomoni, "The Interplay Between Keratinocytes and Immune Cells in the Pathogenesis of Psoriasis.," *Frontiers in Immunology*, vol. 9, p. 1549, 2018. 2

[6] Y. Dombrowski, M. Peric, S. Koglin, C. Kammerbauer, C. Göss, D. Anz, M. Simanski, R. Gläser, J. Harder, V. Hornung, R. L. Gallo, T. Ruzicka, R. Besch, and J. Schauber, "Cytosolic DNA triggers inflammasome activation in keratinocytes in psoriatic lesions.," *Science translational medicine*, vol. 3, pp. 82ra38–82ra38, May 2011. 2

[7] R. Lande, J. Gregorio, V. Facchinetti, B. Chatterjee, Y.-H. Wang, B. Homey, W. Cao, Y.-H. Wang, B. Su, F. O. Nestle, T. Zal, I. Mellman, J.-M. Schröder, Y.-J. Liu, and M. Gilliet, "Plasmacytoid dendritic cells sense self-DNA coupled with antimicrobial peptide.," *Nature*, vol. 449, pp. 564–569, Oct. 2007. 2

[8] K. E. Nograles and J. G. Krueger, "Anti-cytokine therapies for psoriasis.," *Experimental cell research*, vol. 317, pp. 1293–1300, May 2011. 3

[9] C. Leonardi, R. Matheson, C. Zachariae, G. Cameron, L. Li, E. Edson-Heredia, D. Braun, and S. Banerjee, "Anti-interleukin-17 monoclonal antibody ixekizumab in chronic plaque psoriasis.," *The New England journal of medicine*, vol. 366, pp. 1190–1199, Mar. 2012. 3

[10] A. Bouslimani, C. Porto, C. M. Rath, M. Wang, Y. Guo, A. Gonzalez, D. Berg-Lyon, G. Ackermann, G. J. Moeller Christensen, T. Nakatsuji, L. Zhang, A. W. Borkowski, M. J. Meehan, K. Dorrestein, R. L. Gallo, N. Bandeira, R. Knight, T. Alexandrov, and P. C. Dorrestein, "Molecular cartography of the human skin

surface in 3D.," *Proceedings of the National Academy of Sciences of the United States of America*, vol. 112, pp. E2120–9, Apr. 2015. 3

[11] E. A. Grice, H. H. Kong, G. Renaud, A. C. Young, NISC Comparative Sequencing Program, G. G. Bouffard, R. W. Blakesley, T. G. Wolfsberg, M. L. Turner, and J. A. Segre, "A diversity profile of the human skin microbiota.," *Genome research*, vol. 18, pp. 1043–1050, July 2008. 3

[12] E. Fuchs, "Skin stem cells: rising to the surface," *The Journal of Cell Biology*, vol. 180, pp. 273–284, Jan. 2008. 4

[13] E. Fuchs and S. Raghavan, "GETTING UNDER THE SKIN OF EPIDERMAL MORPHOGENESIS," *Nature Reviews Genetics*, vol. 3, pp. 199–209, Mar. 2002. 4

[14] F. M. Watt and K. B. Jensen, "Epidermal stem cell diversity and quiescence," *EMBO Molecular Medicine*, vol. 1, pp. 260–267, Aug. 2009. 4

[15] C. Blanpain and E. Fuchs, "Plasticity of epithelial stem cells in tissue regeneration," *Science*, vol. 344, pp. 1242281–1242281, June 2014. 4

[16] M. P. Alcolea and P. H. Jones, "Lineage Analysis of Epidermal Stem Cells," *Cold Spring Harbor perspectives in medicine*, vol. 4, pp. a015206–a015206, Jan. 2014. 4, 17

[17] G. Mascré, S. Dekoninck, B. Drogat, K. K. Youssef, S. Brohée, P. A. Sotiropoulou, B. D. Simons, and C. Blanpain, "Distinct contribution of stem and progenitor cells to epidermal maintenance," *Nature*, vol. 489, pp. 257–262, Sept. 2012. 4, 19

[18] C. S. Potten, R. Saffhill, and H. I. Maibach, "Measurement of the transit time for cells through the epidermis and stratum corneum of the mouse and guinea-pig.," *Cell and tissue kinetics*, vol. 20, pp. 461–472, Sept. 1987. 4

[19] Y. S. Choi, Y. Zhang, M. Xu, Y. Yang, M. Ito, T. Peng, Z. Cui, A. Nagy, A.-K. Hadjantonakis, R. A. Lang, G. Cotsarelis, T. Andl, E. E. Morrisey, and S. E. Millar, "Distinct Functions for Wnt/β-Catenin in Hair Follicle Stem Cell Proliferation and Survival and Interfollicular Epidermal Homeostasis," *Stem Cell*, vol. 13, pp. 720–733, Dec. 2013. 4

[20] X. Lim, S. H. Tan, W. L. C. Koh, R. M. W. Chau, K. S. Yan, C. J. Kuo, R. van Amerongen, A. M. Klein, and R. Nusse, "Interfollicular epidermal stem cells self-renew via autocrine Wnt signaling.," *Science (New York, N.Y.)*, vol. 342, pp. 1226–1230, Dec. 2013. 4

[21] S. Park, D. G. Gonzalez, B. Guirao, J. D. Boucher, K. Cockburn, E. D. Marsh, K. R. Mesa, S. Brown, P. Rompolas, A. M. Haberman, Y. Bellaïche, and V. Greco, "Tissue-scale coordination of cellular behaviour promotes epidermal wound repair in live mice.," *Nature Cell Biology*, vol. 19, pp. 155–163, Mar. 2017. 4

[22] B. E. Keyes, S. Liu, A. Asare, S. Naik, J. Levorse, L. Polak, C. P. Lu, M. Nikolova, H. A. Pasolli, and E. Fuchs, "Impaired Epidermal to Dendritic T Cell Signaling Slows Wound Repair in Aged Skin.," *Cell*, vol. 167, pp. 1323–1338.e14, Nov. 2016. 4, 5, 6, 14, 25, 84

[23] M. Perez-Moreno, M. A. Davis, E. Wong, H. A. Pasolli, A. B. Reynolds, and E. Fuchs, "p120-Catenin Mediates Inflammatory Responses in the Skin," *Cell*, vol. 124, pp. 631–644, Feb. 2006. 5

[24] Y. Ge, N. C. Gomez, R. C. Adam, M. Nikolova, H. Yang, A. Verma, C. P.-J. Lu, L. Polak, S. Yuan, O. Elemento, and E. Fuchs, "Stem Cell Lineage Infidelity Drives Wound Repair and Cancer.," *Cell*, vol. 169, pp. 636–650.e14, May 2017. 5

[25] B. Flutter and F. O. Nestle, "TLRs to cytokines: Mechanistic insights from the imiquimod mouse model of psoriasis," *European Journal of Immunology*, vol. 43, pp. 3138–3146, Nov. 2013. 5, 15, 31, 37

[26] B. M. Lichtenberger, P. A. Gerber, M. Holcmann, B. A. Buhren, N. Amberg, V. Smolle, H. Schrumpf, E. Boelke, P. Ansari, C. Mackenzie, A. Wollenberg, A. Kislat, J. W. Fischer, K. Röck, J. Harder, J. M. Schröder, B. Homey, and M. Sibilia, "Epidermal EGFR controls cutaneous host defense and prevents inflammation.," *Science translational medicine*, vol. 5, pp. 199ra111–199ra111, Aug. 2013. 5

[27] K. Lay, S. Yuan, S. Gur-Cohen, Y. Miao, T. Han, S. Naik, H. A. Pasolli, S. B. Larsen, and E. Fuchs, "Stem cells repurpose proliferation to contain a breach in their niche barrier.," *eLife*, vol. 7, p. 1272, Dec. 2018. 6, 14

[28] C. M. Schürch, C. Riether, and A. F. Ochsenbein, "Cytotoxic CD8+ T cells stimulate hematopoietic progenitors by promoting cytokine release from bone marrow mesenchymal stromal cells.," *Cell stem cell*, vol. 14, pp. 460–472, Apr. 2014. 6

[29] H. Takizawa, K. Fritsch, L. V. Kovtonyuk, Y. Saito, C. Yakkala, K. Jacobs, A. K. Ahuja, M. Lopes, A. Hausmann, W.-D. Hardt, Á. Gomariz, C. Nombela-Arrieta, and M. G. Manz, "Pathogen-Induced TLR4-TRIF Innate Immune Signaling in Hematopoietic Stem Cells Promotes Proliferation but Reduces Competitive Fitness.," *Cell stem cell*, vol. 21, pp. 225–240.e5, Aug. 2017. 7

[30] S. L. Masters, M. Gerlic, D. Metcalf, S. Preston, M. Pellegrini, J. A. O'Donnell, K. McArthur, T. M. Baldwin, S. Chevrier, C. J. Nowell, L. H. Cengia, K. J. Henley, J. E. Collinge, D. L. Kastner, L. Feigenbaum, D. J. Hilton, W. S. Alexander, B. T. Kile, and B. A. Croker, "NLRP1 inflammasome activation induces pyroptosis of hematopoietic progenitor cells.," *Immunity*, vol. 37, pp. 1009–1023, Dec. 2012. 7

[31] J. L. Zhao, C. Ma, R. M. O'Connell, A. Mehta, R. DiLoreto, J. R. Heath, and D. Baltimore, "Conversion of danger signals into cytokine signals by hematopoietic stem and progenitor cells for regulation of stress-induced hematopoiesis.," *Cell stem cell*, vol. 14, pp. 445–459, Apr. 2014. 7

[32] C. A. Lindemans, M. Calafiore, A. M. Mertelsmann, M. H. O'Connor, J. A. Dudakov, R. R. Jenq, E. Velardi, L. F. Young, O. M. Smith, G. Lawrence, J. A. Ivanov, Y.-Y. Fu, S. Takashima, G. Hua, M. L. Martin, K. P. O'Rourke, Y.-H. Lo, M. Mokry, M. Romera-Hernandez, T. Cupedo, L. Dow, E. E. Nieuwenhuis, N. F. Shroyer, C. Liu, R. Kolesnick, M. R. M. van den Brink, and A. M. Hanash, "Interleukin-22 promotes intestinal-stem-cell-mediated epithelial regeneration.," *Nature*, vol. 528, pp. 560–564, Dec. 2015. 7

[33] M. Kleppe, M. H. Spitzer, S. Li, C. E. Hill, L. Dong, E. Papalexi, S. De Groote, R. L. Bowman, M. Keller, P. Koppikar, F. T. Rapaport, J. Teruya-Feldstein, J. Gandara, C. E. Mason, G. P. Nolan, and R. L. Levine, "Jak1 Integrates Cytokine Sensing to Regulate Hematopoietic Stem Cell Function and Stress Hematopoiesis.," *Cell stem cell*, vol. 21, pp. 489–501.e7, Oct. 2017. 8

[34] G. Nigro, R. Rossi, P.-H. Commere, P. Jay, and P. J. Sansonetti, "The cytosolic bacterial peptidoglycan sensor Nod2 affords stem cell protection and links microbes to gut epithelial regeneration.," *Cell host & microbe*, vol. 15, pp. 792–798, June 2014. 8

[35] M. Biton, A. L. Haber, N. Rogel, G. Burgin, S. Beyaz, A. Schnell, O. Ashenberg, C.-W. Su, C. Smillie, K. Shekhar, Z. Chen, C. Wu, J. Ordovas-Montanes, D. Alvarez, R. H. Herbst, M. Zhang, I. Tirosh, D. Dionne, L. T. Nguyen, M. E. Xifaras, A. K. Shalek, U. H. von Andrian, D. B. Graham, O. Rozenblatt-Rosen, H. N. Shi, V. Kuchroo, O. H. Yilmaz, A. Regev, and R. J. Xavier, "T Helper Cell Cytokines Modulate Intestinal Stem Cell Renewal and Differentiation.," *Cell*, vol. 175, pp. 1307–1320.e22, Nov. 2018. 8

[36] K. Gronke, P. P. Hernández, J. Zimmermann, C. S. N. Klose, M. Kofoed-Branzk, F. Guendel, M. Witkowski, C. Tizian, L. Amann, F. Schumacher, H. Glatt, A. Triantafyllopoulou, and A. Diefenbach, "Interleukin-22 protects intestinal stem cells against genotoxic stress.," *Nature*, vol. 566, pp. 249–253, Feb. 2019. 9

[37] X. Wu, V. L. Dao Thi, Y. Huang, E. Billerbeck, D. Saha, H.-H. Hoffmann, Y. Wang, L. A. V. Silva, S. Sarbanes, T. Sun, L. Andrus, Y. Yu, C. Quirk, M. Li, M. R. MacDonald, W. M. Schneider, X. An, B. R. Rosenberg, and C. M. Rice, "Intrinsic Immunity Shapes Viral Resistance of Stem Cells.," *Cell*, vol. 172, pp. 423–438.e25, Jan. 2018. 9

[38] K. Yang, J. Wang, M. Wu, M. Li, Y. Wang, and X. Huang, "Mesenchymal stem cells detect and defend against gammaherpesvirus infection via the cGAS-STING pathway.," *Scientific reports*, vol. 5, p. 7820, Jan. 2015. 10

[39] S. M. Man, Q. Zhu, L. Zhu, Z. Liu, R. Karki, A. Malik, D. Sharma, L. Li, R. K. S. Malireddi, P. Gurung, G. Neale, S. R. Olsen, R. A. Carter, D. J. McGoldrick, G. Wu, D. Finkelstein, P. Vogel, R. J. Gilbertson, and T.-D. Kanneganti, "Critical Role for the DNA Sensor AIM2 in Stem Cell Proliferation and Cancer.," *Cell*, vol. 162, pp. 45–58, July 2015. 10

[40] J. Agudo, E. S. Park, S. A. Rose, E. Alibo, R. Sweeney, M. Dhainaut, K. S. Kobayashi, R. Sachidanandam, A. Baccarini, M. Merad, and B. D. Brown, "Quiescent Tissue Stem Cells Evade Immune Surveillance.," *Immunity*, vol. 48, pp. 271–285.e5, Feb. 2018. 10

[41] C. D. Allis and T. Jenuwein, "The molecular hallmarks of epigenetic control.," *Nature Reviews Genetics*, vol. 17, pp. 487–500, Aug. 2016. 11, 60

[42] A. M. Deaton and A. Bird, "CpG islands and the regulation of transcription.," *Genes & Development*, vol. 25, pp. 1010–1022, May 2011. 11

[43] M. Lawrence, S. Daujat, and R. Schneider, "Lateral Thinking: How Histone Modifications Regulate Gene Expression.," *Trends in genetics : TIG*, vol. 32, pp. 42–56, Jan. 2016. 11, 12

[44] A. J. Bannister and T. Kouzarides, "Regulation of chromatin by histone modifications.," *Cell research*, vol. 21, pp. 381–395, Mar. 2011. 11, 12

[45] J. F. Flanagan, L.-Z. Mi, M. Chruszcz, M. Cymborowski, K. L. Clines, Y. Kim, W. Minor, F. Rastinejad, and S. Khorasanizadeh, "Double chromodomains cooperate to recognize the methylated histone H3 tail.," *Nature*, vol. 438, pp. 1181–1185, Dec. 2005. 12

[46] H. Li, S. Ilin, W. Wang, E. M. Duncan, J. Wysocka, C. D. Allis, and D. J. Patel, "Molecular basis for site-specific read-out of histone H3K4me3 by the BPTF PHD finger of NURF.," *Nature*, vol. 442, pp. 91–95, July 2006. 12

[47] K. Nishioka, S. Chuikov, K. Sarma, H. Erdjument-Bromage, C. D. Allis, P. Tempst, and D. Reinberg, "Set9, a novel histone H3 methyltransferase that facilitates transcription by precluding histone tail modifications required for heterochromatin formation.," *Genes & Development*, vol. 16, pp. 479–489, Feb. 2002. 12

[48] R. Schneider, A. J. Bannister, C. Weise, and T. Kouzarides, "Direct binding of INHAT to H3 tails disrupted by modifications.," *The Journal of biological chemistry*, vol. 279, pp. 23859–23862, June 2004. 12

[49] E. Calo and J. Wysocka, "Modification of enhancer chromatin: what, how, and why?," *Molecular cell*, vol. 49, pp. 825–837, Mar. 2013. 12, 61

[50] A. J. Ruthenburg, C. D. Allis, and J. Wysocka, "Methylation of lysine 4 on histone H3: intricacy of writing and reading a single epigenetic mark.," *Molecular cell*, vol. 25, pp. 15–30, Jan. 2007. 12

[51] M. P. Creyghton, A. W. Cheng, G. G. Welstead, T. Kooistra, B. W. Carey, E. J. Steine, J. Hanna, M. A. Lodato, G. M. Frampton, P. A. Sharp, L. A. Boyer, R. A. Young, and R. Jaenisch, "Histone H3K27ac separates active from poised enhancers and predicts developmental state.," *Proceedings of the National Academy of Sciences of the United States of America*, vol. 107, pp. 21931–21936, Dec. 2010. 12, 68

[52] M. U. Kaikkonen, N. J. Spann, S. Heinz, C. E. Romanoski, K. A. Allison, J. D. Stender, H. B. Chun, D. F. Tough, R. K. Prinjha, C. Benner, and C. K. Glass, "Remodeling of the enhancer landscape during macrophage activation is coupled to enhancer transcription.," *Molecular cell*, vol. 51, pp. 310–325, Aug. 2013. 13, 76

[53] Y.-I. Kawabe, Y. X. Wang, I. W. McKinnell, M. T. Bedford, and M. A. Rudnicki, "Carm1 regulates Pax7 transcriptional activity through MLL1/2 recruitment during asymmetric satellite stem cell divisions.," *Cell stem cell*, vol. 11, pp. 333–345, Sept. 2012. 13

[54] T.-D. Kanneganti, N. Özören, M. Body-Malapel, A. Amer, J.-H. Park, L. Franchi, J. Whitfield, W. Barchet, M. Colonna, P. Vandenabeele, J. Bertin, A. Coyle, E. P. Grant, S. Akira, and G. Núñez, "Bacterial RNA and small antiviral compounds activate caspase-1 through cryopyrin/Nalp3," *Nature*, vol. 440, pp. 233–236, Jan. 2006. 15

[55] L. van der Fits, S. Mourits, J. S. A. Voerman, M. Kant, L. Boon, J. D. Laman, F. Cornelissen, A. M. Mus, E. Florencia, E. P. Prens, and E. Lubberts, "Imiquimod-Induced Psoriasis-Like Skin Inflammation in Mice Is Mediated via the IL-23/IL-17 Axis," *The Journal of Immunology*, vol. 182, pp. 5836–5845, Apr. 2009. 15

[56] M. Ito, Y. Liu, Z. Yang, J. Nguyen, F. Liang, R. J. Morris, and G. Cotsarelis, "Stem cells in the hair follicle bulge contribute to wound repair but not to homeostasis of the epidermis," *Nature Medicine*, vol. 11, pp. 1351–1354, Nov. 2005. 17

[57] M. E. Page, P. Lombard, F. Ng, B. Göttgens, and K. B. Jensen, "The Epidermis Comprises Autonomous Compartments Maintained by Distinct Stem Cell Populations," *Cell stem cell*, vol. 13, pp. 471–482, Oct. 2013. 17

[58] V. Vasioukhin, L. Degenstein, B. Wise, and E. Fuchs, "The magical touch: genome targeting in epidermal stem cells induced by tamoxifen application to mouse skin.," *Proceedings of the National Academy of Sciences of the United States of America*, vol. 96, pp. 8551–8556, July 1999. 19

[59] M. Li, P. Hener, Z. Zhang, S. Kato, D. Metzger, and P. Chambon, "Topical vitamin D3 and low-calcemic analogs induce thymic stromal lymphopoietin in mouse keratinocytes and trigger an atopic dermatitis.," *Proceedings of the National Academy of Sciences of the United States of America*, vol. 103, pp. 11736–11741, Aug. 2006. 23

[60] C. A. Thomson, A. McColl, J. Cavanagh, and G. J. Graham, "Peripheral inflammation is associated with remote global gene expression changes in the brain.," *Journal of neuroinflammation*, vol. 11, p. 73, Apr. 2014. 23

[61] V. Levy, C. Lindon, Y. Zheng, B. D. Harfe, and B. A. Morgan, "Epidermal stem cells arise from the hair follicle after wounding.," *FASEB journal : official publication of the Federation of American Societies for Experimental Biology*, vol. 21, pp. 1358–1366, May 2007. 23

[62] S. Naik, N. Bouladoux, J. L. Linehan, S.-J. Han, O. J. Harrison, C. Wilhelm, S. Conlan, S. Himmelfarb, A. L. Byrd, C. Deming, M. Quinones, J. M. Brenchley, H. H. Kong, R. Tussiwand, K. M. Murphy, M. Merad, J. A. Segre, and Y. Belkaid, "Commensal-dendritic-cell interaction specifies a unique protective skin immune signature.," *Nature*, vol. 520, pp. 104–108, Apr. 2015. 23, 31

[63] L. L. Dunn, S. de Valence, J.-C. Tille, P. Hammel, B. H. Walpoth, R. Stocker, B. A. Imhof, and M. Miljkovic-Licina, "Biodegradable and plasma-treated electrospun scaffolds coated with recombinant Olfactomedin-like 3 for accelerating wound healing and tissue regeneration.," *Wound repair and regeneration : official publication of the Wound Healing Society [and] the European Tissue Repair Society*, vol. 24, pp. 1030–1035, Nov. 2016. 25

[64] S. Naik, N. Bouladoux, C. Wilhelm, M. J. Molloy, R. Salcedo, W. Kastenmuller, C. Deming, M. Quinones, L. Koo, S. Conlan, S. Spencer, J. A. Hall, A. Dzutsev, H. Kong, D. J. Campbell, G. Trinchieri, J. A. Segre, and Y. Belkaid, "Compartmentalized control of skin immunity by resident commensals.," *Science*, vol. 337, pp. 1115–1119, Aug. 2012. 29

[65] R. A. Clark, "Resident memory T cells in human health and disease.," *Science translational medicine*, vol. 7, pp. 269rv1–269rv1, Jan. 2015. 31

[66] M. G. Netea, L. A. B. Joosten, E. Latz, K. H. G. Mills, G. Natoli, H. G. Stunnenberg, L. A. J. O'Neill, and R. J. Xavier, "Trained immunity: A program of innate immune memory in health and disease.," *Science*, vol. 352, pp. aaf1098–aaf1098, Apr. 2016. 33, 71

[67] S. L. Foster, D. C. Hargreaves, and R. Medzhitov, "Gene-specific control of inflammation by TLR-induced chromatin modifications," *Nature*, vol. 447, pp. 972–978, May 2007. 33

[68] J. D. Buenrostro, B. Wu, H. Y. Chang, and W. J. Greenleaf, *ATAC-seq: A Method for Assaying Chromatin Accessibility Genome-Wide*. ATAC-seq for Assaying Chromatin Accessibility, Hoboken, NJ, USA: John Wiley & Sons, Inc., May 2001. 33

[69] J. Feng, T. Liu, B. Qin, Y. Zhang, and X. S. Liu, "Identifying ChIP-seq enrichment using MACS.," *Nature Protocols*, vol. 7, pp. 1728–1740, Sept. 2012. 36

[70] C. Y. McLean, D. Bristor, M. Hiller, S. L. Clarke, B. T. Schaar, C. B. Lowe, A. M. Wenger, and G. Bejerano, "GREAT improves functional interpretation of cis-regulatory regions.," *Nature biotechnology*, vol. 28, pp. 495–501, May 2010. 37

[71] E. L. Abel, J. M. Angel, K. Kiguchi, and J. DiGiovanni, "Multi-stage chemical carcinogenesis in mouse skin: fundamentals and applications.," *Nature Protocols*, vol. 4, no. 9, pp. 1350–1362, 2009. 55

[72] K. Brown, A. Buchmann, and A. Balmain, "Carcinogen-induced mutations in the mouse c-Ha-ras gene provide evidence of multiple pathways for tumor progression.," *Proceedings of the National Academy of Sciences of the United States of America*, vol. 87, pp. 538–542, Jan. 1990. 55

[73] S. H. Yuspa, T. Ben, H. Hennings, and U. Lichti, "Divergent responses in epidermal basal cells exposed to the tumor promoter 12-O-tetradecanoylphorbol-13-acetate.," *Cancer research*, vol. 42, pp. 2344–2349, June 1982. 55

[74] S. Naik, S. B. Larsen, N. C. Gomez, K. Alaverdyan, A. Sendoel, S. Yuan, L. Polak, A. Kulukian, S. Chai, and E. Fuchs, "Inflammatory memory sensitizes skin epithelial stem cells to tissue damage.," *Nature*, vol. 550, pp. 475–480, Oct. 2017. 60, 91

[75] R. Ostuni, V. Piccolo, I. Barozzi, S. Polletti, A. Termanini, S. Bonifacio, A. Curina, E. Prosperini, S. Ghisletti, and G. Natoli, "Latent Enhancers Activated by Stimulation in Differentiated Cells," *Cell*, vol. 152, pp. 157–171, Jan. 2013. 61, 68, 70, 76

[76] J. van der Veeken, A. J. Gonzalez, H. Cho, A. Arvey, S. Hemmers, C. S. Leslie, and A. Y. Rudensky, "Memory of Inflammation in Regulatory T Cells.," *Cell*, vol. 166, pp. 977–990, Aug. 2016. 61

[77] B. E. Bernstein, T. S. Mikkelsen, X. Xie, M. Kamal, D. J. Huebert, J. Cuff, B. Fry, A. Meissner, M. Wernig, K. Plath, R. Jaenisch, A. Wagschal, R. Feil, S. L. Schreiber, and E. S. Lander, "A bivalent chromatin structure marks key developmental genes in embryonic stem cells.," *Cell*, vol. 125, pp. 315–326, Apr. 2006. 62

[78] A. Local, H. Huang, C. P. Albuquerque, N. Singh, A. Y. Lee, W. Wang, C. Wang, J. E. Hsia, A. K. Shiau, K. Ge, K. D. Corbett, D. Wang, H. Zhou, and B. Ren, "Identification of H3K4me1-associated proteins at mammalian enhancers.," *Nature genetics*, vol. 50, pp. 73–82, Jan. 2018. 68

[79] S. K. T. Ooi, C. Qiu, E. Bernstein, K. Li, D. Jia, Z. Yang, H. Erdjument-Bromage, P. Tempst, S.-P. Lin, C. D. Allis, X. Cheng, and T. H. Bestor, "DNMT3L connects unmethylated lysine 4 of histone H3 to de novo methylation of DNA.," *Nature*, vol. 448, pp. 714–717, Aug. 2007. 68

[80] A. Rada-Iglesias, "Is H3K4me1 at enhancers correlative or causative?," *Nature genetics*, vol. 50, pp. 4–5, Jan. 2018. 68

[81] S. C. Biddie, S. John, P. J. Sabo, R. E. Thurman, T. A. Johnson, R. L. Schiltz, T. B. Miranda, M.-H. Sung, S. Trump, S. L. Lightman, C. Vinson, J. A. Stamatoyannopoulos, and G. L. Hager, "Transcription factor AP1 potentiates chromatin accessibility and glucocorticoid receptor binding.," *Molecular cell*, vol. 43, pp. 145–155, July 2011. 70

[82] J. M. Pattison, S. P. Melo, S. N. Piekos, J. L. Torkelson, E. Bashkirova, M. R. Mumbach, C. Rajasingh, H. H. Zhen, L. Li, E. Liaw, D. Alber, A. J. Rubin, G. Shankar, X. Bao, H. Y. Chang, P. A. Khavari, and A. E. Oro, "Retinoic acid and BMP4 cooperate with p63 to alter chromatin dynamics during surface epithelial commitment.," *Nature genetics*, vol. 50, pp. 1658–1665, Dec. 2018. 70

[83] E. Kaufmann, J. Sanz, J. L. Dunn, N. Khan, L. E. Mendonça, A. Pacis, F. Tzelepis, E. Pernet, A. Dumaine, J.-C. Grenier, F. Mailhot-Léonard, E. Ahmed, J. Belle, R. Besla, B. Mazer, I. L. King, A. Nijnik, C. S. Robbins, L. B. Barreiro, and M. Divangahi, "BCG Educates Hematopoietic Stem Cells to Generate Protective Innate Immunity against Tuberculosis.," *Cell*, vol. 172, pp. 176–190.e19, Jan. 2018. 72

[84] I. Mitroulis, K. Ruppova, B. Wang, L.-S. Chen, M. Grzybek, T. Grinenko, A. Eugster, M. Troullinaki, A. Palladini, I. Kourtzelis, A. Chatzigeorgiou, A. Schlitzer, M. Beyer, L. A. B. Joosten, B. Isermann, M. Lesche, A. Petzold, K. Simons, I. Henry, A. Dahl, J. L. Schultze, B. Wielockx, N. Zamboni, P. Mirtschink, Ü. Coskun, G. Hajishengallis, M. G. Netea, and T. Chavakis, "Modulation of Myelopoiesis Progenitors Is an Integral Component of Trained Immunity.," *Cell*, vol. 172, pp. 147–161.e12, Jan. 2018. 73

[85] A. Christ, P. Günther, M. A. R. Lauterbach, P. Duewell, D. Biswas, K. Pelka, C. J. Scholz, M. Oosting, K. Haendler, K. Baßler, K. Klee, J. Schulte-Schrepping, T. Ulas, S. J. C. F. M. Moorlag, V. Kumar, M. H. Park, L. A. B. Joosten, L. A. Groh, N. P. Riksen, T. Espevik, A. Schlitzer, Y. Li, M. L. Fitzgerald, M. G. Netea, J. L. Schultze, and E. Latz, "Western Diet Triggers NLRP3-Dependent Innate Immune Reprogramming.," *Cell*, vol. 172, pp. 162–175.e14, Jan. 2018. 73

[86] J. Ordovas-Montanes, D. F. Dwyer, S. K. Nyquist, K. M. Buchheit, M. Vukovic, C. Deb, M. H. Wadsworth, T. K. Hughes, S. W. Kazer, E. Yoshimoto, K. N. Cahill, N. Bhattacharyya, H. R. Katz, B. Berger, T. M. Laidlaw, J. A. Boyce, N. A. Barrett, and A. K. Shalek, "Allergic inflammatory memory in human respiratory epithelial progenitor cells.," *Nature*, vol. 139, p. 1752, Aug. 2018. 74

[87] S.-C. Cheng, J. Quintin, R. A. Cramer, K. M. Shepardson, S. Saeed, V. Kumar, E. J. Giamarellos-Bourboulis, J. H. A. Martens, N. A. Rao, A. Aghajanirefah, G. R. Manjeri, Y. Li, D. C. Ifrim, R. J. W. Arts, B. M. J. W. van der Veer, B. M. J. W. van der Meer, P. M. T. Deen, C. Logie, L. A. O'Neill, P. Willems, F. L. van de Veerdonk, J. W. M. van der Meer, A. Ng, L. A. B. Joosten, C. Wijmenga, H. G. Stunnenberg, R. J. Xavier, and M. G. Netea, "mTOR- and HIF-1α-mediated aerobic glycolysis as metabolic basis for trained immunity.," *Science*, vol. 345, pp. 1250684–1250684, Sept. 2014. 75

[88] R. J. W. Arts, A. Carvalho, C. La Rocca, C. Palma, F. Rodrigues, R. Silvestre, J. Kleinnijenhuis, E. Lachmandas, L. G. Gonçalves, A. Belinha, C. Cunha, M. Oosting, L. A. B. Joosten, G. Matarese, R. van Crevel, and M. G. Netea,

"Immunometabolic Pathways in BCG-Induced Trained Immunity.," *Cell reports*, vol. 17, pp. 2562–2571, Dec. 2016. 75

[89] R. J. W. Arts, B. Novakovic, R. Ter Horst, A. Carvalho, S. Bekkering, E. Lachmandas, F. Rodrigues, R. Silvestre, S.-C. Cheng, S.-Y. Wang, E. Habibi, L. G. Gonçalves, I. Mesquita, C. Cunha, A. van Laarhoven, F. L. van de Veerdonk, D. L. Williams, J. W. M. van der Meer, C. Logie, L. A. O'Neill, C. A. Dinarello, N. P. Riksen, R. van Crevel, C. Clish, R. A. Notebaart, L. A. B. Joosten, H. G. Stunnenberg, R. J. Xavier, and M. G. Netea, "Glutaminolysis and Fumarate Accumulation Integrate Immunometabolic and Epigenetic Programs in Trained Immunity.," *Cell metabolism*, vol. 24, pp. 807–819, Dec. 2016. 75, 78

[90] S. Saeed, J. Quintin, H. H. D. Kerstens, N. A. Rao, A. Aghajanirefah, F. Matarese, S.-C. Cheng, J. Ratter, K. Berentsen, M. A. van der Ent, N. Sharifi, E. M. Janssen-Megens, M. Ter Huurne, A. Mandoli, T. van Schaik, A. Ng, F. Burden, K. Downes, M. Frontini, V. Kumar, E. J. Giamarellos-Bourboulis, W. H. Ouwehand, J. W. M. van der Meer, L. A. B. Joosten, C. Wijmenga, J. H. A. Martens, R. J. Xavier, C. Logie, M. G. Netea, and H. G. Stunnenberg, "Epigenetic programming of monocyte-to-macrophage differentiation and trained innate immunity.," *Science (New York, N.Y.)*, vol. 345, pp. 1251086–1251086, Sept. 2014. 76

[91] S. Fanucchi, E. T. Fok, E. Dalla, Y. Shibayama, K. Börner, E. Y. Chang, S. Stoychev, M. Imakaev, D. Grimm, K. C. Wang, G. Li, W.-K. Sung, and M. M. Mhlanga, "Publisher Correction: Immune genes are primed for robust transcription by proximal long noncoding RNAs located in nuclear compartments.," *Nature genetics*, vol. 51, pp. 364–364, Feb. 2019. 76

[92] G. D. Barish, R. T. Yu, M. Karunasiri, C. B. Ocampo, J. Dixon, C. Benner, A. L. Dent, R. K. Tangirala, and R. M. Evans, "Bcl-6 and NF-kappaB cistromes mediate opposing regulation of the innate immune response.," *Genes & Development*, vol. 24, pp. 2760–2765, Dec. 2010. 76

[93] J. Quintin, S. Saeed, J. H. A. Martens, E. J. Giamarellos-Bourboulis, D. C. Ifrim, C. Logie, L. Jacobs, T. Jansen, B.-J. Kullberg, C. Wijmenga, L. A. B. Joosten, R. J. Xavier, J. W. M. van der Meer, H. G. Stunnenberg, and M. G. Netea, "Candida albicans infection affords protection against reinfection via functional reprogramming of monocytes.," *Cell host & microbe*, vol. 12, pp. 223–232, Aug. 2012. 76

[94] J. Kleinnijenhuis, J. Quintin, F. Preijers, L. A. B. Joosten, D. C. Ifrim, S. Saeed, C. Jacobs, J. van Loenhout, D. de Jong, H. G. Stunnenberg, R. J. Xavier, J. W. M. van der Meer, R. van Crevel, and M. G. Netea, "Bacille Calmette-Guerin induces NOD2-dependent nonspecific protection from reinfection via epigenetic reprogramming of monocytes.," *Proceedings of the National Academy of Sciences of the United States of America*, vol. 109, pp. 17537–17542, Oct. 2012. 76

[95] B. Novakovic, E. Habibi, S.-Y. Wang, R. J. W. Arts, R. Davar, W. Megchelenbrink, B. Kim, T. Kuznetsova, M. Kox, J. Zwaag, F. Matarese, S. J. van Heeringen, E. M. Janssen-Megens, N. Sharifi, C. Wang, F. Keramati, V. Schoonenberg, P. Flicek, L. Clarke, P. Pickkers, S. Heath, I. Gut, M. G. Netea, J. H. A. Martens, C. Logie, and H. G. Stunnenberg, "β-Glucan Reverses the Epigenetic State of LPS-Induced Immunological Tolerance.," *Cell*, vol. 167, pp. 1354–1368.e14, Nov. 2016. 76, 78

[96] G. D. Norata, G. Caligiuri, T. Chavakis, G. Matarese, M. G. Netea, A. Nicoletti, L. A. J. O'Neill, and F. M. Marelli-Berg, "The Cellular and Molecular Basis of Translational Immunometabolism.," *Immunity*, vol. 43, pp. 421–434, Sept. 2015. 78

[97] K. Yoshida, T. Maekawa, Y. Zhu, C. Renard-Guillet, B. Chatton, K. Inoue, T. Uchiyama, K.-i. Ishibashi, T. Yamada, N. Ohno, K. Shirahige, M. Okada-Hatakeyama, and S. Ishii, "The transcription factor ATF7 mediates lipopolysaccharide-induced epigenetic changes in macrophages involved in innate immunological memory.," *Nature Immunology*, vol. 16, pp. 1034–1043, Oct. 2015. 78

[98] L. Zhang, Y. Ge, and E. Fuchs, "miR-125b can enhance skin tumor initiation and promote malignant progression by repressing differentiation and prolonging cell survival.," *Genes & Development*, vol. 28, pp. 2532–2546, Nov. 2014. 89

[99] P. van Galen, A. D. Viny, O. Ram, R. J. H. Ryan, M. J. Cotton, L. Donohue, C. Sievers, Y. Drier, B. B. Liau, S. M. Gillespie, K. M. Carroll, M. B. Cross, R. L. Levine, and B. E. Bernstein, "A Multiplexed System for Quantitative Comparisons of Chromatin Landscapes.," *Molecular cell*, vol. 61, pp. 170–180, Jan. 2016. 90